# $GABA_B$ receptor-associated KCTD proteins as molecular linkers to downstream signaling complexes

**Inauguraldissertation**

Zur

Erlangung der Würde eines Doktors der Philosophie

vorgelegt der

Philosophisch-Naturwissenschaftlichen Fakultät

der Universität Basel

von

**David Berner**

aus Rupperswil (AG)

Basel, 2018

Genehmigt von der Philosophisch-Naturwissenschaftlichen Fakultät auf Antrag von

Prof. Dr. Bernhard Bettler

Prof. Dr. Markus Rüegg

Basel, den 21.6.2016

Prof. Dr. Jörg Schibler

Dekan

*To my friends and family*

# Table of Contents

# I Summary

$GABA_B$ receptors are metabotropic receptors of the prevalent inhibitory neurotransmitter gamma-aminobutyric acid (GABA), playing important roles in modulating overall neurotransmission and synaptic plasticity processes. The two principal subunits $GABA_{B1}$ and $GABA_{B2}$ form an obligate heterodimeric receptor, which is coupled to $G_{i/o}$ (reviewed in Gassmann and Bettler, 2012). Additionally, $GABA_B$ receptors are found in complexes with members of a subfamily of potassium channel tetramerization domain proteins (KCTDs). Precisely, KCTD8, KCTD12, KCTD12b and KCTD16 function as auxiliary subunits, further increasing molecular diversity of $GABA_B$ receptors and specifically modulating receptor responses, e.g. KCTD12-mediated desensitization of $GABA_B$ responses (Schwenk et al., 2010, Turecek et al., 2014). It has been described that $GABA_B$ receptors together with their KCTD subunits are present in large signaling complexes, e.g. in conjunction with the presynaptic N-type voltage-gated calcium channels and elements of the synaptic release machinery (Müller et al., 2010). However, the precise function of KCTDs in these complexes is not fully understood at the moment.

This thesis aims to study some of the roles that the KCTD subunits play in $GABA_B$ signaling, especially with regard to the interconnection of $GABA_B$ receptors to downstream signaling complexes. The main hypothesis was that KCTDs are molecular scaffolds for these protein complexes, thereby enlarging the functional repertoire of $GABA_B$ receptors.

The thesis is divided in two independent chapters. In the first chapter, I found that KCTD8 and KCTD16 are novel interactors of Cullin 3-RING E3 ubiquitin ligases (CRL3). The hypothesis that the $GABA_B$-associated KCTDs may bind to Cullin 3 was based on the fact that other KCTD family members were shown to be CRL3 substrate adaptors (Skoblov et al., 2013). Surprisingly, these newly-discovered interactions with Cullin 3 depended on the homology 2 (H2) domains of KCTD16 and KCTD8, even though Cullin 3-interactions of other KCTD family members are mediated by so-called Bric-a-brac, Tramtrack, Broad-complex (BTB) motifs found in their tetramerization (T1) domains (Furukawa et al., 2003, Skoblov et al., 2013). In the case of KCTD8 and KCTD16, their T1 domains were shown to lack Cullin 3-binding. Similar to other BTB substrate adaptors, KCTD16 was found to bind to the N-terminus of Cullin 3. The unusual Cullin 3-binding domains of KCTD16 and KCTD8 were confirmed by BRET measurements. Finally, I found that KCTD16 provides a linker between the $GABA_B$ receptor and the Cullin 3 complex. Co-expression of KCTD16 with $GABA_B$ receptors did not down-regulate $GABA_B$ receptors. Thus, the functional consequences of these novel CRL3 complexes are still unknown.

In the second chapter, I studied the function of the KCTDs in the complex of $GABA_B$ receptors and N-type voltage-gated calcium channels (VGCCs). I discovered that the CaV2.2 α1 subunit specifically interacts

with KCTD16 but not with KCTD12 and KCTD8. Interaction domain-mapping showed that this CaV2.2-KCTD16 interaction relied on the H2 domain of KCTD16. Strikingly, the CaV2.2-binding property could be transferred to KCTD12 by fusing the H2 domain of KCTD16 to KCTD12. Interestingly, the Gβγ-binding intracellular loop I-II of CaV2.2 was sufficient for the association with KCTD16. Finally, I confirmed the protein-protein interactions of $GABA_B$ receptors with both CaV2.2 and the synaptic protein syntaxin-1 in mouse brain tissue in co-IP experiments.

To understand the physiological relevance of this direct CaV2.2-KCTD16 interaction, its electrophysiological effects were characterized. It was found that KCTD16 changes the biophysical properties of N-type VGCCs in several ways. First, KCTD16 shifts the voltage-dependence of the channel to more hyperpolarized potentials. Second, KCTD16 increases the permeability of N-type VGCCs for divalent cations. Third, KCTD16 accelerates the kinetics of the channel activation. Perhaps most important for *in vivo* function, KCTD16 decreases the sensitivity and speed of response of N-type VGCCs to $GABA_B$-mediated inhibition.

In conclusion, the results of this thesis corroborate the concept that $GABA_B$ receptor-associated KCTDs act as molecular linkers of $GABA_B$ receptors to downstream signaling complexes, as shown here for CRL3 and N-type VGCCs. Furthermore, the results presented here also have functional implications for $GABA_B$-modulation of presynaptic neurotransmitter release.

# II Abbreviations

| | |
|---|---|
| AID | Alpha interaction domain (of VGCCs) |
| BACURD | BTB/POZ domain-containing adapter for Cul3-mediated RhoA degradation protein |
| BRET | Bioluminescence resonance energy transfer |
| BTB | Bric-a-brac, Tramtrack, Broad-complex domain |
| CaV2.1 | Pore-forming α1 subunit of P/Q-type voltage-gated calcium channels |
| CaV2.2 | Pore-forming α1 subunit of N-type voltage-gated calcium channels |
| CaMKII | Calmodulin-dependent kinase II |
| CHO | Chinese hamster ovary cells |
| CHO N-VGCC | CHO cell line stably expressing N-type VGCC |
| CNS | Central nervous system |
| Co-IP | Co-immunoprecipitation |
| COS-1 | Immortalized African green monkey cell line |
| CRL | Cullin-RING E3 ligase |
| Cul1 | Cullin 1 |
| Cul3 | Cullin 3 |
| E1, E2, E3 | Enzymes of the ubiquitination cascade |
| ER | Endoplasmic reticulum |
| ERAD | Endoplasmic reticulum-associated degradation |
| GABA | Gamma-aminobutyric acid |
| $GABA_A$ | Gamma-aminobutyric acid type A |
| $GABA_B$ | Gamma-aminobutyric acid type B |
| GHB | Gamma-hydroxybutyric acid |
| GIRK | G-protein-gated inwardly rectifying potassium channel |
| GK | Guanylate kinase |
| GPCR | G protein-coupled receptor |
| GRK | G protein-coupled receptor kinase |
| H1 | Homology domain 1 (of KCTDs) |
| H2 | Homology domain 2 (of KCTDs) |
| HCN2 | Hyperpolarization-activated cyclic nucleotide–gated cation channel 2 |
| HDAC1 | Histone deacetylase 1 |

| | |
|---|---|
| HEK293T | Human Embryonic Kidney 293 cells containing the large T antigen |
| HVA | High-voltage-activated (calcium channels) |
| IP | Immunoprecipitation |
| IPSP | Inhibitory postsynaptic potential |
| KCTD | Potassium channel tetramerization domain protein |
| Kir | Potassium inwardly-rectifying channel |
| KO | Knock-out |
| LTP | Long-term potentiation |
| LVA | Low-voltage-activated (calcium channels) |
| NMDA | N-methyl-D-aspartate receptor |
| PAM | Positive allosteric modulator |
| PKA | cAMP-dependent protein kinase |
| PKC | Protein kinase C |
| POZ | Pox virus and zinc finger (domain) |
| PTX | Pertussis toxin |
| RING | Really Interesting New Gene |
| Rluc | *Renilla reniformis* luciferase |
| SH3 | Src homology 3 |
| SNARE | Soluble N-ethylmaleimide-sensitive-factor attachment receptor |
| SNP | Single nucleotide polymorphism |
| Synprint | Synaptic protein interaction domain (of VGCCs) |
| Syt11 | Synaptotagmin 11 |
| T1 | Tetramerization domain (of KCTDs) |
| Ub | Ubiquitin |
| VFTD | Venus flytrap domain |
| WT | Wild-type |
| YFP | Yellow fluorescent protein |

# III General Introduction

## $GABA_B$ receptors

Gamma-aminobutyric acid (GABA) is the prevalent inhibitory neurotransmitter in the brain. The receptors for GABA can be classified into the $GABA_A$ ion channels and the metabotropic $GABA_B$ receptors (Olsen and Sieghart, 2008). Both $GABA_A$ and $GABA_B$ receptors mediate inhibitory postsynaptic potentials (IPSP). The ionotropic $GABA_A$ receptors are responsible for fast IPSPs acting within the order of a few milliseconds (Olsen and Sieghart, 2008). On the other hand, postsynaptic activation of metabotropic $GABA_B$-receptors causes slower IPSPs with durations of hundreds of milliseconds (reviewed in Gassmann and Bettler, 2012).

$GABA_B$ receptors belong to the family C of GPCRs and are structurally related to metabotropic glutamate receptors (Pin et al., 2003). Classical work of Bowery et al. showed that there are GABA receptors that are bicuculline-insensitive, these unusual GABA receptors were then termed $GABA_B$ receptors (reviewed in Bowery, 1993). The molecular cloning of the principal $GABA_B$ receptor subunits was accomplished in the late 1990s (Kaupmann et al., 1997). On a molecular level, $GABA_B$ receptors consist of two principal subunits, so-called $GABA_{B1}$ and $GABA_{B2}$ (Kaupmann et al., 1998a). Like other members of the GPCR family C, both $GABA_B$ receptor subunits are consisting of an N-terminal signal peptide, a large extracellular Venus flytrap domain (VFTD), a seven-transmembrane domain and an intracellular C-terminus important for signaling (Pin et al., 2003). The VFTD harbors the ligand-binding site in $GABA_{B1}$. The $GABA_{B1}$ subunit exists in two different isoforms, $GABA_{B1a}$ and $GABA_{B1b}$, differing by the two sushi domains which are only present in $GABA_{B1a}$ (Gassmann and Bettler, 2012). The sushi domains of $GABA_{B1a}$ have a role in axonal trafficking, causing a different subcellular distribution in neurons for $GABA_{B1a}$ and $GABA_{B1b}$ (Vigot et al., 2006, Biermann et al., 2010). However, $GABA_{B1a}$ and $GABA_{B1b}$ do not differ pharmacologically when expressed in heterologous cells (Bettler et al., 2004). Functional $GABA_B$ receptors are formed by an obligate heterodimer of $GABA_{B1}$ and $GABA_{B2}$, as $GABA_{B1}$ KO or $GABA_{B2}$ KO mice lack electrophysiological $GABA_B$ responses and display strong behavioral abnormalities such as stereotypical circling. The phenotypes of $GABA_B$ KO mice are summarized elsewhere (table 1 in Gassmann and Bettler, 2012). Even though $GABA_{B1}$ contains the ligand-binding site, it is not sufficient to form a functional $GABA_B$ receptor on its own, because $GABA_{B2}$ is required for efficient trafficking of $GABA_{B1}$ to the plasma membrane (Pagano et al., 2001, Robbins et al., 2001). $GABA_{B1}$ is retained by an ER retention motif (RSRR) contained on its intracellular domain that is occluded when $GABA_{B1}$ and $GABA_{B2}$ heterodimerize in the ER (Pagano et al., 2001). In addition to the role in trafficking, $GABA_{B2}$ is also important for G protein-coupling and

contains the binding site for the auxiliary KCTD subunits (Robbins et al., 2001, Schwenk et al., 2010). $GABA_B$ receptors belong to the class of $G_{i/o}$-coupled receptors (Bettler et al., 1998). Activation of $GABA_B$ receptors by GABA or pharmacological agonists such as baclofen leads to the dissociation of Gα and Gβγ from the receptor. Gα inhibits adenylate cyclase and Gβγ signals to downstream effector channels such as G-protein-gated inwardly rectifying potassium (GIRK) channels or N-type VGCCs (Gassmann and Bettler, 2012).

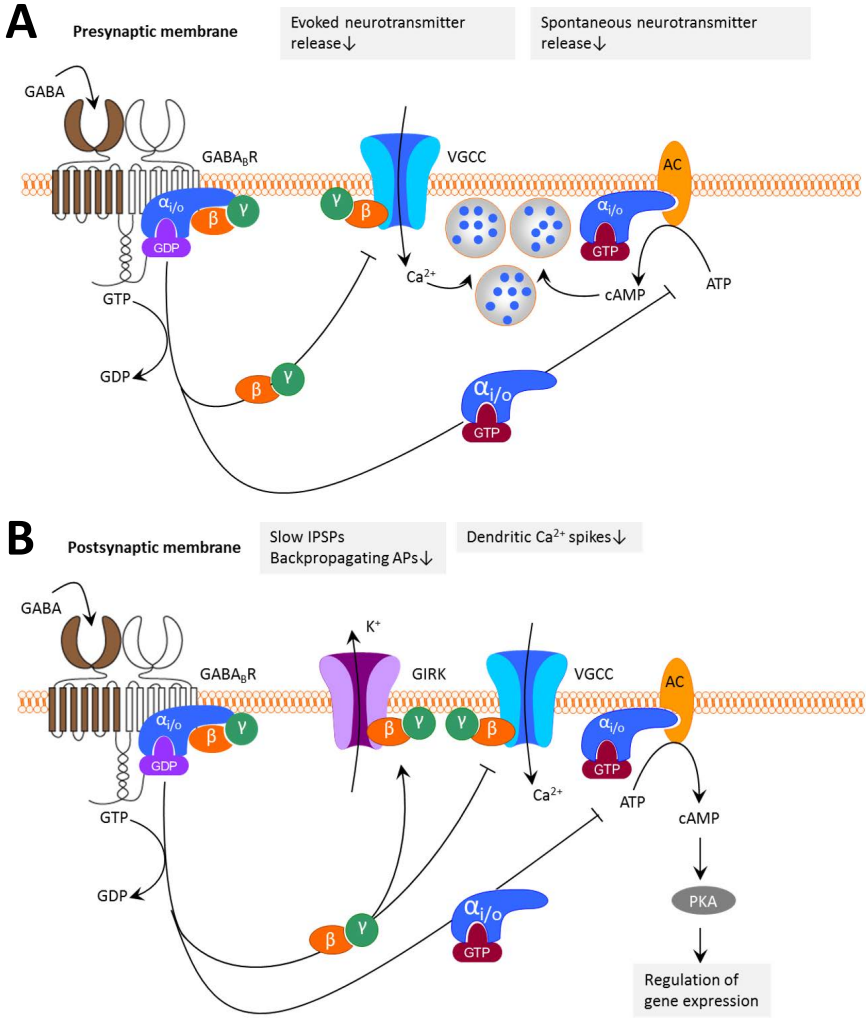


**Figure 1. Major effector systems of the $GABA_B$ receptor at the pre- and postsynapse.**
$GABA_B$ receptors are $G_{i/o}$-coupled GPCRs. Activation of the $GABA_B$ receptor leads to the dissociation of the heterotrimeric G protein. (A) At the presynapse, Gβγ inhibits presynaptic VGCCs and consequentially neurotransmitter release, while Gα inhibits the adenylate cyclase and thus affects spontaneous release of neurotransmitters. (B) At the postsynapse, released Gβγ activates GIRK channels, thereby leading to slow IPSPs. Furthermore, Gβγ decreases dendritic calcium spikes by inhibiting postsynaptic VGCCs. Gα inhibits PKA signaling via inhibition of the adenylate cyclase. Figure adapted from (Gassmann and Bettler, 2012).

In neurons, $GABA_B$ receptors are expressed in both presynaptic and postsynaptic locations (Vigot et al., 2006). Figure 1 illustrates the most important signaling pathways of pre- and postsynaptic $GABA_B$ receptors. $GABA_B$ receptors are found in almost all neurons in the brain. At the presynapse, activation of $GABA_B$ receptors leads to inhibition of neurotransmission via Gβγ-inhibition of presynaptic voltage-gated calcium channels and Gα-mediated inhibition of the adenylate cyclase (Gassmann and Bettler, 2012).

Postsynaptic $GABA_B$ receptors located in the somatodendritic compartment cause a reduction of neuronal excitability by several mechanisms. Release of the Gβγ heterodimer activates GIRK channels, leading to slow IPSPs and additionally inhibits postsynaptic VGCCs (Sodickson and Bean, 1996, Kaupmann et al., 1998b, Pérez-Garci et al., 2006). Gα-signaling inhibits the adenylate cyclase causing reduced PKA activity, which in turn affects NMDA receptors and TREK2 channels (Deng et al., 2009, Chalifoux and Carter, 2010).

The $GABA_B$ receptor is regulated on several levels. First, $GABA_B$ receptor complexes are regulated by their subunit composition, as the KCTD subunits have differential effects on $GABA_B$ signaling (Schwenk et al., 2010). Second, $GABA_B$ membrane levels are regulated through mechanisms like endocytosis, degradation or trafficking. GPCRs often undergo agonist-dependent internalization. The molecular mechanism involves receptor phosphorylation by G protein-coupled receptor kinases (GRKs) and β arrestin recruitment. Internalized receptors can then be either recycled back to the plasma membrane or degraded by lysosomal degradation. $GABA_B$ receptors do not undergo this classical agonist-dependent internalization (Raveh et al., 2015). Instead, $GABA_B$ receptors are constitutively internalized and glutamatergic neurotransmission leads to a decrease in $GABA_B$ receptor levels by reducing the fraction of recycled receptors (Maier et al., 2010). In another study, NMDA receptor activity was shown to cause $GABA_B$ receptor internalization by CaMKII-phosphorylation at S867 in the c-tail of $GABA_{B1}$ subunit (Guetg et al., 2010). PKA-mediated phosphorylation of $GABA_{B2}$ at S892 increases receptor stability by inhibiting constitutive receptor endocytosis (Couve et al., 2002). Proteasomal degradation also influences plasma membrane $GABA_B$ levels, as blocking the endoplasmic reticulum-associated degradation (ERAD) pathway leads to increased $GABA_B$ receptor levels (Zemoura et al., 2013). This form of degradation of $GABA_B$ is mediated by the ERAD E3 ligase Hrd1, which ubiquitinates the intracellular lysines 767/771 of $GABA_{B2}$ with K48-linked-polyubiquitin chains (Zemoura et al., 2013). K48-polyubiquitination is a classical signal for proteasomal degradation (Thrower et al., 2000).

Synaptic plasticity, the phenomenon of changing individual synaptic connections between neurons by long-term potentiation (LTP) or its opposite long-term depression (LTD), is widely thought to be crucial for learning and memory (reviewed in Sweatt, 2016). $GABA_B$ receptors are well known to regulate

synaptic strength by LTP (Davies et al., 1991). Given the importance of $GABA_B$ receptors in the brain, it is not surprising that $GABA_B$–signaling has been implicated in many neurological diseases such as epilepsy, depression, addiction and anxiety (reviewed in Gassmann and Bettler, 2012).

Only two drugs with $GABA_B$-affinity are in clinical use nowadays, notably the archetypical $GABA_B$-specific agonist baclofen has clinical utility as a muscle relaxant for treating spasticity (Bettler et al., 2004). The property as a muscle relaxant and other side effects like sedation or confusion make baclofen unfavorable for treating psychiatric disorders (Bettler et al., 2004). Gamma-hydroxybutyric acid (GHB) is a substance naturally occurring in the brain in trace amounts as well as a psychoactive compound, when administered exogenously. GHB is known to act as a $GABA_B$ receptor agonist, but has diverse effects on other pathways as well (Maitre et al., 2016). However, it is unknown whether the low concentrations of GHB found in healthy people affect $GABA_B$ signaling (Gassmann and Bettler, 2012). In a metabolic disease called succinic semialdehyde dehydrogenase deficiency, high amounts of GHB accumulate in the brain due to lack of degradation (Maitre et al., 2016). Due to its depressant properties, GHB is utilized in the treatment of narcolepsy and as a therapeutic substitute for alcohol (Leone et al., 2010, Gowda and Lundt, 2014). Furthermore, GHB is illicitly used as a recreational drug and date-rape drug (Maitre et al., 2016).

The $GABA_B$ antagonist SGS742 was tested in Phase II clinical studies for mild cognitive impairment and Alzheimer's disease, but the clinical development for this indication was discontinued later (Froestl et al., 2004). Positive allosteric modulators (PAMs) of $GABA_B$ receptors are promising for a number of diseases such as addiction and are currently being developed by pharmaceutical companies (Filip et al., 2015). Compared to $GABA_B$ agonists, the $GABA_B$ PAMs are supposed to modulate the $GABA_B$ receptors in a more physiological way, because they only enhance signaling that is already present endogenously. This mechanism of action improves their safety and side effect profile (Filip et al., 2015). PAMs are thought to bind to the transmembrane domain of $GABA_{B2}$ and consequentially influence $GABA_B$ signaling (Urwyler, 2011).

## KCTDs as auxiliary $GABA_B$ receptor subunits

For some time, several elements of electrophysiological $GABA_B$ responses recorded in native tissue could not be fully explained with the respective responses in recombinant cells expressing the two principal $GABA_B$ receptor subunits (Gassmann and Bettler, 2012). This fact pointed towards more underlying molecular complexity. In a proteomics analysis of native $GABA_B$ complexes, the intracellular proteins KCTD12, KCTD12b, KCTD16 and KCTD8 were found and proposed as auxiliary subunits of the $GABA_B$

receptor (Schwenk et al., 2010), on the basis of their stable and tight association with $GABA_B$ receptors. Furthermore, they specifically modulate $GABA_B$ receptor responses, e.g. KCTD12 plays a role in the fast desensitization of $GABA_B$-mediated GIRK currents (Schwenk et al., 2010, Adelfinger et al., 2014, Turecek et al., 2014). The existence of KCTD auxiliary subunits could partially explain some differences seen between recombinant and native $GABA_B$ responses, however an important discrepancy still remains unexplained, namely the 10-fold higher agonist affinity seen in native brain membranes compared to recombinant systems (Kaupmann et al., 1998a, Rajalu et al., 2015).

The KCTD protein family encompasses at least 26 different intracellular proteins involved in diverse cellular functions like development, proliferation, protein degradation, transcription regulation and regulation of potassium conductances (Skoblov et al., 2013). All KCTD proteins contain an eponymous tetramerization domain (T1 domain), which exhibits homology to the tetramerization domain found in potassium channels (Liu et al., 2013). The KCTD family of proteins belongs to the larger family of BTB domain proteins, as their T1 domains contain the BTB structural motif (Skoblov et al., 2013). BTB proteins are thought to be the substrate adaptors for the Cullin 3-RING E3 ubiquitin ligases (Furukawa et al., 2003).

KCTD8, KCTD12, KCTD12b and KCTD16 share their overall protein domain structure and constitute one subclade of the KCTD family (Schwenk et al., 2010, Liu et al., 2013). Their protein domain structure is shown in Fig. 2A. They all contain the T1 domain at their very N-terminus followed by the homology domain 1 (H1 domain) (Skoblov et al., 2013). KCTD8 and KCTD16 additionally possess the homology domain 2 (H2 domain) at their very C-terminus (Schwenk et al., 2010). Both H1 and H2 domains do not resemble any known protein domain found in other proteins and are also not related to each other. As all KCTD proteins feature a tetramerization domain, the KCTD proteins are thought to form oligomers, e.g. for KCTD5 a pentameric stoichiometry was observed (Dementieva et al., 2009). In the case of the $GABA_B$-associated KCTD proteins, it is assumed that they all form tetramers (Schwenk et al., 2010). The gene coding for KCTD12b is found in many vertebrates, but humans only possess KCTD8, KCTD12 and KCTD16 (Seddik et al., 2012, Skoblov et al., 2013).

The expression pattern of the $GABA_B$-associated KCTDs is subtype-specific (Fig. 2B) and not restricted to neuronal tissue, therefore at least some of these KCTDs may have additional roles other than $GABA_B$-modulation (Schwenk et al., 2010, Metz et al., 2011). For example, KCTD12 can be found in many tissues like intestine, colon, kidney, heart, testis and bone marrow and is reported to be relevant in some gastrointestinal tumors (Suehara et al., 2008, Kikuta et al., 2010, Metz et al., 2011). In the adult mouse brain, KCTD12 and KCTD16 are most widely expressed, whereas the distributions of KCTD8 and KCTD12b

are quite confined to specific brain areas (Metz et al., 2011). KCTD12b is found exclusively in the medial habenula. KCTD8 is localized in the medial habenula, cerebellum and in parts of the brainstem. KCTD12 is found in several brain regions like the hippocampus and the cerebellum. KCTD16 is widely expressed in the cortex, hippocampus, thalamus and amygdala. Pyramidal and granule cells in the hippocampus can express both KCTD12 and KCTD16, so their expression is not mutually exclusive (Metz et al., 2011).

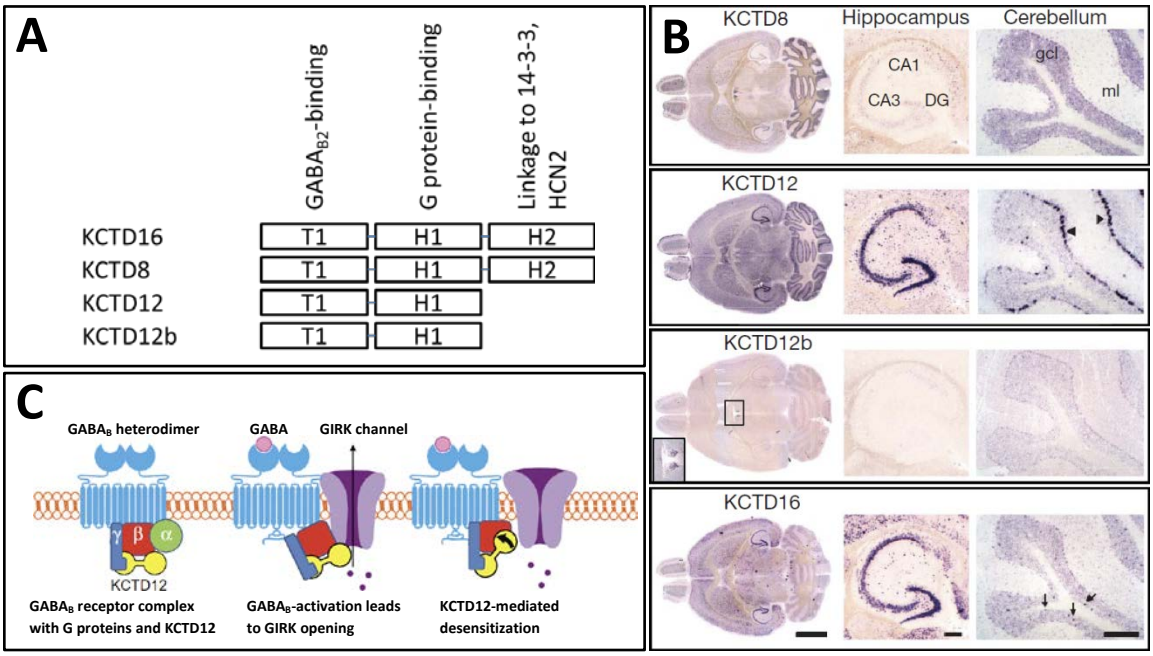


**Figure 2. KCTD proteins are auxiliary subunits of the GABA$_B$ receptor.**
(A) Schematic illustration of the protein domain structure of the GABA$_B$-associated KCTDs. All contain a T1 domain, where the GABA$_{B2}$-binding site is located and a H1 domain, which enables G protein-binding. KCTD8 and KCTD16 feature an additional H2 domain, which enables further protein-interactions.
(B) KCTD tissue distribution in adult mice brains as observed by in situ hybridization. KCTD12 and KCTD16 are widely expressed, e.g. in the hippocampus. In contrast, the expression of KCTD8 and KCTD12b is restricted to a few brain areas, such as the medial habenula. Panel adapted from (Schwenk et al., 2010)
(C) KCTDs affect GABA$_B$-effector channel signaling by interacting with Gβγ. As shown here, KCTD12 mediates desensitization of GIRK currents by inhibiting the Gβγ-activation of the GIRK channel. Panel adapted from (Raveh et al., 2015).

KCTD8, KCTD12, KCTD12b and KCTD16 are binding to the intracellular tail of GABA$_{B2}$ through their T1 domains (Schwenk et al., 2010). Residues 901-906 of GABA$_{B2}$ are particularly important, as the point mutation Y902A abolishes KCTD-binding (Schwenk et al., 2010). Interestingly, this critical Y902 residue is conserved among vertebrates but absent in invertebrates, therefore the function of KCTDs as GABA$_B$-associated subunits evolved in vertebrates (Seddik et al., 2012). The specific H1 domain of KCTD12 and

the absence of an H2 domain are important for the KCTD12-mediated desensitization of the $GABA_B$ response (Seddik et al., 2012). KCTD8, KCTD12 and KCTD16 are also known to interact with G proteins even in the absence of the $GABA_B$ receptor (Turecek et al., 2014). They specifically bind to the Gβγ heterodimer and also to the trimeric G protein complex (Turecek et al., 2014). Their isolated H1 domain is sufficient for interaction with the G proteins (T. Fritzius, personal communication). Besides its inhibitory role in desensitization, the H2 domain of KCTD16 is known to interact with the HCN2 channel and 14-3-3 proteins (Schwenk et al., 2016).

Even though $GABA_B$-associated KCTDs do not have a major allosteric effect on ligand-binding to the $GABA_B$ receptor per se (Rajalu et al., 2015), $GABA_B$-mediated GIRK currents differ significantly depending on the molecular composition of individual $GABA_B$ receptor complexes. $GABA_B$ receptors associated with KCTD12 and KCTD12b showed strong desensitization, whereas KCTD8 and KCTD16 displayed much less desensitization in the continued presence of baclofen (Schwenk et al., 2010). The mechanism for this desensitization is illustrated in Fig. 2C. The same pattern of response kinetics was observed when the $GABA_B$-regulated CaV2.1- and CaV2.2-currents were studied in oocytes (Schwenk et al., 2010). All four KCTDs accelerate the rise-time of the GIRK-mediated $GABA_B$ receptor response, but differ individually in the degree of acceleration (Schwenk et al., 2010). KCTD12 and KCTD16 also strongly increase agonist potency for $GABA_B$ receptors (Schwenk et al., 2010).

$GABA_B$-associated KCTDs have been implicated in a number of diseases. As $GABA_B$ receptor signaling itself is known to be implicated in many neuropsychological disorders such as epilepsy, it is not surprising that the auxiliary KCTDs also have some importance for this type of diseases. In this context, a genome-wide association study (GWAS) implicated KCTD12 in bipolar I disorder in a population sample of Han Chinese (Lee et al., 2011). In another study, the expression of KCTD12 was found to be upregulated in the hippocampus of schizophrenic patients (Benes, 2009). KCTD12 was also identified as a risk modifier in chronic tinnitus (Sand et al., 2012). Furthermore, KCTD12 is relevant for depression, as KCTD12 is upregulated in the amygdala of patients with major depressive disorder (Surget et al., 2008, Sibille et al., 2009). Another genetic study identified KCTD16 as a candidate gene for a special form of inherited temporal lobe epilepsy, but a molecular mechanism for this was not proposed (Angelicheva et al., 2009). Given their tissue expression profiles, the $GABA_B$-associated KCTDs likely play $GABA_B$-independent roles too, therefore these proteins could be relevant for diseases in a broader context (Metz et al., 2011). A large body of work showed that the KCTD12 expression level is a robust prognostic marker in gastrointestinal tumors (Suehara et al., 2008, Kikuta et al., 2010, Kubota et al., 2012, Hasegawa et al., 2013, Kubota et al., 2013, Orita et al., 2014). Similar to gastrointestinal tumors, KCTD12-positivity also

leads to a better survival prognosis for sarcoma patients (Kondo et al., 2013). KCTD12 was also analyzed in the context of glucose regulation and diabetes, but found to be of comparatively little importance (Cauchi et al., 2008).

# IV Aim of the Thesis

$GABA_B$ receptors are metabotropic receptors for the prevalent inhibitory neurotransmitter in the brain GABA. A large body of work already clarified the basic molecular constituents of functional $GABA_B$ receptors and their general electrophysiological responses (Gassmann and Bettler, 2012). Recently, it became apparent that $GABA_B$ receptors together with their auxiliary subunits KCTD8, KCTD12 and KCTD16 are found in large protein complexes in vivo, e.g. $GABA_B$ receptors are linked to N-type VGCCs and synaptic proteins of the presynaptic release machinery (Müller et al., 2010, Schwenk et al., 2010, Schwenk et al., 2016). The precise biochemical constitution of these signaling complexes and their functional consequences are still unclear.

The main goal of this thesis was to study novel protein interactions of the $GABA_B$-associated KCTDs, in order to gain more knowledge about the interconnections of $GABA_B$ receptors to other protein complexes. This thesis is based on two chapters: In the first chapter, I wanted to test the hypothesis that $GABA_B$-associated KCTDs are novel interactors of Cullin 3-RING E3 ubiquitin ligases (CRL3). In the second chapter, I wanted to study the function of KCTDs in the interaction of $GABA_B$ receptors with N-type voltage-gated calcium channels.

In chapter one, the hypothesis that KCTD12, KCTD16 and KCTD8 may be novel interactors of Cullin 3-RING E3 ubiquitination ligases was investigated (see 1.3.1). This hypothesis is mainly based on the homology between different KCTD family protein members. Most of the KCTD proteins have been found to be interacting with Cul3; for some KCTDs a substrate adaptor function has been demonstrated (Skoblov et al., 2013). The discovered Cul3-KCTD16 and Cul3-KCTD8 protein-protein interactions were then further characterized in terms of the necessary protein domains (see 1.3.2 and 1.3.3). As I found that the Cul3-KCTD16 interaction was dependent on an unexpected protein domain (the H2 domain rather than the T1 domain), I wanted to confirm this finding by another method. Therefore, I decided to do BRET measurements to corroborate my previous interaction domain-mapping (see 1.3.4). Based on the results of the interaction domain-mapping, the hypothesis that KCTD16 and KCTD8 are molecular linkers for Cullin 3 and $GABA_B$ receptors was studied (1.3.5). Finally, the plausible hypothesis that KCTD16 plays a role in the constitutive degradation of $GABA_B$ receptors was tested (1.3.6).

In chapter two, I wanted to study the important presynaptic complex of $GABA_B$ receptors with N-type voltage gated calcium channels, particularly the role that KCTDs play in this complex. First, I wanted to study whether the $GABA_B$ auxiliary subunits KCTD8, KCTD12 or KCTD16 interact with N-type calcium channels (see 2.3.1 and 2.3.2). I then decided to further characterize the newly-discovered CaV2.2-KCTD16 interaction (see 2.3.3 and 2.3.4). Finally, I chose to confirm the biochemical interactions of the

$GABA_B$ receptor with N-type VGCCs and the synaptic protein syntaxin-1 in mouse brain membranes (see 2.3.5). In order to understand the physiological relevance of the CaV2.2-KCTD16 interaction, electrophysiological recordings were carried out (R. Turecek), see 2.3.6.

# Chapter 1: KCTD8 and KCDT16 are novel Cullin 3-interactors

## 1.1 Introduction

### 1.1.1 Ubiquitination

Ubiquitination is the process of modifying protein substrates with a protein called Ubiquitin (Ub). Ub itself is a small (8.5kDa) and highly conserved protein in eukaryotes, is expressed ubiquitously and comprises only 76 amino acid residues (Goldstein et al., 1975). Since its Nobel-prized discovery in the 1980s, ubiquitination has emerged as an important post-translational modification rivalling phosphorylation, reflected by the fact that several thousands of proteins are regulated by some form of ubiquitination (Wilkinson, 2005, Kim et al., 2011, Wagner et al., 2011). Ubiquitination occurs in many different ways (reviewed in Komander and Rape, 2012). The least complex form of ubiquitination is mono-ubiquitination, where exactly one ubiquitin moiety is attached to a protein. In contrast, in the process of poly-ubiquitination, several Ubs are transferred to the substrate. The different forms of poly-ubiquitination differ in the way the individual ubiquitin molecules are linked together. Ubiquitin has seven lysines and all of them can be used for linkage. The K48-linked-poly-ubiquitination is a classical signal for proteasomal degradation, where four Ubs is the minimum amount required for efficient degradation. (Thrower et al., 2000). K63-linked-poly-ubiquitination is often a signal for endocytosis (Galan and Haguenauer-Tsapis, 1997). There are also more complex forms of poly-ubiquitination known where the association between the Ub molecules is heterogenous, although they are not well characterized (Komander and Rape, 2012). The post-translational modification of ubiquitination is carried out by an enzymatic cascade starting with the activation of Ub by an E1 enzyme in an ATP-dependent manner (Hershko and Ciechanover, 1998, Berndsen and Wolberger, 2014). In a next step, Ub is transferred from E1 to a cysteine residue of an E2 enzyme (Hershko and Ciechanover, 1998). The active E2 enzyme is then recruited to a large E3 ubiquitin ligase complex, which finally modifies certain lysine residues or the N-termini of specific substrates (Berndsen and Wolberger, 2014).

### 1.1.2 Cullin-RING E3 ubiquitination ligases

There are three different classes of E3 ligases (E3s): the RING, HECT and RBR protein families (reviewed in Berndsen and Wolberger, 2014). Together, there are more than 600 different E3 ligases present in the human genome (Li et al., 2008). The Cullin protein family (Cullin 1, Cullin 2, Cullin 3, Cullin 4a, Cullin 4b, Cullin 5 and Cullin 7 in mammals) is part of the RING E3 ligase family and it is the most prevalent class of E3s (Metzger et al., 2014). An additional but rather atypical member of the Cullin family is the p53-

associated parkin-like cytoplasmic protein (Parc) (Marín, 2009). The Cullin family was initially discovered in *C. elegans*, with Cullin 1 being a negative regulator of the cell-cycle and its null-mutation leading to hyperplasia in early development (Kipreos et al., 1996). An early study of CDC53/Cullin 1 in yeast demonstrated its role in ubiquitination and protein degradation (Mathias et al., 1996).

In the modular Cullin-RING E3 ligase (CRL) complexes, the Cullin proteins themselves act as molecular scaffolds for the assembly of these complexes, where their main function is to join together the ubiquitination target substrate and the activated E2 enzyme into one protein complex (Furukawa et al., 2002). The E2 enzyme provides the Ub moiety to be transferred to the ubiquitination substrate. The Cullin proteins all share a conserved Cullin homology domain at the C-terminus. This domain is required for the recruitment of the RING finger proteins Rbx1 and Rbx2, which act as adaptors for the E2 enzyme (Furukawa et al., 2002). To recognize their specific substrates, CRLs rely on specific substrate adaptor proteins. The general molecular organization is conserved in all Cullin E3 ligases, as the substrate adaptors associate with the N-termini of Cullin scaffolds and RING finger proteins interact with their C-termini (Fig. 3).

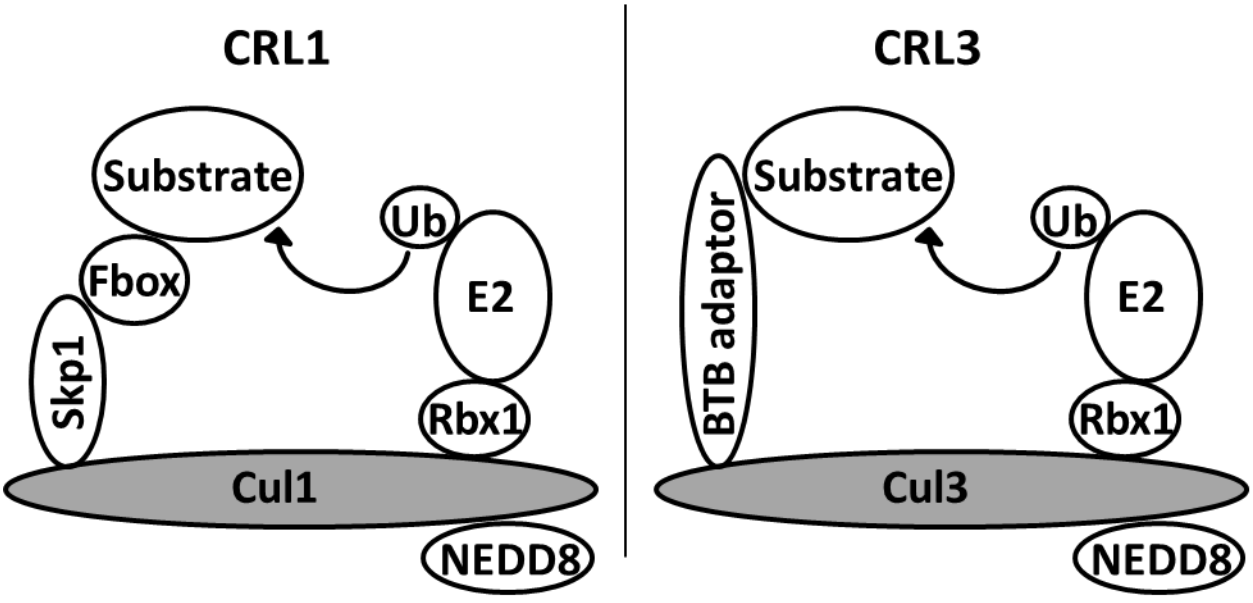


**Figure 3. The molecular organization of CRL1 and CRL3 complexes.**
The Cullin scaffold proteins arrange the E3 ligase complexes. The substrate recognition module binds to the N-termini of the Cullin scaffold and the RING finger protein Rbx1 recruits the E2 enzyme to their C-termini. The major difference between CRL1 and CRL3 complexes is the way of substrate recognition. CRL1 targets substrates by Skp1 and one of many F-box proteins, while CRL3 target their substrate by means of a single BTB substrate adaptor. NEDD8 acts as a regulator for both CRL complexes.

Cullin 3-RING E3 ubiquitin ligases (CRL3) differ from the other Cullin-RING E3 ligases in their way of substrate recognition (Furukawa et al., 2003). In Cullin 1-RING E3 ubiquitin ligases (CRL1), the substrate

specificity is regulated by two proteins, the Skp1 adaptor as well as one of many F-Box proteins, which serve as the actual substrate recognition proteins (Skaar et al., 2013). In CRL3 on the other hand, the substrate specificity is provided by one single substrate adaptor protein, which belongs to the BTB protein superfamily (Furukawa et al., 2003, Sarikas et al., 2011). Figure 3 illustrates the general molecular organization of CRL1 and CRL3.

### 1.1.3 Regulation of Cullin-RING E3 ligases

The E3 ligase activity of CRL complexes themselves is regulated by an ubiquitin-like modifier called NEDD8, the respective posttranslational modification is called neddylation (Osaka et al., 1998, Ohh et al., 2002). Similar to ubiquitination, neddylation is governed by an E1/E2/E3 enzymatic cascade (Osaka et al., 1998). In CRLs, the Cullin scaffolds are neddylated at a conserved lysine in the Cullin homology domain which promotes the ubiquitination activity of the CRLs by a structural reorganization. Deneddylation and inactivation of CRLs, is mediated by the COP9 signalosome (CSN). Another important regulator of CRLs is Cullin-associated NEDD8-dissociated protein 1 (CAND1). CAND1 molecules bind to unneddylated Cullins and inhibit E3 ligase activity (Zheng et al., 2002). Neddylation of Cullins displaces CAND1 from the complex (Liu et al., 2002). The precise mechanisms and functions of CAND1 are still debated (Sarikas et al., 2011).

### 1.1.4 Substrate adaptors of Cullin 3-RING E3 ligases

Several protein families including the KCTD proteins contain a BTB structural domain (Genschik et al., 2013, Skoblov et al., 2013). About 180 different BTB proteins are known in humans, although not all of them may form E3 ligases (Stogios et al., 2005).

In contrast to CRL1, in CRL3s the substrate specificity is mediated by one single BTB protein (Furukawa et al., 2003). One of the best characterized BTB substrate adaptors is the SPOP protein. A high-resolution crystal structure of the Cul3-SPOP complex was solved (Errington et al., 2012). For the Cullin 3-SPOP interaction, the N-terminal alpha helices H2 and H5 of Cullin 3 were shown to be crucial (Errington et al., 2012). Similar to SPOP, the BTB substrate adaptor KLHL11 also interacts with alpha helices H2 and H5 of Cul3 (Canning et al., 2013).

Conceptually, the KCTDs are thought to bind to the Cullin 3 scaffold through their BTB domain (within T1 domain) and to their specific ubiquitination substrates through their more variable C-term (Skoblov et al., 2013). This overall model was confirmed for several KCTD members, such as KCTD5, KCTD6, KCTD7, KCTD21 (Bayón et al., 2008, Azizieh et al., 2011, De Smaele et al., 2011). Recently, Smaldone and

coauthors showed that not all KCTD proteins associate with Cullin 3, as KCTD12 and KCTD15 were shown to lack the Cullin 3-binding property (Smaldone et al., 2015). This inability to interact with Cullin 3 likely stems from a structural alteration of the BTB domain of KCTD12 compared to members of other KCTD subfamilies. On the basis of their Cul3-binding experiments with the isolated BTB domain of KCTD12, they assumed that the other members of the subclade of KCTD12, namely KCTD8 and KCTD16, are also deficient in binding to Cul3 (Smaldone et al., 2015). Apart from the mentioned study, the subfamily of the $GABA_B$-associated KCTDs is not studied with regard to ubiquitination signaling via Cullin 3 (Skoblov et al., 2013).

### 1.1.5 Ubiquitination and degradation of $GABA_B$ receptors

Like other GPCRs, the plasma membrane levels of $GABA_B$ receptors are regulated by ubiquitination and degradation processes. Several lysines on both $GABA_{B1}$ and $GABA_{B2}$ were found to be ubiquitinated in vivo (Na et al., 2012). According to Lahaie et al., the residues K887, K893, K900 and K905 are potential ubiquitination sites on $GABA_{B1b}$, while the same is true for residues K767 and K771 on $GABA_{B2}$ (Lahaie et al., 2016).

At the beginning of its life cycle, $GABA_B$ receptor is a substrate for the ER-associated degradation (ERAD) system, probably as part of the quality control system in the ER. In the ERAD pathway, substrates are ubiquitinated by specific E3 ligases while they reside in the ER and get degraded by the proteasome afterwards. The ERAD E3 ligase Hrd1 was shown to ubiquitinate the $GABA_{B2}$ subunit at lysines 767/771, targeting $GABA_{B2}$ to the proteasomal degradation pathway (Zemoura et al., 2013). Consequentially, surface levels of $GABA_B$ are influenced by this mechanism, as blockade of the proteasome or ERAD leads to increased $GABA_B$ on the plasma membrane (Zemoura et al., 2013).

At the end of the life cycle of a GPCR, the receptors are typically endocytosed from the plasma membrane and either recycled back to the membrane or degraded in lysosomes. In many cases, receptor internalization is agonist-dependent. The $GABA_B$ receptor is an exception in this regard, as $GABA_B$ receptors do not undergo classical agonist-dependent internalization by β arrestin recruitment (Raveh et al., 2015). It is known that $GABA_B$ is internalized in a rapid constitutive manner (Grampp et al., 2008). Glutamate signaling also leads to endocytosis of $GABA_B$ receptors (Guetg et al., 2010, Maier et al., 2010). Furthermore, coordinated action of NSF and phosphorylation by PKC was shown to induce $GABA_B$ receptor internalization (Pontier et al., 2006).

Recently, overexpression of ubiquitin specific protease 14 (USP14) was shown to lead to decreased ubiquitination of $GABA_B$ but to increased degradation of $GABA_B$ (Lahaie et al., 2016). This USP14-

promoted degradation of $GABA_B$ was lysosomal-dependent. Interestingly, the deubiquitination activity of USP14 was shown to be independent of its degradation of $GABA_B$, suggesting that USP14-deubiquitination might play a role in the recycling of ubiquitin. Lahaie et al. propose that $GABA_B$ receptors are ubiquitinated in a PKC-dependent manner at the plasma membrane, which leads to the USP14-mediated degradation after endocytosis.

In this chapter, I describe the unexpected finding that KCTD16 and KCTD8 are actually novel protein interaction partners of Cullin 3. Furthermore, I show that they bind to Cul3 by their C-terminal H2 domains and not by their BTB domains. I also demonstrate that KCTD16 is recruiting Cul3 to the $GABA_B$ receptor.

## 1.2 Materials and Methods

**Expression plasmids**

The pCI-Myc-KCTD constructs (myc-KCTD12, myc-KCTD16, myc-KCTD8, myc-KCTD16T1-12H1, myc-KCTD16ΔH2, myc-KCTD16H2, myc-KCTD8ΔH2, myc-KCTD16H1H2, myc-KCTD12-16H2, myc-KCTD12-16H2 Δ60) were described earlier (Seddik et al., 2012).

For pCI-Myc-KCTD12-16H2 Δ39, a stop codon was inserted after residue Leu388.

The pCI-Cullin 3-Flag was generated by overlap extension PCR and subsequent subcloning into the pCI vector (Promega, WI, US), so that the Flag tag directly follows after the human Cullin 3 coding sequence. The pCDNA3-myc-Cul3 plasmid served as a template for this PCR. The pCI-Cullin 1–Flag plasmid was generated in the same way as the pCI-Cullin 3-Flag plasmid, using the pCDNA3-myc-Cul1 plasmid as a template. The two plasmids pcDNA3-myc3-Cul1 (Addgene plasmid #19896) and pcDNA3-myc-CUL3 (Addgene plasmid #19893) were gifts from Yue Xiong (Ohta et al., 1999).

To generate pCI-Rluc-Cul3 with overlap extension PCR, the Rluc gene was cloned directly in front of human Cullin 3 without a linker peptide. For pCI-KCTD16-Venus and pCI-KCTD8-Venus, the linker peptide DIGGGSGGGGS followed by the Venus tag were fused to the C-termini of KCTD16 and KCTD8. The pEGFP-Venus-KCTD16 and pEGFP-Venus-KCTD8 plasmids were made by changing GFP to Venus followed by the EcoRI restriction site in front of the N-termini of KCTD16 and KCTD8.

**Cell culture**

COS-1 and HEK293T cells were maintained in DMEM + 10% FCS in a cell culture incubator set to 37°C with 5% $CO_2$. Cells were split twice a week. Cell transfection was done using Lipofectamine 2000 (Life Technologies) according to the manufacturer's protocol. DNA amounts were equalized by empty pCI Vector DNA (Promega, WI, US).

**Co-immunoprecipitation and Western Blot**

Between 24 and 48 hours after transfection, COS-1 cells were washed in ice-cold PBS and lysed in NETN buffer (100mM NaCl, 20 mM Tris, 1mm EDTA, 0.5% NP40, pH 7.4) supplemented with EDTA-free cOmplete protease inhibitors (Roche). Lysates were then used for Western Blot (Input) or immunoprecipitations. Immunoprecipitations were done using magnetic Protein G beads (Dynabeads, 10004D, Life Technologies) according to the manufacturer’s protocol. Briefly, lysates and antibody coupled to beads were incubated for 10min at room temperature, beads were washed four times with

NETN buffer and eluted with 1x Lämmli Buffer. Input and IPs were resolved with standard SDS-PAGE on 8-12% acrylamide gels.

**Co-immunoprecipitation using mouse brain tissue**

For the immunoprecipitation experiment with mouse brain lysates, full brains from 4-week old mice were homogenized in ice-cold NETN buffer, using a glass-teflon homogenizer (30 strokes). Brain homogenates were centrifuged at 15'000g for 10min at 4°C. Proteins were immunoprecipitated with antibodies coupled to protein G-agarose (Roche Applied Science) and NETN buffer was used as a washing buffer.

**BRET experiments**

HEK293T cells were transiently transfected with indicated plasmids by Lipofectamine 2000 transfection. Five hours later, cells were trypsinized and plated into 96-wellplates (Greiner Bio-One, Kremsmünster, Austria). One day later, the cells were washed with PBS with $MgCl_2$ and $CaCl_2$ (Sigma-Aldrich, D8862) and incubated with the coelenterazine substrate (NanoLight Technologies, AZ, US) diluted in PBS with $MgCl_2$ and $CaCl_2$. BRET signals were measured with an Infinite® F500 Microplate Reader (Tecan, Männedorf, Switzerland).

**Immunostainings of hippocampal neurons**

Dissociated hippocampal cultures of WT mice (DIV14) were fixed by incubation with 4% PFA + 4% sucrose in PBS for 10min. Permeabilization was performed with 0.25% Triton-X in PBS with $MgCl_2$ and $CaCl_2$ (Sigma-Aldrich, D8862) for 10min at room temperature. PBS with $MgCl_2$ and $CaCl_2$ was used for the washing steps. Unspecific binding sites were blocked by incubation with 5% BSA in PBS with $MgCl_2$ and $CaCl_2$ for one hour at room temperature. Primary antibodies were incubated in blocking solution for one hour at room temperature. Secondary antibodies were incubated in blocking solution for 45min at room temperature. Finally, the stained samples were mounted using Fluoromount (Sigma-Aldrich, F4680).

**Primary antibodies used for IPs and Western Blots**

| Name | Host | Company | Product Nr. | WB | IP |
|---|---|---|---|---|---|
| Anti-Flag M2 | Mouse | Sigma | F1804 | - | 2µl |
| Anti-Flag | Rabbit | Sigma | F7425 | 1:1000 | - |
| Anti-myc 9e10 | Mouse | Santa Cruz | sc-40 | - | 5µl |
| Anti-myc | Rabbit | Sigma | C3956 | 1:1000 | - |
| Anti-Cul3 | Rabbit | Abcam | ab75851 | 1:1000 | 2µl |
| Anti-KCTD16 | Rabbit | Metz et al., 2011 | - | 1:1000 | - |
| Anti-KCTD16 | Guinea pig | Metz et al., 2011 | - | 1:1000 | 4µl |
| Anti-GB2 | Rabbit | Alomone | AGB-002 | 1:1000 | - |
| Anti-K48-Ub | Rabbit | Millipore | 05-1307 | 1:1000 | - |

**Antibodies used for immunostainings of hippocampal neurons**

| Name | Host | Company | Product Nr. | Dilution |
|---|---|---|---|---|
| Anti-KCTD16 | Rabbit | Metz et al., 2011 | - | 1:250 |
| Anti-Cullin 3 | Mouse | Sigma-Aldrich | SAB4200180 | 1:250 |
| Anti-MAP2 | Chicken | Abcam | ab5292 | 1:5000 |
| Anti-Rabbit Alexa 488 | Donkey | Life Technologies | A21206 | 1:1000 |
| Anti-Mouse Alexa 555 | Donkey | Life Technologies | A31570 | 1:1000 |
| Anti-Chicken Alexa 647 | Donkey | Millipore | AP194SA6 | 1:1000 |

## 1.3 Results

### 1.3.1 KCTD16 and KCTD8 but not KCTD12 bind to the Cullin 3-RING E3 ubiquitin ligase

Several members of the KCTD protein family are known to have a role as substrate adaptors of Cullin 3-RING E3 ubiquitin ligases, regulating diverse biological processes (Skoblov et al., 2013). To test whether KCTD12, KCTD16 and KCTD8 also associate with Cullin 3, co-immunoprecipitation experiments using transfected COS-1 cells were conducted. Figure 4A shows that both KCTD16 and KCTD8 bind to Cullin 3, while KCTD12 does not. Of note, KCTD8 displayed a weaker affinity for Cullin 3 when compared to KCTD16.

KCTD16 and KCTD8 have different expression patterns in the mouse brain, with KCTD16 being relatively abundant compared to KCTD8 (Metz et al., 2011). Notably, KCTD16 is strongly expressed in hippocampal neurons, while KCTD8 expression in the hippocampus is very weak (Metz et al., 2011). To study the endogenous expression patterns of KCTD16 and Cullin 3 in hippocampal neurons, I carried out immunostainings of dissociated hippocampal neurons of WT mice at DIV14. As shown in Fig. 4B, both KCTD16 and Cullin 3 are endogenously co-expressed in hippocampal neurons. Of note, both proteins are well expressed in the dendritic compartment (stained with the marker MAP2), as shown in the insets of Fig. 4B. This endogenous co-expression of KCTD16 and Cullin 3 in hippocampal neurons supports a possible biochemical association *in vivo*.

Finally, in order to check whether the KCTD16 interaction with Cullin 3 can also be demonstrated in neurons, I performed co-immunoprecipitation experiments with whole brain lysates from WT or KCTD16 KO mice. As shown in Figure 4C, the KCTD16-Cul3 interaction was also observed in mouse brain lysates in both directions. Therefore, the protein-protein interaction previously obtained with the recombinant assay using overexpression (in Fig. 4A) was confirmed using mouse brain tissue.

In summary, KCTD16 and KCTD8 were found to be novel protein-protein interaction partners of Cullin 3, whereas KCTD12 is not a direct interactor of Cullin 3-RING E3 ubiquitin ligases. For the more widely expressed KCTD16, this novel association with Cullin 3 was also confirmed in mouse brain tissue.

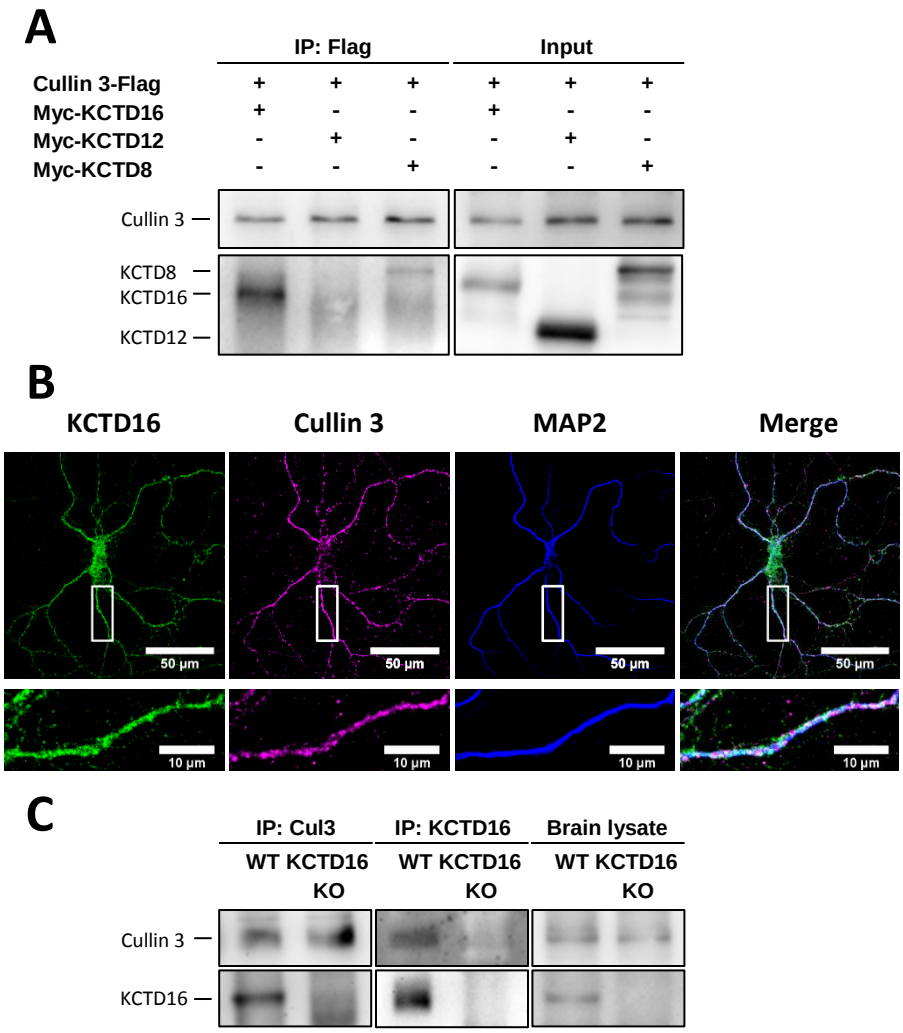


**Figure 4. KCTD16 and KCTD8 but not KCTD12 bind to the Cullin 3-RING E3 ubiquitin ligase.**
(A) Co-immunoprecipitation experiment using COS-1 cells transfected with Cullin 3-Flag and myc-KCTD16, myc-KCTD8 or myc-KCTD12. Cullin 3 was immunoprecipitated and detected with anti-Flag antibodies, while KCTDs were detected with anti-myc antibodies. KCTD16 and KCTD8 but not KCTD12 co-precipitate with Cullin 3. (B) Immunostainings of hippocampal neurons. KCTD16 and Cullin 3 are endogenously co-expressed in hippocampal neurons, MAP2 is a dendritic marker. Insets show a proximal dendrite of the neuron. (C) Co-immunoprecipitation experiment with mouse brain lysates of WT and KCTD16 KO mice. Endogenous Cullin 3 and KCTD16 were immunoprecipitated and detected using anti-KCTD16 and anti-Cullin 3 antibodies. KCTD16 is binding to Cullin 3 in mouse brain lysates.

### 1.3.2 The H2 domains of KCTD16 and KCTD8 are important for Cullin 3-binding

Generally, substrate adaptors for CRL3 complexes bind to the Cullin 3 scaffolds through their BTB domains (Furukawa et al., 2003, Genschik et al., 2013). The KCTDs also possess BTB domains, which are located in their T1 domains. To study whether the BTB domain is required for KCTD16-binding to Cullin 3, I tested different constructs of KCTD16 and KCTD12 by performing co-IP experiments using transfected COS-1 cells (Fig. 5A). Identical to the results in Fig. 4, full length KCTD16 binds to Cullin 3, while KCTD12 does not. Unexpectedly, both constructs containing the T1 domain of KCTD16 (16T1-12H1 and 16ΔH2) do not bind to Cullin 3, suggesting a non-conventional BTB-independent binding of KCTD16 to Cullin 3. Deletion of the KCTD16 H2 domain abolished Cullin 3-binding (16ΔH2), suggesting that the H2 domain is required for this protein interaction. Strikingly, attaching the H2 domain of KCTD16 to KCTD12 renders this construct (12-16H2) capable of Cullin 3-binding, confirming the necessity of the H2 domain for the interaction with Cullin 3. Next, I wanted to test whether the H2 domain of KCTD8 is also relevant for Cullin 3-binding. By performing co-IP experiments, I found that the H2 domain of KCTD8 was also necessary for the association with Cullin 3 (Fig. 5B), as binding was abolished when the H2 domain was deleted (8ΔH2). As the H2 domains of both KCTD16 and KCTD8 are required for Cullin 3-binding, I wanted to test whether the isolated H2 domain of KCTD16 is not only necessary but also sufficient for this interaction. I found that the isolated H2 domain of KCTD16 (16H2 construct) was not sufficient to bind to Cullin 3 (Fig. 5C), in contrast to the 16H1H2 construct. This 16H1H2 construct consists of both H1 and H2 domains of KCTD16 and represents the minimal Cullin 3-binding construct identified in this experiment. Potentially, the low expression level of 16H2 or a problem with proper folding might explain the inability of 16H2 to interact with Cullin 3. Altogether, I found that the BTB-containing T1 domains are not required for the Cullin 3 association, while the H2 domains of KCTD16 and KCTD8 play an important role in these protein-protein interactions, describing for the first time an interaction between KCTDs and Cullin 3 that is not BTB domain-dependent.

The importance of the H2 domain for Cullin 3-binding was demonstrated in Fig. 5A-C. In order to define the binding site more closely, two C-terminal deletion mutants of the H2 domain were tested. These constructs were made on the background of the H2 domain of KCTD16 fused to KCTD12. The last 39 or 60 amino acids of the H2 domain were deleted. Co-immunoprecipitations show that both constructs (12-16H2Δ60 and 12-16H2Δ39) were unable to bind to Cullin 3 (Fig. 5D). These results confirm the requirement of the H2 domain and further suggest that the C-terminal part of the H2 domain is necessary. A summary of the used constructs and their ability of Cullin 3-binding is given in Fig. 5E.

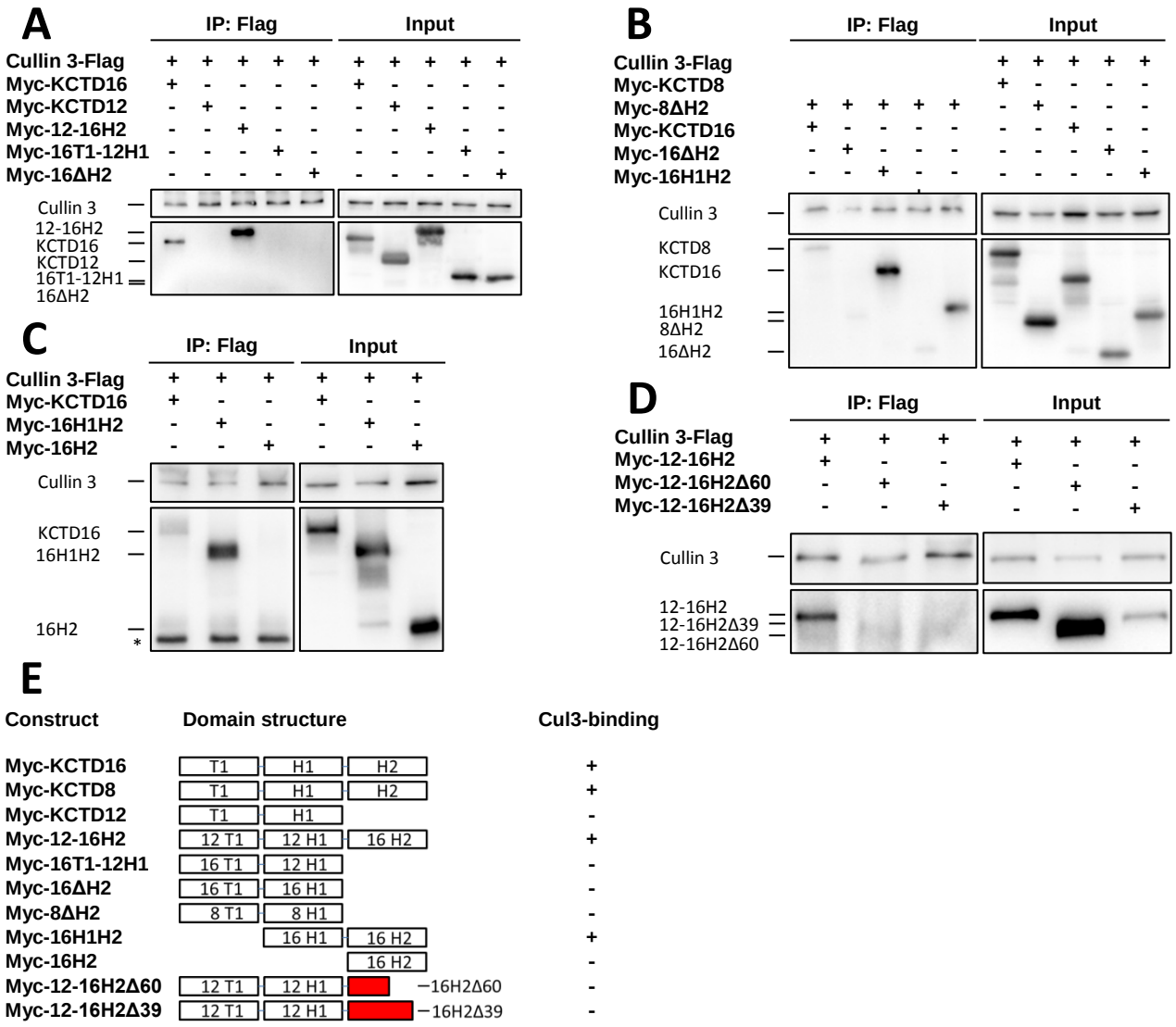


**Figure 5. The H2 domains of KCTD16 and KCTD8 are required for binding to Cullin 3.**

Cell lysates and co-immunoprecipitations of COS-1 cells transfected with Cullin 3-Flag and various KCTD constructs. Immunoprecipitations were done with indicated antibodies. KCTDs and Cullin 3 were detected using anti-myc and anti-Flag antibodies. (A) Domain mapping of the Cullin 3-binding site on KCTD16 using full length and chimeric constructs of KCTD16 and KCTD12. Full length KCTD16 binds to Cullin 3, KCTD12 serves as a negative control. Both constructs containing the T1 domain of KCTD16 (16T1-12H1 and 16ΔH2) do not bind to Cullin 3, whereas attaching the H2 domain of KCTD16 to KCTD12 transfers Cullin 3-binding to KCTD12. (B) Deletion of the H2 domains of KCTD16 and KCTD8 abolishes binding to Cullin 3 demonstrating the importance of the H2 domains for Cullin 3-binding. (C) The isolated H2 domain of KCTD16 (16H2) is not sufficient for binding to Cullin 3, in contrast to the combination of the H1 and H2 domains of KCTD16 (16H1H2) or full length KCTD16. Asterisk indicates a nonspecific band in the immunoprecipitations. (D) C-terminal 39 or 60 amino acids of the H2 domain were deleted on the background of the 12-16H2 construct (12-16H2Δ39 and 12-16H2Δ60). Both C-terminal H2 deletion constructs result in loss of binding to Cullin 3. (E) Overview of the protein domain structure of the used KCTD constructs and summary of their ability to associate with Cullin 3.

### 1.3.3 The N-terminus of Cullin 3 is sufficient for binding to KCTD16

In general, substrate adaptors of Cullin 3 are thought to bind to the N-terminal part of Cullin 3, in order to sterically position the substrate for ubiquitination by the E2 ubiquitination enzyme, which is linked to the C-terminus of the Cullin 3 (Furukawa et al., 2002, Furukawa et al., 2003). To test the hypothesis that KCTD16 similarly binds to the N-terminus of Cullin 3, two deletion constructs of Cullin 3 were made: Cul3 N223 consists of amino acids 1-223 of Cullin 3, while in the Cul 3 Δ218 construct amino acids 1-218 are deleted (Fig. 6A). These constructs together with full-length Cullin 3 were then assayed

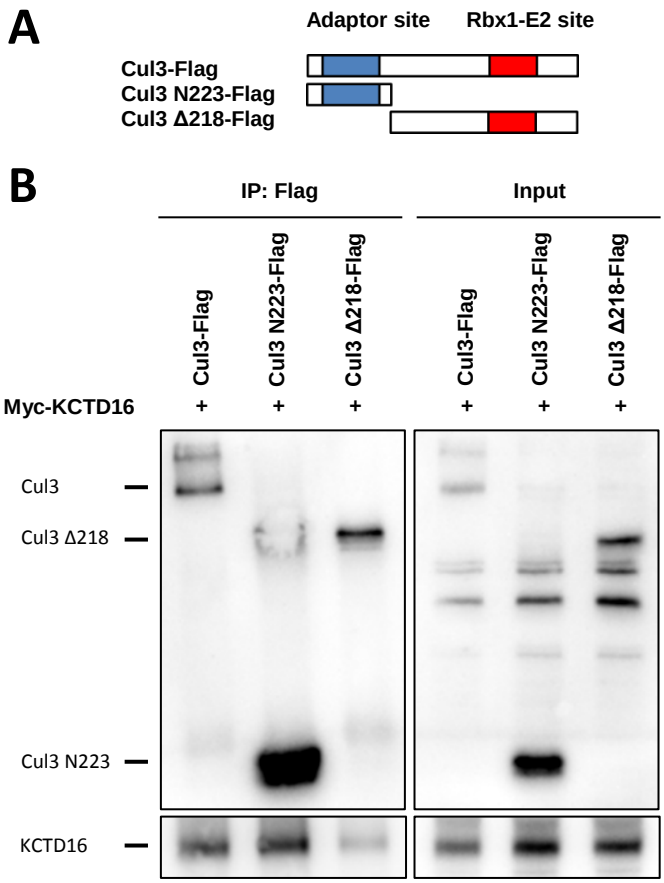


**Figure 6. The N-terminus of Cullin 3 is sufficient for binding to KCTD16.**
(A) Schematic illustration of the Cullin 3 constructs used in the co-immunoprecipitation experiments. To study the importance of the N-terminus of Cullin 3 for KCTD16-binding, I used a full length Cul3-Flag, a Cul3 construct composed of the N-terminal 223 amino acids (Cul3 N223-Flag) and a Cul3 construct consisting of the C-terminal amino acids 219-768 (Cul3 Δ218-Flag). (B) Co-immunoprecipitation experiment using transfected COS-1 cells. Cells were transfected with myc-KCTD16 together with Cul3-Flag, Cul3 N223-Flag or Cul3 Δ218-Flag. The Cullin 3 constructs were immunoprecipitated by using their Flag tag. Western Blot detection of the samples was done using anti-myc and anti-Flag antibodies.

for KCTD16-binding by performing co-immunoprecipitation experiments with transfected COS-1 cells (Fig. 6B). These co-IP experiments show that the N-terminus of Cullin 3 (Cul3 N223) is sufficient to interact with KCTD16. The strength of interaction is similar to full length Cullin 3. In contrast, KCTD16 binding for Cul3 Δ218 was significantly diminished to about 30% of Cul3 full length control, demonstrating that deletion of the N-terminus dramatically weakens the binding to KCTD16. The residual KCTD16-binding of Cul3 Δ218 could potentially be explained by association of this construct with endogenous Cullin 3, as Cullin 3 is endogenously expressed in COS-1 cells. Overall, these results are in agreement with the proposed binding of KCTD16 to the N-terminus of Cullin 3, similar to what was observed for other BTB protein family members (Genschik et al., 2013).

### 1.3.4 BRET studies confirm interactions of KCTD16 and KCTD8 with the N-terminus of Cullin 3

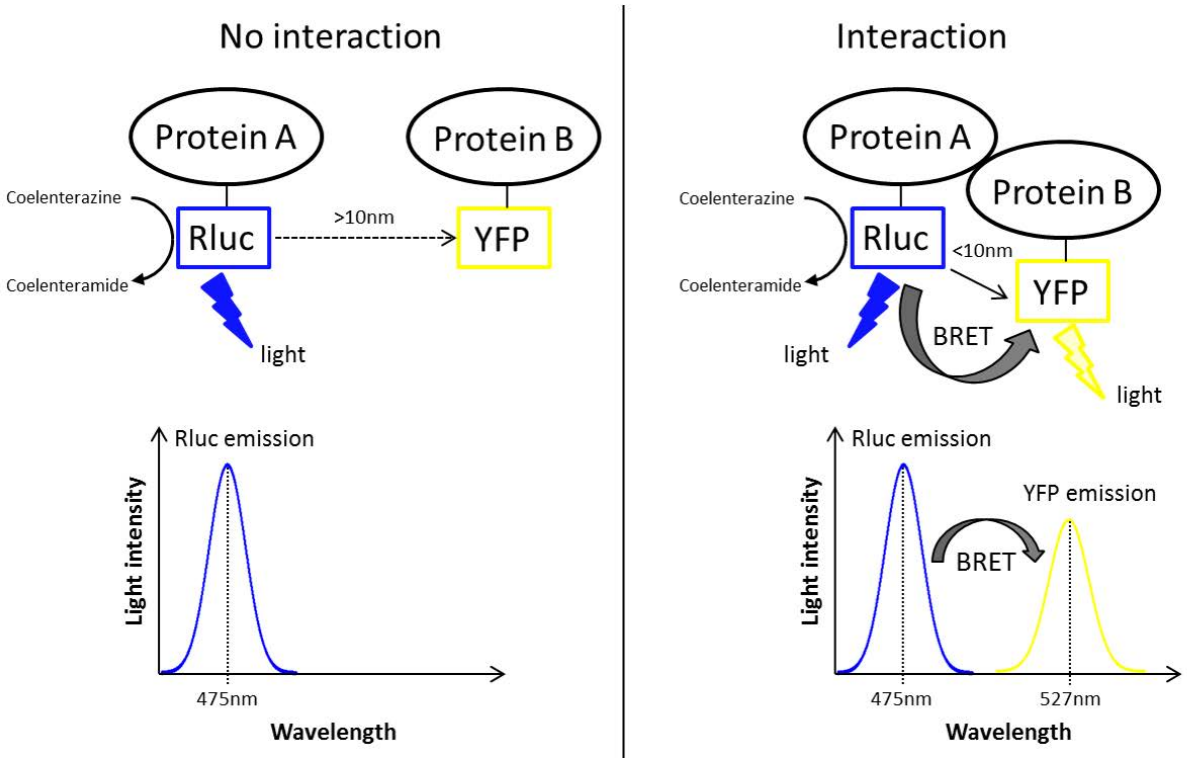


**Figure 7. Bioluminescence resonance energy transfer (BRET) experiments to measure protein-protein interactions in living cells.** Two fusion-proteins are co-expressed in cells. Protein A is tagged with Rluc and protein B is tagged with YFP. Blue light (475nm) is emitted when the cells are incubated with the substrate coelenterazine, being the substrate for a bioluminescent reaction catalyzed by the Rluc enzyme. Upon interaction of proteins A and B, the distance between Rluc and YFP is permissive for BRET. A distance of less than 10nm is considered to be required for BRET. Energy is transferred from the Rluc donor to the YFP acceptor, which emits yellow light (527nm). BRET efficiency is strongly dependent on the distance between donor and acceptor.

The previous co-IP experiments led me to a model where the C-termini of KCTD16 or KCTD8 bind to the N-terminus of Cullin 3. At this point, I decided to confirm this interaction model by a different experimental technique. Another method often used to study protein-protein interactions is based on the principle of bioluminescence resonance energy transfer (BRET). The general mechanism for BRET experiments is shown in Fig. 7.

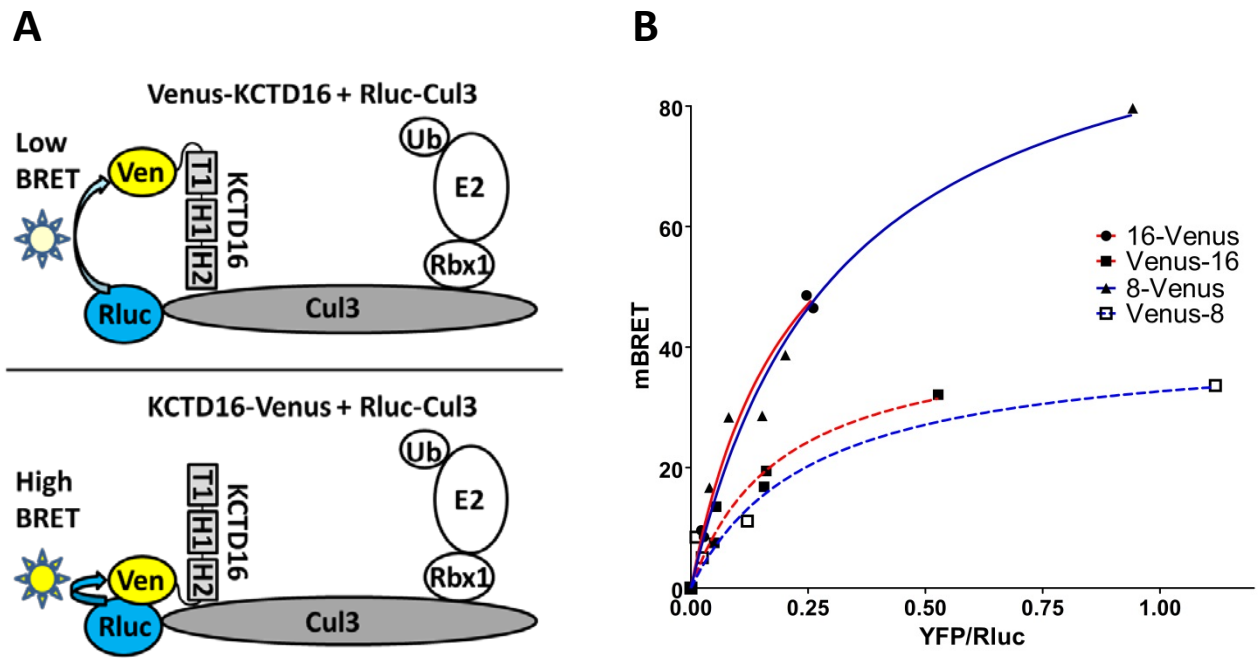


**Figure 8. BRET measurements confirm the C-terminal binding of KCTD16 and KCTD8 to the N-terminus of Cullin 3 in living cells.** (A) Experimental setup of the Cullin 3-KCTD16 BRET assay. If KCTD16 and KCTD8 bind to Cullin 3 as proposed, it is expected that the N-terminally Venus-tagged KCTD proteins induce weaker BRET than their C-terminally-tagged counterparts. (B) To generate the BRET saturation curves, increasing amounts of the Venus-tagged KCTD constructs were co-expressed together with constant amounts of Rluc-Cullin 3 in HEK293 cells. The result confirms the proposed binding of the N-terminus of Cullin 3 to the C-termini of KCTD16 and KCTD8.

The rationale of my BRET experiments is outlined in Fig. 8A. Venus tags were attached to KCTD16/8, at their C-termini or their N-termini and co-expressed with Cullin 3 with a Rluc tag attached to its N-terminus in HEK 293 cells. BRET saturation curves (Fig. 8B) show that the highest BRET signals, meaning closer physical distance, were obtained when the Venus tag was attached at the C-termini of KCTD16 or KCTD8, compared to the Venus tag at the N-termini. This result confirms my previous observation that the binding site for Cullin 3 in KCTD8/16 is located at the C-terminus which contains the H2 domain. Furthermore, this is clear evidence that the KCTD16/8-Cul3 interactions also happen in living cells.

### 1.3.5 KCTD16 is able to recruit Cullin 3 to the $GABA_B$ receptor complex

As KCTD16 and KCTD8 are described as auxiliary subunits of $GABA_B$ receptors (Schwenk et al., 2010, Gassmann and Bettler, 2012), the question arose whether there is recruitment of the CRL3 complex to the $GABA_B$ receptor by these KCTDs acting as molecular linkers (Figure 9B). To test this hypothesis, I performed co-IP experiments using transfected COS-1 cells. The $GABA_B$-associated KCTDs bind to the $GABA_{B2}$ subunit (Schwenk et al., 2010), therefore I co-expressed Cullin 3 and $GABA_{B2}$ together with

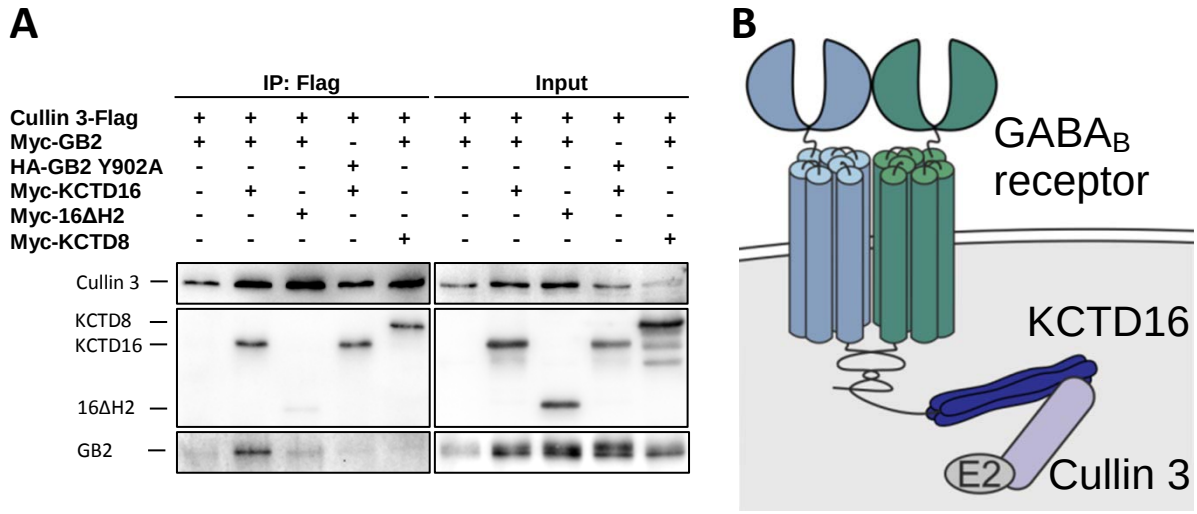


**Figure 9. KCTD16 but not KCTD8 recruits Cullin 3 to the $GABA_B$ receptor complex.**
(A) Co-immunoprecipitation experiment using transfected COS-1 cells showing the ability of KCTD16 to link Cullin 3 to the $GABA_{B2}$ subunit. Cullin 3 was immunoprecipitated with anti-Flag antibodies followed by Western Blot detection with anti-Flag, anti-myc and anti-$GABA_{B2}$ antibodies. Asterisk indicates a non-specific band in the inputs. Expectedly, no Cul3-recruitment to $GABA_B$ was observed for the negative controls 16ΔH2 and $GABA_{B2}$ Y902A. Surprisingly, KCTD8 was unable to bridge $GABA_B$ and Cul3. (B) Model showing the recruitment of CRL3 to the $GABA_B$ receptor via KCTD16.

KCTD16 or KCTD8. Next, Cullin 3 was immunoprecipitated using its Flag-tag and the indirect co-IP of $GABA_{B2}$ was assessed. KCTD16ΔH2 and the KCTD-binding deficient mutant $GABA_{B2}$ Y902A were used as negative controls. These co-IP experiments demonstrated that KCTD16 is able to link Cullin 3 to the $GABA_{B2}$ subunit (Fig. 9A). On the other hand, KCTD8 could not be demonstrated to recruit the $GABA_B$ receptor to Cullin 3 complexes. A possible reason might be the weaker affinity of KCTD8 for Cullin 3 compared to KCTD16, which renders it more difficult to show an indirect protein interaction with $GABA_{B2}$. As expected, neither the KCTD16ΔH2 nor the $GABA_{B2}$ Y902A conditions were showing CRL3 recruitment to $GABA_B$ receptors.

### 1.3.6 KCTD16 co-expression does not constitutively down-regulate $GABA_B$ receptors

In the previous experiment, I demonstrated that KCTD16 is able to link Cullin 3 to $GABA_B$ receptors. This posed the obvious question whether the $GABA_B$ receptor itself is a target for ubiquitination and degradation by KCTD16-CRL3 complexes. To test whether co-expression of KCTD16 has a direct effect on $GABA_B$ receptor total levels, COS-1 cells were transfected with the two principal subunits $GABA_{B1b}$ and

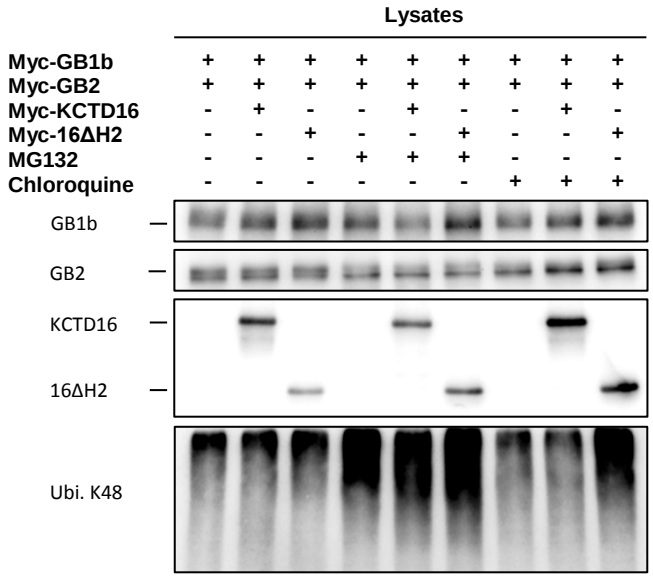


**Figure 10. Co-expression of KCTD16 with $GABA_B$ receptors does not down-regulate $GABA_B$ receptor total levels in transfected COS-1 cells.** In order to test for a direct effect of KCTD16 on $GABA_B$ receptor total levels, $GABA_B$ receptors were co-transfected with or without KCTD16. The co-transfection with KCTD16ΔH2 served as a negative control. The proteasome inhibitor MG-132 (10µM) or the lysosomal inhibitor chloroquine (100µM) was incubated to dissect a possible effect regarding the route of degradation. However, co-expression of KCTD16 does not down-regulate $GABA_B$ receptor total levels.

$GABA_{B2}$ together with or without KCTD16. KCTD16ΔH2 served as a negative control. Of note, Cullin 3 is endogenously expressed, thus functional KCTD16-CRL3 complexes are expected to form in these transfected cells and overexpression of CRL substrate adaptors alone is usually enough to produce pronounced effects on protein levels of their ubiquitination substrate, e.g. overexpression of KCTD21 and KCTD6 drastically decrease their substrate Histone deacetylase 1 (HDAC1) (De Smaele et al., 2011). To dissect a possible degradation effect on protein levels, the proteasomal inhibitor MG132 (10µM, Sigma Aldrich, M7449) and the lysosomal inhibitor chloroquine (100µM, Tocris, 4109) were incubated overnight in the indicated samples. It turned out that co-expression of KCTD16 does not down-regulate total protein levels of both principal $GABA_B$ receptor subunits under these conditions (Fig. 10). This

argues against a hypothesized constitutive ubiquitination and degradation of $GABA_B$ receptors by KCTD16-CRL3 complexes.

In conclusion, I found that $GABA_B$ receptor-associated KCTD16 and KCTD8 are novel Cullin 3 interaction partners, in contrast to KCTD12. Furthermore, the KCTD16 and KCTD8 interactions with Cullin 3 are non-conventional and BTB-independent, as they rely on their H2 domains. KCTD16 was also shown to recruit the CRL3 complex to the $GABA_B$ receptor.

## 1.4 Discussion

Many KCTDs have been reported to be interactors of Cullin 3-RING E3 ubiquitin ligases (reviewed in Skoblov et al., 2013). In these large multi-subunit E3 complexes, BTB proteins such as the KCTDs are thought to function as the substrate adaptors for these complexes (Furukawa et al., 2003). One last subclade of the KCTD family is mostly unstudied in this regard (Skoblov et al., 2013). This subfamily encompasses KCTD12, KCTD16 and KCTD8, all of them are known to be auxiliary subunits of $GABA_B$ receptors, where they specifically modulate receptor responses (Schwenk et al., 2010). In this chapter, I performed a systematic Cullin 3-binding assay of this unstudied subfamily and I concluded that KCTD16 and KCTD8 are indeed interacting with Cullin 3 (Fig. 4A). These interactions were observed in recombinant system, in live cells as well as in brain tissue.

Interestingly, I found that KCTD16 and KCTD8 bind Cullin 3 not through the canonical Cullin 3-interacting BTB domains, but rather through their C-terminal H2 domains. As shown in Figure 5, I found that H2 domain deletion constructs of KCTD16 or KCTD8 as well as full length KCTD12, which lacks an H2 domain, are unable to bind to Cullin 3. In contrast, I demonstrated that full-length KCTD16 and KCTD8 show the unexpected property of Cullin 3-binding and strikingly, this trait can be transferred to KCTD12, when the H2 domain of KCTD16 is fused to KCTD12 (Fig. 5A). Of note, the isolated H2 domain was unable to interact with Cullin 3, therefore the H2 domain is necessary but not sufficient for this interaction. I speculate that the low expression of this construct and possibly improper folding of the isolated H2 domain explain this result. The minimum Cullin 3-binding construct of KCTD16 was found to be 16H1H2, further corroborating that the T1 domain, which contains the BTB domain, is completely dispensable for this protein interaction.

In this thesis, I described a new H2 domain-dependent mechanism of KCTD16 and KCTD8 interaction with Cullin 3, opening up the possibility that not just BTB-domain containing proteins could be adaptors for CRL3 complexes. This possibility would further expand the number of potential CRL3 substrate adaptors. This atypical binding pattern explains two important points: First, it directly follows why only KCTD16 and KCTD8 are interacting with Cullin 3 (as both contain an H2 domain), but KCTD12 does not (as KCTD12 lacks the necessary H2 domain). Second, it fully explains Smaldone and coauthors observations. This group proposed that this KCTD subfamily is unable to interact with Cullin 3, based on their Cullin 3-interaction experiments with the purified BTB domain of KCTD12 (Smaldone et al., 2015). In this work, I used full-length KCTD proteins to assay for a Cullin 3-interaction rather than purified BTB domains, allowing us to find this new H2 domain-based binding mechanism. Also, I confirmed their previous observation that KCTD12 is unable to bind to Cullin 3 (Smaldone et al, 2015). I know now that the reason

of this result is that KCTD12 lacks the H2 domain and that its BTB domain is also incapable of binding. The inability to directly interact with Cullin 3 renders KCTD12 an exception in its subclade of the KCTD family. The fact that KCTD12 was found to be associated with Cullin 3 in a proteomic study (Bennett et al., 2010) might be explained by its heteromerization with either KCTD16 or KCTD8 (T. Fritzius, personal communication). For unknown reasons, KCTD16 and KCTD8 were not found as Cullin 3 interactors in the mentioned proteomic study (Bennett et al., 2010).

Classically, BTB proteins are thought to be the molecular substrate adaptors for Cullin 3-RING E3 ubiquitination ligases (Furukawa et al., 2003). In analogy to other BTB proteins, it is conceivable that KCTD16 and KCTD8 are functioning as substrate adaptors. The finding that KCTD16 associates with the N-terminus of Cullin 3 (Fig. 6) is in agreement with this hypothesis. However, the fact, that the BTB domain is actually dispensable for binding to Cullin 3, complicates the picture. In order to convincingly show that KCTD16 and KCTD8 are novel substrate adaptors similar to other BTB proteins, their substrates would need to be identified. Substrate identification for substrate adaptors of E3 ligases is a technically challenging task due to the principally short-lived nature of the interaction between substrates and their adaptors. Orphan substrate adaptors for E3 ligases are common in the literature (Liu et al., 2013).

My results further show that Cullin 3 and $GABA_{B2}$ can be found in the same complex in the presence of KCTD16 (Fig. 9). In this regard, the physiological function of KCTD16 may be a molecular linker that recruits the CRL3 complex to the $GABA_B$ receptor. KCTD16 has been found to act as a molecular linker in other contexts as well, for example linking $GABA_B$ with effector channels such as HCN2 channels (Schwenk et al., 2016). As shown in the second chapter, KCTD16 may also link $GABA_B$ to the CaV2.2 signaling complex. In the case of KCTD8, I was not able to demonstrate a similar molecular linker function in the same experiment. Possibly, technical reasons such as lower signal strength and the measurement of indirect protein interactions might explain this finding. It should be noted that in my co-IP experiments, I observed that KCTD8 has a weaker affinity to Cullin 3 compared to KCTD16, as an example see Figure 4A. Based on this lower affinity, one should expect a lower signal for the indirect $GABA_B$ co-IP in these experiments. I cannot exclude the possibility that a linker function of KCTD8 could be demonstrated by another experimental method. The reason for the weaker Cullin 3-binding affinity of KCTD8 compared to KCTD16 is unknown, but it is likely attributable to amino acid differences in their H2 domains.

An obvious hypothesis was that the KCTD16-CRL3 complex directly ubiquitinates and degrades $GABA_B$ receptors. The KCTD16-CRL3 complex does not constitutively down-regulate $GABA_B$ receptor levels (as shown in Fig. 10), arguing against this hypothesis. Thus, at the moment the question of the substrates of

the observed $GABA_B$-KCTD16-CRL3 and KCTD8-CRL3 complexes remains open. Possible substrates include other constituents of the large $GABA_B$ interactome. Alternatively, $GABA_B$ receptor-independent functions of the KCTD16/8-CRL3 complexes remain a plausible possibility as well, as the $GABA_B$-associated KCTDs are also expressed in non-neuronal tissues (Metz et al., 2011).

In conclusion, my results suggest that through the association with Cullin 3, KCTD16 and KCTD8 play a role in ubiquitination signaling *in vivo*, possibly in the context of $GABA_B$ receptors. However, their precise functions remain to be elucidated. Recent work has firmly established CRL3s as major regulators of different cellular and developmental processes. In humans, several mutations in CRL3 complex components have been associated with various pathologies, including metabolic disorders, muscle, and nerve degeneration, as well as cancer (Genschik et al., 2013). In this context, I demonstrated that not just BTB-domain containing proteins could be adaptors for CRL3 complexes and as a direct consequence this suggests a potential increase of putative adaptors and substrates which are regulated by these complexes. Elucidating the molecular mechanism and the functional consequence of the $GABA_B$-KCTD16-Cul3 complex will be important to better understand the regulation of $GABA_B$ receptor signaling.

# Chapter 2: KCTD16 directly interacts with N-type voltage-gated calcium channels

## 2.1 Introduction

### 2.1.1 Voltage-gated calcium channels

Voltage-gated calcium channels (VGCCs) play important roles in all excitable tissues, e.g. in the CNS or in the heart. As their name implies, their main function is to transduce electrical activity into changes of the intracellular level of the important second messenger calcium (Simms and Zamponi, 2014). Historically, VGCCs were classified into high-voltage-activated (HVA) and low-voltage-activated (LVA) channels based on early electrophysiological recordings (Fedulova et al., 1985, Mitra and Morad, 1986). Several types of VGCCs are known today (as shown in Fig. 11A), which mostly differ in their CaVα1 subunit: the L-type (CaV1.1-CaV1.4), the P/Q-type (CaV2.1), the N-type (Cav2.2), the R-type (Cav2.3) and the T-type (Cav3.1-Cav3.3) (Ertel et al., 2000, Simms and Zamponi, 2014). As shown in Fig. 11B and C, HVA channels are consisting of several subunits: the channel-forming CaVα1 subunits and the auxiliary CaVβ and CaVα2δ subunits (Simms and Zamponi, 2014). L-type VGCCs also incorporate CaVγ subunits (Simms and Zamponi, 2014). The auxiliary CaVβ1-4 and CaVα2δ1-4 subunits are promiscuous and associate with many different CaVα1 subunits (Dolphin, 2003). Native T-type VGCCs may lack auxiliary subunits (Perez-Reyes, 2003).

Predominantly P/Q-type and N-type VGCCs are crucial for synaptic transmission, as they couple neuronal activity with vesicle release in the presynapse (Simms and Zamponi, 2014). R-type VGCCs are also found in the presynapse. L-type VGCCs are mainly found in muscle and cardiac tissue. T-type VGCCs are present in both cardiac and neuronal tissue. The different types of VGCC can be distinguished pharmacologically, e.g. N-type VGCC are specifically inhibited by ω-conotoxin-GVIA, a toxin isolated from the marine cone snail *Conus geographus* (Kerr and Yoshikami, 1984).

### 2.1.2 The pore-forming CaVα1 subunits

As mentioned above, the different VGCCs are classified into different electrophysiological types on the basis of their CaVα1 subunit (Ertel et al., 2000). The pore-forming CaVα1 subunits are large proteins of around 250kDa consisting of four transmembrane domains, each of them made up of six transmembrane alpha-helices (Simms and Zamponi, 2014). The intracellular linkers between the four transmembrane segments (labeled I-IV) contain binding sites for diverse signaling modulators and scaffolds.

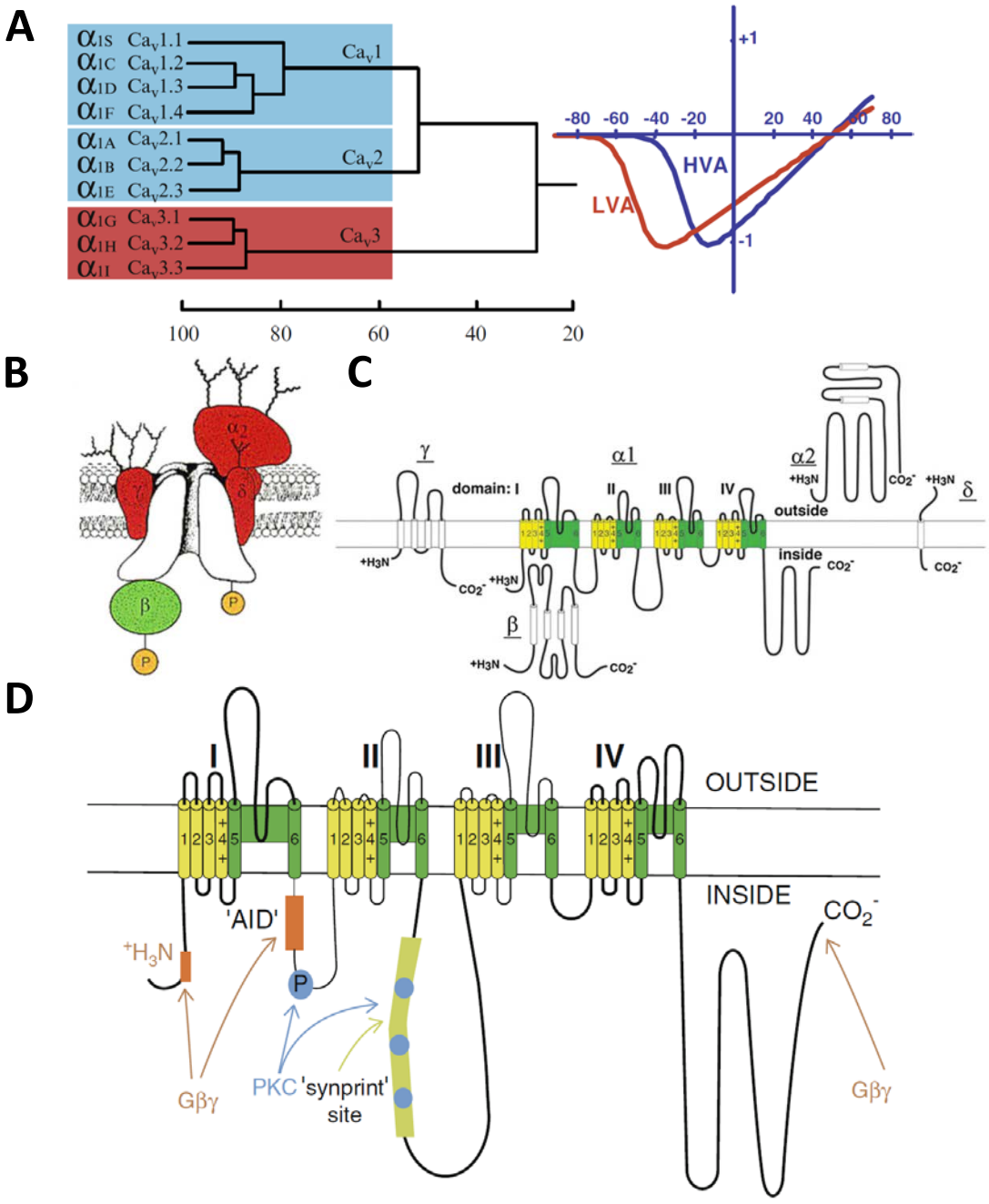


**Figure 11. Voltage-gated calcium channels.**

(A) The family of VGCC is subdivided in several subfamilies. High-voltage-activated (HVA) channels open when the membrane is heavily depolarized, in contrast to Low-voltage-activated (LVA) channels that activate already at less depolarized potentials. The HVA channels are further divided into CaV1 and CaV2 channels. (B) + (C) Schemes of the subunit composition for HVA channels. The principal pore-forming α1 subunit associates with regulatory β, α2δ and γ subunits. (D) Regulation of CaV2 channels. Gβγ inhibits the channel by binding to three sites distributed on the CaVα1 subunit. PKC phosphorylation is another major regulation mechanism. Synaptic proteins such as syntaxin-1 and SNAREs bind to the so-called Synprint site, thereby coupling the VGCC to the synaptic release machinery. Images adapted from (Catterall and Few, 2008) and (Stephens and Mochida, 2013).

In order to form functional VGCCs, α1 subunits associate with auxiliary subunits (Arikkath and Campbell, 2003). Interestingly, recombinantly expressed α1 subunits of T-type channels elicit similar currents as recorded in vivo, therefore it is unclear whether T-type channels need or are associated with auxiliary subunits in vivo (Perez-Reyes, 2003).

The presynaptic CaV2.1 and CaV2.2 contain several regulatory binding sites (Fig. 11D), to allow modulation of their $Ca^{2+}$-influx and consequentially of neurotransmission (Zamponi and Currie, 2013). An important binding site is the alpha interaction domain (AID) found on intracellular loop I-II, where the modulatory CaVβ subunits bind (Pragnell et al., 1994). A major regulatory site is found on linker I-II, where Gβγ leads to inhibition of calcium currents (Herlitze et al., 1997). Another crucial site is the so-called synaptic protein interaction site (Synprint), which is located on linker II-III (Rettig et al., 1996). SNAP-25 and syntaxin-1 are binding to the Synprint site, thereby tethering the VGCC and the release machinery together (Rettig et al., 1996, Catterall and Few, 2008). The important calcium sensor synaptotagmin 1 also binds to the Synprint site (Sheng et al., 1997). As the presynaptic VGCCs together with the vesicle release machinery constitute the core of the presynapse, many different signaling pathways converge at this site. Thus, it is not surprising that a multitude of interacting proteins of the CaVα1 subunits exist (Müller et al., 2010). VGCCs can also be regulated by phosphorylation through PKC and CaMKII kinases using specific sites on the α1 subunit (Zamponi and Currie, 2013).

### 2.1.3 CaVβ subunits

In mammalian cells, there are four genes coding for VGCC β subunits (CaVβ1-4). Additionally, several alternative splice forms exist for these genes. The Cavβ subunits consist of variable N- and C-termini as well as highly conserved Src homology 3 (SH3) and guanylate kinase (GK) domains, linked together by a HOOK domain. The GK domain is catalytically inactive but binds to the CaVα1 AID motif. The SH3 domain functions as a protein-protein interaction module. Overall the structures of CaVβs resemble membrane-associated guanylate kinases (MAGUKs). CaVβ subunits are promiscuous and bind to all Cav1 and CaV2 α1 subunits in heterologous systems (Dolphin, 2003). On the other hand, Cavβ subunits are not found in CaV3-based channels. The CaVβ subunits are soluble intracellular proteins and affect trafficking of the VGCCs, thereby strongly enhancing their calcium currents when co-expressed together with the CaVα1 subunits (Singer et al., 1991). The β subunits bind to the I-II linker of the α1 subunits and enhance surface expression of VGCCs and $Ca^{2+}$-currents (Pragnell et al., 1994). Recently, another VGCC-independent function of CaVβ subunits is emerging, as CaVβ subunits regulate the transcriptional activity of a certain Pax-6 isoform (Zhang et al., 2010).

### 2.1.4 CaVα2δ subunits

Four genes coding for the α2δ subunits are known (CaVα2δ1-4) (Obermair et al., 2008). Similar to the CaVβ subunits, α2δ subunits are promiscuous in their binding to different α1 subunits in recombinant systems (Obermair et al., 2008). The α2δ subunits are post-translationally cleaved into the α2 and the δ peptides, which then re-associate by a disulphide bridge (De Jongh et al., 1990). The α2δ subunit binds to CaVα1 in a completely extracellular interaction (Gurnett et al., 1997). Like the CaVβ subunits, the CaVα2δ proteins have a role in trafficking of VGCCs and/or enhancing of $Ca^{2+}$-currents (Arikkath and Campbell, 2003). Notably, the α2δ subunit is the pharmacological target for the anti-epileptic drugs Gabapentin and Pregabalin (Gee et al., 1996, Field et al., 1997).

### 2.1.5 Presynaptic voltage-gated calcium channels

N-type and P/Q-type calcium channels are crucial for neurotransmitter release at the presynaptic terminal (Simms and Zamponi, 2014). Voltage changes are sensed by these VGCCs and translated into a calcium ion influx that in turn leads to the release of neurotransmitter vesicles (Takahashi and Momiyama, 1993). At a molecular level, these VGCCs are highly interconnected with the synaptic release machinery through their Synprint domain (Rettig et al., 1996). This Synprint domain is located on the II-III linker of the α1 subunits (Rettig et al., 1996). Several SNARE proteins like syntaxin-1, synaptotagmin 1 and SNAP-25 bind to this site of both CaV2.1- and CaV2.2-based channels. Additional interfaces with the synaptic core complex are found on the CaVβ subunits, where the Rab interacting protein (RIM) binds (Kiyonaka et al., 2007). Through these redundant connections, CaV2.1 and CaV2.2 VGCCs are located in close physical proximity to the release machinery, which likely improves reliability and improves efficacy of this pivotal neuronal function (Neher, 1998).

Given the high relevance of N-Type and P/Q-type VGCCs in neurotransmitter release, it is not surprising that their function can be modulated by many different players such as GPCRs, protein kinases and second messengers (reviewed in Zamponi and Currie, 2013). Several neurotransmitters (e.g. GABA) are known to inhibit the calcium currents mediated by these VGCCs and consequentially also presynaptic transmitter release (Zamponi and Currie, 2013). Gβγ inhibition of presynaptic VGCCs is mediated by several binding sites for Gβγ on the α1 subunits (Herlitze et al., 1997, Cantí et al., 1999, Li et al., 2004). Presynaptic calcium channels are found in large protein complexes reflecting their important role in neurotransmission. A proteomics study of rat CaV2 channels (CaV2.1-CaV2.3) has shown a vast interactome of around 200 protein partners associated with these three VGCCs (Müller et al., 2010), 52 protein interactors are shared by all CaV2 channels. N-type VGCCs share an additional 47 putative

binding partners with P/Q-type and 19 interactors with R-type channels. Interestingly, the $GABA_B$ receptor and its auxiliary subunits KCTD12, KCTD8 and KCTD16 were also found to be specifically associated with N-type VGCCs (Müller et al., 2010).

### 2.1.6 GPCR-mediated modulation of presynaptic VGCCs

As a consequence of their pivotal role in neurotransmission, the presynaptic P/Q- and N-type VGCCs are known to be modulated by many different neurotransmitters such as GABA, glutamate, acetylcholine, monoamines (Zamponi and Currie, 2013). The mechanism for this form of modulation of VGCCs mostly consists in activating presynaptic GPCRs. There are two well-known forms of GPCR-mediated inhibitions of presynaptic VGCCs (Zamponi and Currie, 2013).

The first mechanism is a fast-acting inhibition mediated by the released Gβγ heterodimer. As described before, Gβγ is interacting with several sites on the CaVα1 subunit leading to inhibition of the VGCCs (Herlitze et al., 1997, Cantí et al., 1999, Li et al., 2004). Gβγ inhibits VGCCs by causing a positive shift in their voltage-dependence. The shift in voltage-dependence can be overcome by stronger depolarization such as trains of action potentials (Brody and Yue, 2000). This fast, direct Gβγ-inhibition is caused by $G_{i/o}$-coupled receptors such as the $GABA_B$-receptor (Cardozo and Bean, 1995). The Gβγ-inhibition is sensitive to Pertussis toxin (PTX), as PTX inhibits the necessary $G_{i/o}$ protein signaling (Zamponi and Currie, 2013).

In contrast to the fast Gβγ voltage-dependent inhibition, there is a second slower form of inhibition, which is voltage-independent. The mechanisms for this form of inhibition of VGCCs depend on several intracellular signaling pathways. Several $G_q$-coupled receptors like muscarinic and metabotropic glutamate receptors inhibit VGCCs in this manner (Bernheim et al., 1991, Takahashi et al., 1996).

In addition to the two forms of inhibition described above, direct protein interactions of GPCRs with VGCCs might change their signaling and/or expression levels on the plasma membrane. Examples for this type of modulation are that metabotropic glutamate receptors regulate CaV2.1 responses (Kitano et al., 2003) or that nociception receptors change internalization and expression levels of N-type calcium channels (Altier et al., 2006, Evans et al., 2010).

In this chapter, I demonstrate that the $GABA_B$ auxiliary subunit KCTD16 directly binds to CaV2.2 and describe relevant binding sites for this protein-protein interaction. Furthermore, I confirm the interactions between the $GABA_B$ receptor and N-type VGCCs as well as syntaxin-1 in mouse brains. The described protein CaV2.2-KCTD16 interaction has important electrophysiological effects on N-type VGCCs.

## 2.2 Materials and Methods

**Expression plasmids**

pCI-Myc-KCTD constructs (myc-KCTD12, myc-KCTD16, myc-KCTD8, myc-KCTD16ΔH2, myc-KCTD16H1H2, myc-KCTD16H2, myc-KCTD12-16H2) were described earlier (Seddik et al., 2012).

The pCDNA3-CaVβ1b and pCDNA3-CaV2.2 plasmids were gifts from Linda Haugaard-Kedstrom.

pCI-GFP-I-II-Flag was made by standard PCR cloning. First, CaV2.2 loop I-II was amplified with a C-terminally Flag tag peptide flanked by the restriction sites MluI on the N-terminus and XmaI on the C-term. This fragment was subcloned into an empty pCI expression vector. Afterwards, EGFP was amplified flanked by EcoRI and MluI and ligated into pCI-I-II-Flag to give rise to pCI-GFP-I-II-Flag.

**Cell culture**

COS-1 cells were maintained in DMEM (Life Technologies, CA, US) + 10% FCS (GE Healthcare, Buckinghamshire, UK) in a cell culture incubator set to 37°C with 5% $CO_2$. A stably transfected CHO-CaV2.2 cell line (CHO N-VGCC) was provided by B. Fakler (Universität Freiburg). CHO N-VGCC were maintained in MEM Alpha (Gibco, 2271-020) + 10% FCS (GE Healthcare, Buckinghamshire, UK) supplemented with 700µg/ml G418 (Geneticin), 250µg/ml Hygromycin B, and 5µg/ml Blasticidin.

Cells were split twice a week for regular cultivation.

Cell transfection was done using Lipofectamine 2000 (Life Technologies) according to the manufacturer's protocol. DNA amounts were equalized by empty pCI Vector DNA (Promega, WI, US).

**Co-immunoprecipitation and Western Blot**

Between 24 and 48 hours after transfection, COS-1 or CHO N-VGCC cells were washed in ice-cold PBS and lysed in NETN buffer (100mM NaCl, 20 mM Tris, 1mm EDTA, 0.5% NP40, pH 7.4) supplemented with complete protease inhibitors (Roche, Basel, Switzerland). Lysates were then used for Western Blot (Input) or immunoprecipitations. Immunoprecipitations were done using magnetic Protein G beads (Dynabeads, 10004D, Life Technologies) according to the manufacturer's protocol. Briefly, lysates and antibody coupled to beads were incubated for 10min at room temperature, beads were washed four times with NETN buffer and eluted with 1x Lämmli Buffer. Input and IPs were resolved with standard SDS-PAGE on 6-12% acrylamide gels.

**Antibodies list**

| Name | Host | Company | Product Nr. | WB | IP |
|---|---|---|---|---|---|
| Anti-Flag M2 | mouse | Sigma | F1804 | - | 2µl |
| Anti-Flag | rabbit | Sigma | F7425 | 1:1'000 | - |
| Anti-myc, 9e10 | mouse | Santa Cruz | sc-40 | - | 5µl |
| Anti-myc | rabbit | Sigma | C3956 | 1:1'000 | - |
| Anti-CaV2.2 | rabbit | Millipore | AB5154 | 1:500 | - |
| Anti-CaVβ1 | rabbit | Abcam | ab28502 | 1:1'000 | - |
| Anti-GFP | Rabbit | Invitrogen | A-11122 | 1:1000 | - |

## 2.3. Results

### 2.3.1 The CaV2.2 α1 subunit specifically interacts with KCTD16 in absence of $GABA_B$

As both the $GABA_B$-receptor as well as the associated KCTDs have been identified to be part of the interactome of N-type voltage-gated calcium channels (Müller et al., 2010), it is of interest whether the KCTD proteins are able to directly bind to CaV2.2 channel complexes themselves. To test KCTD-binding to the CaV2.2 in absence of the $GABA_B$ receptor, I carried out co-immunoprecipitation experiments in a CHO cell line stably expressing CaV2.2, CaVβ- and CaVα2δ-subunits (CHO N-VGCC). The results show that the CaV2.2 α1 subunit specifically binds to KCTD16 (Fig. 12A). On the other hand, KCTD12 and KCTD8 did not show significant CaV2.2-binding under these conditions. In another set of experiments done in transfected COS-1 cells, this specific CaV2.2-KCTD16 interaction was confirmed (Fig. 12B). In these experiments, only CaV2.2 and CaVβ1b were co-transfected with the KCTDs. Therefore, the requirement of CaVα2δ subunits for the CaV2.2-KCTD16 interaction can be excluded on the basis of these experiments. Next, I tested the requirement of the CaVβ1b subunit for the CaV2.2-KCTD16 interaction in transfected COS-1 cells. In these co-immunoprecipitation experiments, I found that the isolated CaV2.2 α1 subunit was sufficient for the interaction with KCTD16 (Fig. 12C). This suggests that KCTD16 could act as a molecular linker between the $GABA_B$ receptor and N-type VGCCs (see 2.4).

### 2.3.2 KCTD16 does not interact with the β subunit of voltage-gated calcium channels

Voltage-gated calcium channels are consisting of three principal subunits: a channel-forming α1 subunit, a CaVβ subunit and a CaVα2δ subunit. So far, I found the specific interaction of KCTD16 with CaV2.2, which is the α1 subunit of N-type VGCCs. It is interesting to know whether KCTD16 binds to other subunits of VGCCs as well. A priori, the α2δ subunit is not very likely to bind to KCTD16, as α2δ only has a small intracellular portion. Therefore, I checked for a possible interaction of KCTD16 with the CaVβ subunit. To test binding of KCTD16 to the VGCC β subunit, co-immunoprecipitation experiments in COS-1 cells were conducted (Fig. 12D). The obtained results indicate that neither KCTD16 nor KCTD12 directly bind to the CaVβ1b subunit. Although I only tested CaVβ1b, it is likely that KCTD16 does not directly bind to CaVβ subunits (see 2.4).

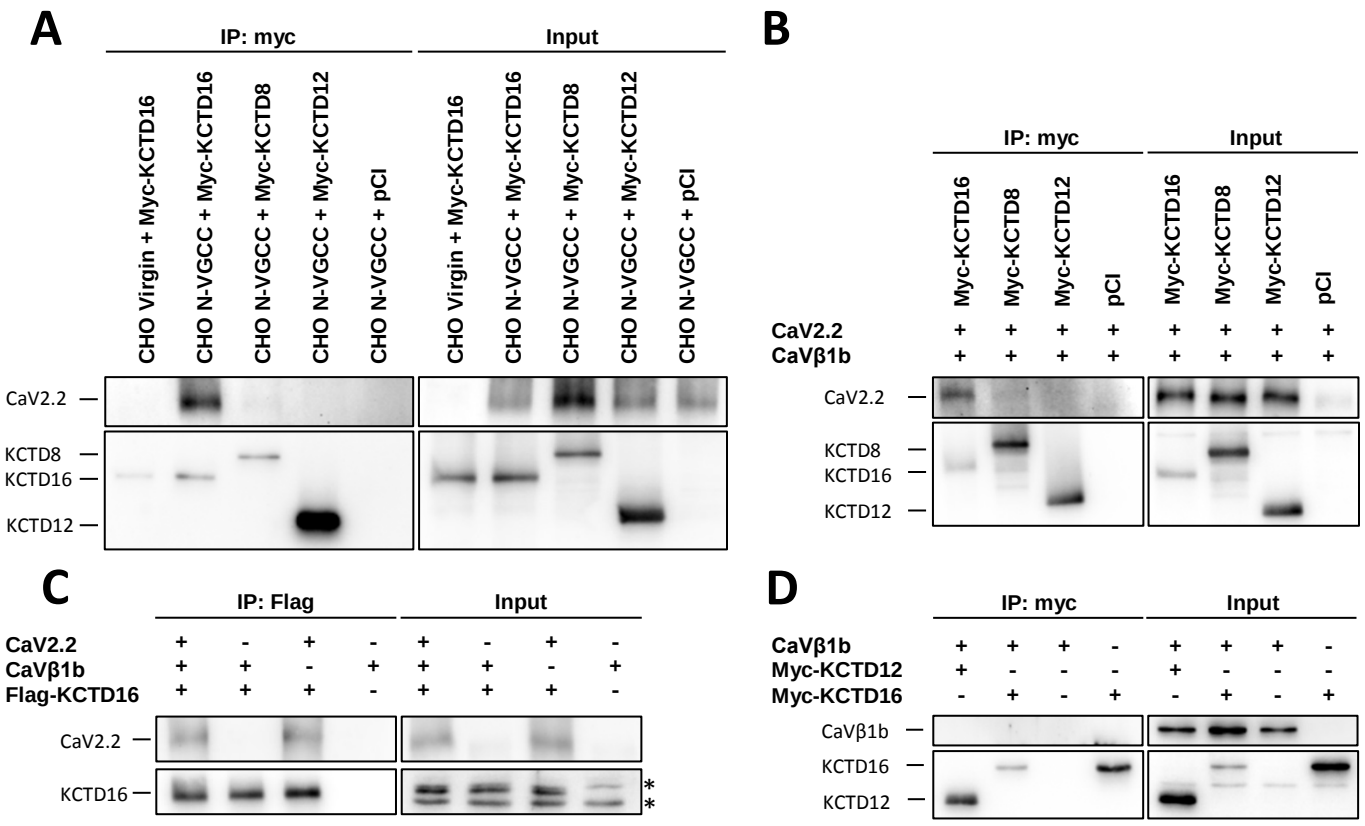


**Figure 12. The CaV2.2 α1 subunit specifically binds to KCTD16.**

(A) Co-immunoprecipitation experiments using transfected CHO N-VGCC cells. The CaV2.2 channel complex specifically binds to KCTD16. (B) Co-immunoprecipitation experiments using transfected COS-1 cells. KCTD16 binds to CaV2.2 in the presence of CaVβ1b. (C) Co-immunoprecipitation experiments using transfected COS-1 cells. KCTD16 also binds to the isolated CaV2.2 α1 subunit; therefore the presence of the CaVβ1b subunit is not required for the CaV2.2-KCTD16 interaction. Asterisks indicate non-specific bands in the input. Note that there are two non-specific bands in the KCTD16 input, the higher one of them is overlapping with the specific band of KCTD16. (D) Co-immunoprecipitation experiments using transfected COS-1 cells. Neither KCTD16 nor KCTD12 bind to the isolated CaVβ1b subunit.

### 2.3.3 The H2 domain of KCTD16 is important for the CaV2.2-KCTD16 interaction

In order to identify the KCTD16 domain involved in the interaction with CaV2.2, I expressed different KCTD constructs in CHO N-VGCC cells and carried out co-immunoprecipitation experiments (Fig. 13A+B). I found that full length KCTD16 bound strongest to CaV2.2, while KCTD12 was completely unable to bind. The deletion of the H2 domain of KCTD16 dramatically diminished the binding. The 16H1H2 construct, consisting of the H1 and H2 domains of KCTD16, was found to be the minimal construct capable of binding to CaV2.2. Interestingly, CaV2.2-binding can be transferred to KCTD12 by fusing the H2 domain of KCTD16 to KCTD12. As the H1 domain in this chimeric construct stems from KCTD12, which alone is unable to bind to CaV2.2, this emphasizes the importance of the H2 domain of KCTD16 for CaV2.2-binding. However, the isolated H2 domain of KCTD16 was not sufficient on its own. The reason for the requirement of an H1 domain could be that the isolated H2 domain is weakly expressed and possibly not properly folded.

### 2.3.4 The intracellular loop I-II of CaV2.2 is sufficient to co-precipitate KCTD16

The results gathered so far are consistent with the hypothesis that KCTD16 directly binds to the pore-forming CaV2.2 α1 subunit. Gβγ is known to inhibit VGCCs by binding to several sites on the α1 subunit. A major binding site for Gβγ on CaV2.2 is found on the intracellular loop I-II (Herlitze et al., 1997). As KCTD16 is binding to the Gβγ heterodimer (Turecek et al., 2014), the possibility that KCTD16 interacts with Gβγ at the intracellular loop I-II and thereby change CaV2.2 channel currents is an attractive hypothesis. To check whether KCTD16 interacts with the intracellular loop I-II of CaV2.2, I tagged the intracellular loop I-II with GFP at the N-terminus and with Flag at the C-terminus and performed co-immunoprecipitations in COS-1 cells. I found that the GFP-I-II-Flag construct was able to specifically co-precipitate KCTD16 (Fig. 13D). These results suggest a direct protein-protein interaction between KCTD16 and the intracellular loop I-II, as there are no endogenous VGCC subunits expressed in COS-1 cells (Harry et al., 2004).

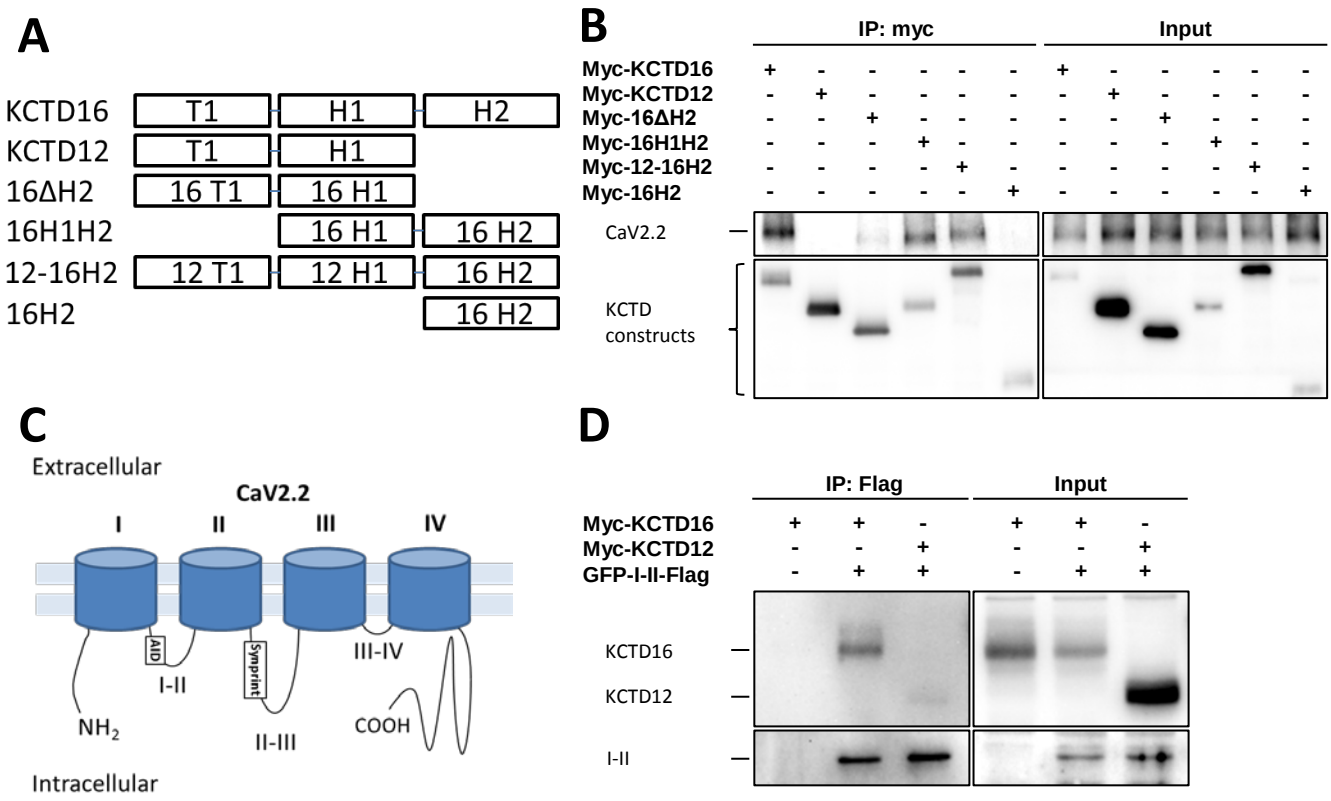


**Figure 13. Characterization of the CaV2.2-KCTD16 interaction.**

(A) Scheme of the KCTD constructs used for domain mapping of the CaV2.2 interaction site on KCTD16. (B) Co-immunoprecipitation experiments with transfected CHO N-VGCC cells using the KCTD constructs depicted in (A). The 16H1H2 construct was found to be the minimal deletion construct to bind to CaV2.2, as the isolated H2 domain was not sufficient. CaV2.2-binding could be transferred to KCTD12 by fusing the H2 domain of KCTD16 to KCTD12 (12-16H2). This highlights the importance of the H2 domain for the interaction with CaV2.2. (C) Diagram of the protein domains of CaV2.2. CaV2.2 consists of four large transmembrane domains connected by intracellular loops. The intracellular loop I-II contains the alpha interaction domain (AID), which interacts with the CaVβ subunits, and also binds to Gβγ. The intracellular loop II-III features the Synprint domain for interacting with several synaptic proteins. (D) Co-immunoprecipitation experiments with transfected COS-1 cells. The intracellular loop I-II of CaV2.2 is sufficient to co-precipitate KCTD16.

### 2.3.5 $GABA_B$ associates with N-type calcium channels and syntaxin-1 in mouse brain tissue

Presynaptic N-type channels are coupled to both $GABA_B$ receptors and the neurotransmitter release machinery. For this reason, I decided to study whether endogenous $GABA_B$ receptors are found in complex with CaV2.2 and syntaxin-1 in mouse brain tissue. To test this, I performed co-immunoprecipitations using mouse brain membrane preparations. By immunoprecipitating with an anti-$GABA_{B1}$-specific antibody, both CaV2.2 and syntaxin-1 were confirmed as part of $GABA_B$ receptor complexes (Fig. 14). The results of these experiments are already published, as Figure S9 in (Vertkin et al., 2015), also see appendix for this publication.

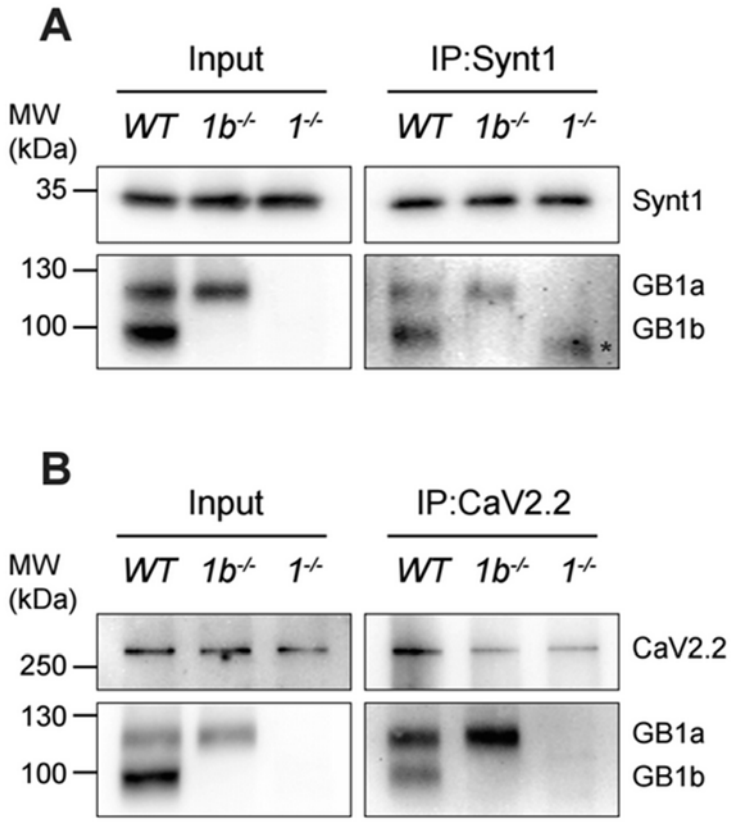


**Figure 14. Endogenous $GABA_B$ receptors co-immunoprecipitate with syntaxin-1 and CaV2.2.**
(A-B) Solubilized brain membranes from WT, 1b-/- and 1-/- mice were immunoprecipitated (IP) with anti-syntaxin-1 (A) and anti-CaV2.2 (B) antibodies and analyzed by western blotting with the indicated antibodies. Of note, the anti-GB1 antibody recognizes the common C-terminus of GB1a and GB1b. Asterisk indicates a cross-reacting band visible after the long exposure required for detection of $GABA_B$ receptors in anti-syntaxin-1 IPs. Left panels show input brain membranes used for immunoprecipitation. MW, molecular weight.

### 2.3.6 Electrophysiological effects of KCTD16 on N-type VGCCs

To understand the physiological relevance of the CaV2.2-KCTD16 interaction, patch-clamp recordings were performed using transfected CHO N-VGCC cells (R. Turecek). These recordings of calcium currents were carried out under blockade of potassium currents and chelation of intracellular calcium by EGTA, to isolate specific calcium currents from N-type VGCCs.

Co-expression of KCTD16 showed a number of effects on the activation of N-type VGCCs. As shown in Fig. 15A-C, KCTD16 shifted the voltage-dependence of N-type VGCCs to more hyperpolarized potentials by about 10mV. Furthermore, KCTD16 strongly increased and accelerated calcium currents in these recordings. This shift in voltage-dependence of N-type VGCCs is clearly KCTD16-specific, as KCTD12 did not similarly alter activation potentials, as shown in Fig. 15D. Furthermore, the effect of KCTD16 on activation of N-type VGCCs persists in the presence of $GABA_B$ receptors (Fig. 15D).

Previously, I found that the intracellular loop I-II of CaV2.2 binds to KCTD16 (see Fig. 13D). To test whether the effect of KCTD16 on N-type VGCCs can be inhibited by co-expression of this intracellular loop construct, patch-clamp recordings were done of CHO N-VGCC cells transfected with different constructs. As was observed before, KCTD16 shifted the activation of N-ype VGCCs to more hyperpolarized potentials. Interestingly, co-expression of the GFP-I-II-Flag construct was able to completely block this KCTD16-induced shift in voltage-dependence (Fig. 15E), whereas transfection of GFP-I-II-Flag alone did not significantly change voltage-dependence. As shown in Fig. 15F, transfection of GFP-I-II-Flag per se did not significantly alter conductance density of these cells compared to the control condition without KCTDs, suggesting that it does not measurably change the expression of N-type VGCCs. These data support my previous finding that KCTD16 interacts with the intracellular loop I-II of CaV2.2 and suggest that this direct interaction changes important physiological parameters of N-type VGCCs such as voltage-dependence and current amplitudes.

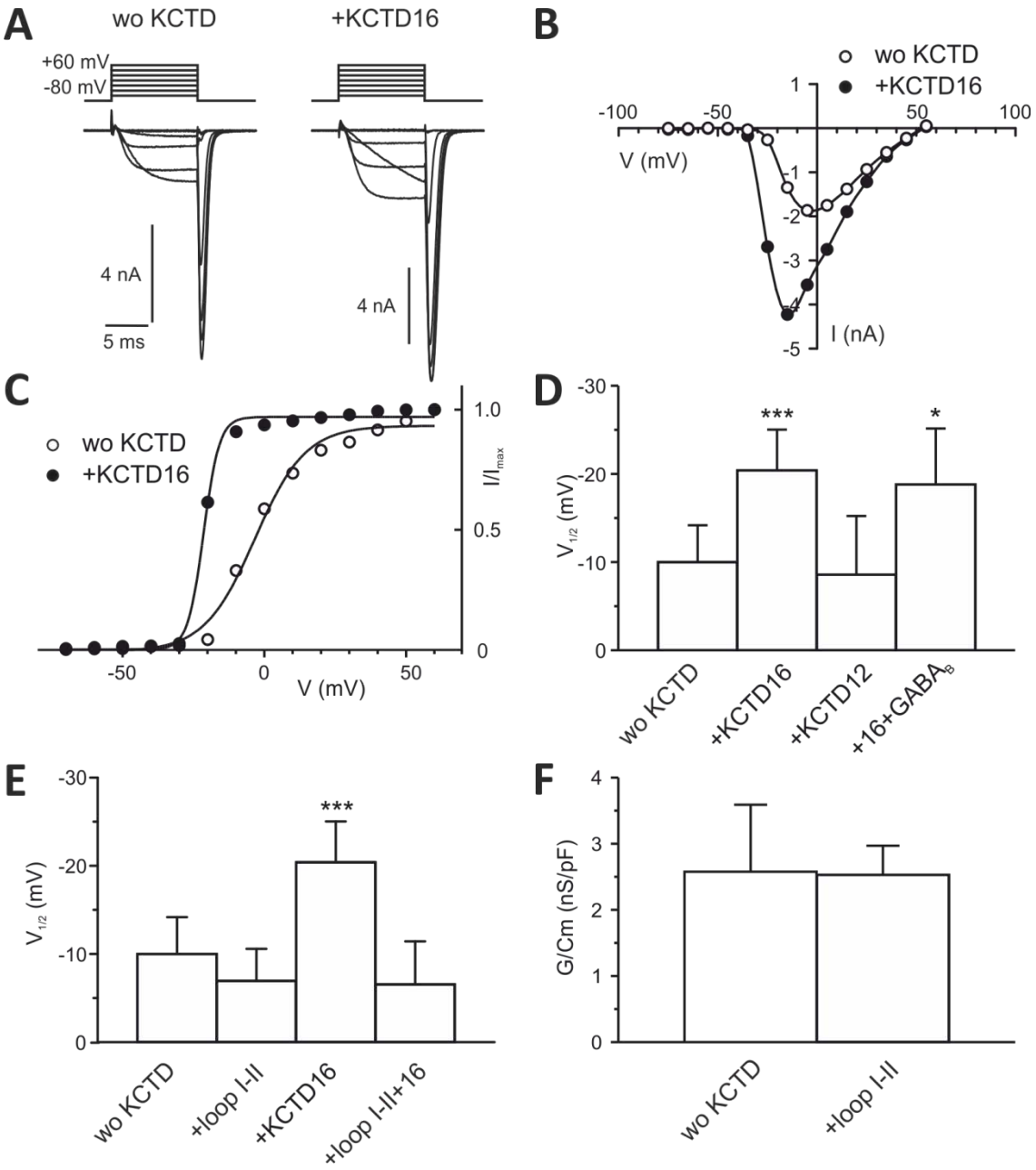


**Figure 15. KCTD16 shifts voltage-dependence of N-type VGCCs to more hyperpolarized potentials.**
(A) Traces of N-type calcium currents evoked by voltage steps from -80 to +60mV in 20mV increments. Recordings were done with CHO N-VGCC cells transfected with or without KCTD16. (B) Current-voltage relationship of calcium currents shown in (A). KCTD16 shifts activation of N-type VGCCs to more hyperpolarized potentials and increases calcium currents. (C) Normalized calcium tail-current amplitudes fitted by Boltzmann equation. (D) KCTD16 significantly shifts activation of N-type calcium channels to more hyperpolarized potentials by about 10mV. KCTD12 does not show this effect. The KCTD16 effect persists in the presence of the $GABA_B$ receptor. (E) The KCTD16 effect on the activation of N-type calcium channels can be blocked by co-transfection of the intracellular loop I-II construct. Transfection of the intracellular loop I-II alone does not significantly affect activation of N-type VGCCs. (F) Transfection of the intracellular loop I-II also does not change conductance density. By courtesy of R. Turecek.

In conclusion, it was demonstrated that the $GABA_B$ auxiliary subunit KCTD16 directly binds to the pore-forming CaV2.2 subunit and the relevant binding sites for this protein-protein interaction were described. Furthermore, the interactions between the $GABA_B$ receptor and N-type VGCCs as well as syntaxin-1 were confirmed in mouse brain tissue. The described protein CaV2.2-KCTD16 interaction has important electrophysiological effects on N-type VGCCs, which can be blocked by co-expression of the KCTD16-binding intracellular loop I-II of CaV2.2.

## 2.4 Discussion

For some time, $GABA_B$ receptors are known to regulate N-type VGCCs through Gβγ inhibition (Cardozo and Bean, 1995). $GABA_B$ receptors as well as their associated KCTDs were shown to be part of the interactome of these channels (Müller et al., 2010). However, the precise biochemical interconnections and functions of these large protein complexes are not yet fully understood. First, I tested whether N-type VGCCs also bind to $GABA_B$-associated KCTDs in absence of $GABA_B$ receptors. In transfected CHO N-VGCC and COS-1 cells, CaV2.2 was found to only directly bind to KCTD16 (Fig. 12). This is in contrast to the available proteomics data of mouse brain tissue, where also KCTD12 and KCTD8 have been found to be associated with CaV2.2 (Müller et al., 2010). It has to be considered that the experiments presented here were done in recombinant systems, so this discrepancy can be explained either by heteromerization of these KCTDs or recruitment of $GABA_B$ complexes to CaV2.2 by additional molecular linkers in native tissue. Both of these possibilities are very plausible, as heteromerization of KCTDs is indeed occurring (T. Fritzius, personal communication) and given the existence of multiple mutual interaction partners of both CaV2.2 and $GABA_B$ receptors such as Gβγ, SNARE proteins, 14-3-3 proteins etc. (Müller et al., 2010). For this reason, I chose to use a recombinant system, where the advantage was to have isolated components, in order to test the specificity of KCTD16-CaV2.2 direct interaction.

I found that the pore-forming CaV2.2 α1 subunit specifically binds to KCTD16. Of course, this does not exclude other VGCC subunits binding to KCTD16 as well. The predominantly transmembrane and extracellular CaVα2δ and CaVγ subunits are unlikely to interact with KCTD16 because of their different intracellular locations. I showed that KCTD16 was unable to bind to the isolated CaVβ1 subunit (Fig. 12D). Of note, there is a high amino acid identity of more than 60% between different CaVβ subunits (Stephens and Mochida, 2013) and CaVβ subunits are promiscuous in their binding to CaVα1 subunits. In electrophysiological recordings of hippocampal neurons, KCTD16 specifically altered N-type VGCC currents, as observed by a pharmacological blocking of N-type channels by ω-Conotoxin-GVIA (R. Turecek, personal communication). If KCTD16 directly interacted with CaVβ subunits, one would expect to see similar electrophysiological changes for several types of HVA channels as well, because of promiscuous CaVβ-CaVα1 associations. On these grounds, I argue that KCTD16 do not interact via CaVβ subunits. Similarly to KCTD16, KCTD12 was also unable to bind to CaVβ1b (Fig. 12D). This finding is interesting, as SNPs for both KCTD12 and CaVβ2 have been identified in a bipolar I disorder genome-wide association study (Lee et al., 2011). CaVβ1b and CaVβ2 are highly similar (Stephens and Mochida, 2013), thus these results tentatively suggest that KCTD12 might not directly bind to CaVβ2. Even in the absence of direct protein-protein interactions with CaVβ subunits, KCTD12 potentially regulates VGCC-

signaling, e.g. by heteromerizing with KCTD16 or by generally interfering with Gβγ-signaling (Turecek et al., 2014).

Furthermore, I have demonstrated the importance of the C-terminal H2 domain of KCTD16 for CaV2.2-binding. This is reminiscent of the HCN2-binding to KCTD16, where deletion of the C-terminus of KCTD16 was shown to abolish the molecular interaction between the HCN2 channel and KCTD16 (Schwenk et al., 2016). Similarly, the H2 domains of KCTD16 and KCTD8 were shown to be required for Cullin 3-binding in the first chapter of this thesis. Of note, KCTD16 is binding to $GABA_{B2}$ by its N-terminal T1 domain. Therefore, KCTD16 is most likely able to bind both the CaV2.2 channel and the $GABA_B$ receptor simultaneously. KCTD16 might therefore act as a molecular linker that couples the $GABA_B$ receptor to the N-type VGCCs. The direct KCTD16-CaV2.2 protein-protein interaction reflects the importance of presynaptic release regulation, physically linking $GABA_B$ receptors to N-type calcium channel complexes. A major function of this interaction is the modulation of biophysical properties of N-type calcium channels, also in a $GABA_B$-activity-dependent way (see discussion below). For quite some time, the $GABA_B$ receptor and other GPCRs have been known to modulate N-type VGCCs. One well established pathway of GPCR-mediated modulation of VGCCs activity consists of Gβγ inhibition through multiple binding sites on presynaptic CaVα1 subunits (Herlitze et al., 1997, Zamponi et al., 1997, Cantí et al., 1999, Li et al., 2004).

The finding that the intracellular loop I-II is able to co-precipitate KCTD16 is interesting, as this site is known to bind to Gβγ as well as to CaVβ subunits. It is known that KCTD16 also interacts with the Gβγ heterodimer (Turecek et al., 2014). This raises the intriguing possibility that KCTD16 changes Gβγ-mediated inhibition of N-type calcium channels by directly interfering with the Gβγ heterodimer. For other effector channels of $GABA_B$ receptors like GIRK and HCN2 channels, it is known that KCTDs play a role in $GABA_B$-mediated effector responses. In the case of GIRK channels, KCTD12 desensitizes channel responses by competing with the released Gβγ heterodimer (Turecek et al., 2014).

Finally, I confirmed the biochemical associations of the $GABA_B$ receptor with both N-type VGCCs and syntaxin-1 by co-immunoprecipitations in mouse brain membranes (Vertkin et al., 2015). Both protein interactions have been previously identified in a large-scale proteomics study (Müller et al., 2010). However, this is the first biochemical study showing that $GABA_B$ receptors are physically linked to both presynaptic VGCCs and the presynaptic vesicle release machinery. My results suggest that KCTD16 could act as a molecular linker that precouples $GABA_B$ receptors, which are bound to KCTD16 through its T1 domain, to N-type VGCCs.

Currently, an electrophysiological characterization of the CaV2.2-KCTD16 interaction is ongoing. So far, the physiological relevance of the interaction was tested by electrophysiological recordings of CHO N-VGCC cells transfected with KCTD16, where the following observations were made (R. Turecek, personal communication). KCTD16 was found to change the biophysical properties of N-type channels in several ways in the absence of $GABA_B$ receptors. First, KCTD16 shifts the voltage-dependence of N-type VGCCs to more hyperpolarized potentials (by about 10 mV). Second, KCTD16 also increases permeability for divalent cations in these channels. Third, KCTD16 accelerates the kinetics of N-type VGCC activation. Fourth, KCTD16 decreases sensitivity of N-type channels to and decelerates the kinetics of $GABA_B$-mediated inhibition.

Interestingly, the KCTD16 effect on N-type calcium channels could be blocked by co-expression of the intracellular loop I-II of CaV2.2 (Fig. 15E), confirming that this loop is a relevant binding site for KCTD16. This short intracellular loop I-II of around 130 amino acids contains several different regulation sites such as a Gβγ-site, the AID as well as phosphorylation sites. A further dissection of the KCTD16-binding site could provide valuable additional information on the mechanism of the KCTD16-modulation of N-type VGCCs.

The same modulation by KCTD16 was also observed for native neuronal N-type channels in hippocampal neurons. This modulation was demonstrated to be N-type specific using pharmacological inhibition of N-type currents, as hippocampal neurons also express different types of VGCC, such as P/Q-type or L-type channels. As both P/Q-type and N-type VGCCs are implicated in the same biological context of presynaptic neurotransmitter release, it remained an open possibility whether KCTD16 binds to other CaVα1 subunits than CaV2.2, as $GABA_B$ receptors were also shown to be slightly enriched in CaV2.1 (Müller et al., 2010). However, based on these observations, this seems not to be the case.

The underlying molecular mechanism for the KCTD16 effects on N-type currents is unknown. It could be mediated by the direct interactions of KCTD16 with the intracellular linker I-II and/or Gβγ. Of note, all effects of KCTD16 on the channel are similar (or synergistic?) to CaVβ-mediated effects, therefore another possibility is that KCTD16 enhances CaV2.2-CaVβ interactions. As mentioned, CaVβ does not seem to be the direct binding partner of KCTD16, as suggested by my co-IP results (Fig. 12D) and by the specificity of KCTD16 effects for N-type currents.

Together, these studies shed light on presynaptic regulation by $GABA_B$ receptors, not just through secondary effectors, but also by direct interaction with the presynaptic release machinery, leading to important implications in synaptic strength modulation and hence for learning and memory.

# Final Conclusions

The prevalent inhibitory neurotransmitter gamma-aminobutyric acid (GABA) acts through the ionotropic $GABA_A$ and the metabotropic $GABA_B$ receptors. Functional $GABA_B$ receptors are $G_{i/o}$ protein-coupled receptors, consisting of an obligate heterodimer of $GABA_{B1}$ and $GABA_{B2}$ subunits (Kaupmann et al., 1998a). Several aspects of $GABA_B$ signaling could not be explained by these two principal subunits alone. A few years ago, a new source of molecular diversity for $GABA_B$ receptors was found with the discovery that the members of a subfamily of KCTDs, consisting of KCTD8, KCTD12, KCTD12b and KCTD16, constitute auxiliary subunits of these receptors (Schwenk et al., 2010).

The aim of this thesis was to study some of the roles that KCTDs play in $GABA_B$ signaling, especially in regard to the interconnection of $GABA_B$ receptors to other downstream signaling complexes. Being intracellular molecules binding to the $GABA_{B2}$ subunit as well as to the heterotrimeric G proteins (Schwenk et al., 2010, Turecek et al., 2014), these KCTDs seem ideally suited to function as scaffold molecules connecting the $GABA_B$ receptor core complex to effector and signaling complexes, thereby enabling or enlarging the functional consequences of $GABA_B$ receptors in neurons.

In conclusion, the results of this thesis corroborate the concept that KCTD16 and KCTD8 extend the connectivity of $GABA_B$ receptors to both classical and non-classical effector and regulatory systems by acting as molecular linkers. In this work, I described two of these directly KCTD16/8-associated protein complexes: chapter one describes the biochemical connection of KCTD16 and KCTD8 with the Cullin 3-RING E3 ligase (CRL3) system, while chapter two is concerned with the KCTD16 interaction with N-type voltage-gated calcium channels.

The results of chapter one are relevant in so far, as the biochemical connections of KCTD16 and KCTD8 to CRL3 are new. These interactions were not reported in published proteomic studies and the $GABA_B$-associated KCTDs were proposed to lack Cullin 3-binding properties, on the basis of limited experimental evidence with KCTD12 (Smaldone et al., 2015). Furthermore, the results show a novel Cullin 3-binding mechanism for KCTD8 and KCTD16 that is not relying on the canonical Cullin 3-binding BTB domain, unlike other substrate adaptors of CRL3 complexes (Furukawa et al., 2003, Genschik et al., 2013). This finding is not only relevant for the $GABA_B$ receptor-associated KCTDs, but might also expand the spectrum of possible Cullin 3 interactors beyond BTB family proteins, as the BTB domains of KCTD16 and KCTD8 were shown to be completely dispensable for their association with Cullin 3. Finally, I demonstrated that the CRL3 complex can be recruited to the $GABA_B$ receptor by KCTD16, suggesting that CRL3 potentially regulates $GABA_B$ receptors or secondary proteins bound in the $GABA_B$ complex through ubiquitination. Unlike with KCTD16, a CRL3-recruitment to $GABA_B$ receptors via KCTD8 could not be

demonstrated with my experiments and two alternatives may explain this finding. The first explanation is a technical one, as the weaker affinity of KCTD8 for Cullin 3 and the expectedly low signal for indirect co-IPs could explain this finding and more sensitive techniques might find these complexes. Second, the possibility that the KCTD16-CRL3 and the KCTD8-CRL3 interactions have functions independently of $GABA_B$ receptors cannot be completely excluded with the data at hand. In this context, it is worth mentioning that the largest fractions of KCTD12 and KCTD16 are co-migrating with $GABA_B$ receptors in native gels of brain tissue suggesting close assembly of the KCTDs with $GABA_B$ receptors in the brain (Schwenk et al., 2010, Turecek et al., 2014). However, these KCTDs are also expressed in other tissues than the brain (Metz et al., 2011), so $GABA_B$-independent functions of KCTDs remain possible in other tissues.

On the other hand, N-type VGCCs are classical effectors of $GABA_B$ receptors and the results of chapter two of this thesis refine understanding of $GABA_B$ signaling with respect to these presynaptic channels crucial for presynaptic regulation of neurotransmission. The Gβγ-inhibition of N-type calcium channels by $GABA_B$ receptors was known for quite some time. Here, I present data that KCTD16 is directly binding to CaV2.2, which represents the pore-forming α1 subunit of N-type VGCCs. Therefore, $GABA_B$ receptors are not solely coupled to CaV2.2 through Gβγ-signaling but also by a direct biochemical assembly via the auxiliary subunit KCTD16. Furthermore, KCTD16 is shown to associate with the intracellular loop I-II of CaV2.2. Interestingly, this important regulatory loop also features the CaVβ- and Gβγ-binding sites, thus this interaction is functionally relevant. The physiological relevance of this protein-protein interaction was further established, as an electrophysiological characterization of the CaV2.2-KCTD16 association showed diverse effects on N-type VGCC currents. Finally, the protein-protein interactions of $GABA_B$ receptors with CaV2.2 and the synaptic protein syntaxin-1 were confirmed in mouse brain tissue, demonstrating that $GABA_B$ receptors are indeed part of the CaV2.2 complex. This last finding is already published (Vertkin et al., 2015).

Interestingly, for all the protein-protein interactions studied in this thesis, the H2 domains of KCTD16 or KCTD8 were identified as the necessary molecular determinants. The H2 domain was previously shown to also have an inhibitory effect on KCTD-mediated desensitization of $GABA_B$ receptor signaling, the proposed mechanism for this was sterical hindrance (Seddik et al., 2012). A steric mechanism also makes sense in the light of the new findings, as protein-protein interactions through the H2 domain dramatically change the three-dimensional surroundings of the H1 domain, which is mediating the desensitization of $GABA_B$ receptors.

Of the KCTDs associated with the $GABA_B$ receptor, especially KCTD16 now emerges as an important hub for different connections of $GABA_B$ receptors to several different signaling complexes (as shown in Fig. 16), such as the hyperpolarization-activated cyclic nucleotide–gated cation 2 (HCN2) channels (Schwenk et al., 2016), two different 14-3-3 proteins (Schwenk et al., 2016), CRL3 complexes and N-type VGCCs. As mentioned, N-type VGCCs are classical effectors of $GABA_B$ receptors (Gassmann and Bettler, 2012), while HCN2 channels represent a new effector system (Schwenk et al., 2016). Cul3 and 14-3-3 proteins may mediate new regulatory mechanisms for $GABA_B$ receptors, perhaps important at specific steps in the life cycle of $GABA_B$, e.g. trafficking or endocytosis. These functional connections also depend on the specific cellular context of the individual receptor, e.g. the KCTD16-connection to N-type VGCCs is relevant for presynaptic release, while HCN2 channels are associated with $GABA_B$ receptors in dopaminergic neurons of the ventral tegmental area (Schwenk et al., 2016).

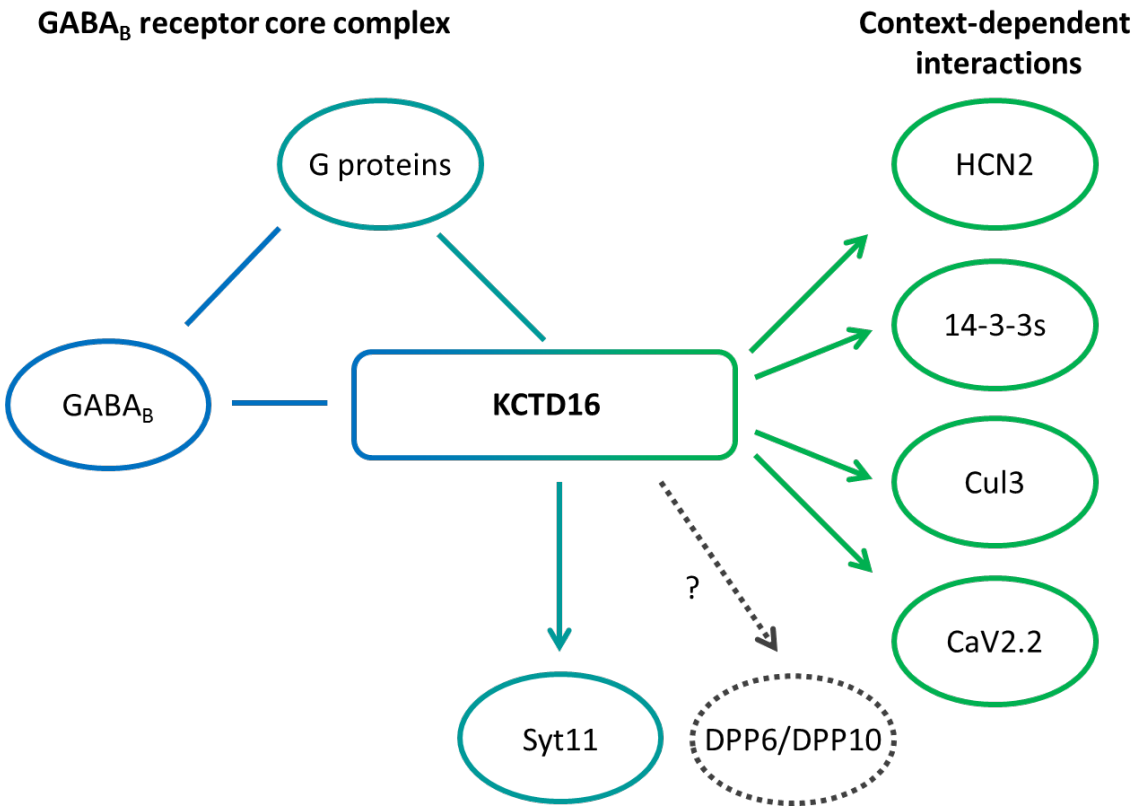


**Figure 16. KCTD16 extends the connectivity of the $GABA_B$ receptor complex to different regulation and effector systems.** The core $GABA_B$ receptor complex (consisting of the $GABA_B$ heterodimer and heterotrimeric G proteins) binds to the T1 and H1 domains of KCTD16, while the C-terminal H2 domain of KCTD16 is necessary for further connectivity to effector systems such as HCN2 or CaV2.2 channels or other regulators like 14-3-3 proteins or the CRL3 system. Other protein-protein interactions of KCTD16 remain to be further studied, one of them is synaptotagmin 11 (Syt11). A role for KCTDs in the connection to DPP was proposed, but remains to be clarified (Schwenk et al., 2016).

In contrast to KCTD16, KCTD12 does not exhibit a similar scaffolding function and its main functions likely remain mediating the desensitization of $GABA_B$ receptor responses through the interaction with Gβγ and upregulation of surface $GABA_B$ levels (Schwenk et al., 2010, Ivankova et al., 2013, Turecek et al., 2014, Booker et al., 2016).

Regarding the scaffolding function, KCTD8 can be seen as a functional intermediate between KCTD12 and KCTD16, as KCTD8 possesses some of the linker functions that were shown for KCTD16. For example in this work, it was demonstrated that KCTD8 associates with CRL3 complexes, albeit with a weaker affinity than KCTD16. However, some of the protein-protein interactions are KCTD16-specific and are not found with KCTD8, as seems to be the case for HCN2 channels (Schwenk et al., 2016) and for N-type VGCCs, as shown in this study. These functional differences likely stem from amino acid differences in the H2 domains of KCTD16 and KCTD8. Of note, expression of KCTD16 is more widespread in the brain compared to KCTD8 (Metz et al., 2011), suggesting that the scaffolding functions for $GABA_B$ receptor complexes *in vivo* is mostly conferred by KCTD16 rather than KCTD8.

It has to be emphasized that an individual $GABA_B$ receptor-heterodimer may not exclusively incorporate only one specific KCTD subunit at a given time, as KCTD proteins generally form oligomers (Skoblov et al., 2013) and the $GABA_B$-associated KCTDs are also able to form heteromers among themselves (T. Fritzius, personal communication). Therefore, $GABA_B$ receptors can be associated with several different KCTD subunits simultaneously, which greatly increases the possible molecular diversity of native $GABA_B$ receptors. The repertoire of available $GABA_B$ receptors in specific neurons is determined by the brain expression patterns of the different KCTD auxiliary subunits (Metz et al., 2011). KCTD16 and KCTD12 are endogenously co-expressed in several brain areas, notably in pyramidal neurons and dentate granule cells of the hippocampus suggesting $GABA_B$ receptors may form complexes with KCTD16/12-heterodimers in these areas (Metz et al., 2011). On the other hand, KCTD12, KCTD12b and KCTD8 are co-expressed together in the medial habenula (Metz et al., 2011). In contrast, cells in the cerebellum probably express only one KCTD subunit at the time, thereby forming $GABA_B$ receptors containing KCTD homomers (Metz et al., 2011).

Interestingly, additional proteins are recruited to $GABA_B$ receptors by linkage through KCTD16 or KCTD8. One of them is synaptotagmin 11 (Syt11), which was found in the interactome of $GABA_B$ receptors and specifically enriched in $GABA_B$- and KCTD16-specific affinity purifications (Schwenk et al., 2016). Recently, the KCTD16-Syt11 interaction was confirmed in co-immunoprecipitation experiments (Y. Tan, personal communication). This might be relevant for presynaptic function, as other members of the synaptotagmin protein family are crucial for synaptic release (Südhof, 2014). Conceivably, $GABA_B$

receptors, KCTD16, Syt11 and N-type VGCCs all form a large protein complex. In this putative complex, KCTD16 recruits both Syt11 and N-type-VGCCs simultaneously to the $GABA_B$ receptor. The precise role of Syt11 in such a complex is not clear a priori, as not much is known about its function. Given the low calcium-affinity of Syt11 (von Poser et al., 1997), a calcium sensor function similar to what was demonstrated for other synaptotagmins is rather unlikely, but cannot be excluded completely, because physical proximity of Syt11 and N-type VGCCs might still enable calcium sensing. However, in contrast to other synaptotagmin proteins, Syt11 was recently demonstrated to be an inhibitor of clathrin-mediated and bulk endocytosis and to have no effect on exocytosis (Wang et al., 2016). Based on this novel finding, Wang et al. argue that Syt11 plays an important role in the recycling of synaptic vesicles in neurons.

For these reasons, Syt11 should be especially important in sustained synaptic neurotransmission, as the recycling of synaptic vesicles is becoming more relevant in phases of heightened neuronal activity. Through a connection to Syt11, $GABA_B$ receptors might be able to disinhibit vesicle endocytosis, in addition to the known inhibitory effect on presynaptic vesicle release through Gβγ inhibition of N-type VGCCs (Zamponi and Currie, 2013).

The results from a recent proteomics study also point towards interactions of the dipeptidyl peptidases 6 and 10 (DPP6, DPP10) with the $GABA_B$ receptor, a role for KCTDs in these connections was suggested but has still to be clarified (Schwenk et al., 2016). DPP6 and DPP10 are reported to be relevant for modulation of potassium channels, but do not seem to possess any peptidase activity despite exhibiting homologies to other peptidases (Nadal et al., 2003, Jerng et al., 2005, Kaulin et al., 2009). At the moment, not much is known about the function of DPPs in $GABA_B$ signaling, so further studies are needed to elucidate the relevance of DPP6 and DPP10 for $GABA_B$ receptors.

In a broader perspective, $GABA_B$ receptors are not only connected to other signaling complexes through their auxiliary KCTD subunits, but also interact with a variety of other proteins through direct binding to the principal $GABA_B$ receptor complex, particularly to $GABA_{B1}$ or specific G proteins (Fig. 17). One category consists of transmembrane proteins such as the amyloid β A4 protein (APP), the amyloid-like protein 2 (APLP2) and the adherens junction-associated protein 1 (AJAP1) (Schwenk et al., 2016). These proteins mainly interact with the $GABA_B$ receptor through binding to the extracellular sushi domains of $GABA_{B1a}$ (Schwenk et al., 2016). Some of them likely have a function in axonal trafficking of $GABA_B$ receptors. Another category of interactors is composed by different proteins that directly interact with the intracellular C-terminus of $GABA_{B1}$. These proteins include regulatory proteins like 14-3-3 proteins (Couve et al., 2001, Brock et al., 2005), the capsaicin receptor TRPV1 (Hanack et al., 2015) as well as the synaptic protein syntaxin-1 (see Fig. 14). Other $GABA_B$ interactors such as regulator of G protein signaling

7 (RGS7) and the Gα inhibitory interacting protein GINIP directly bind and modulate G proteins (Fajardo-Serrano et al., 2013, Gaillard et al., 2014). Furthermore, there are several proteins in the $GABA_B$ interactome, for which the interactions with the $GABA_B$ receptor complex are poorly described at the moment. These include membrane proteins like the previously mentioned DPPs, the neuronal adhesion molecule neuroligin-3, the PILR-associating neural protein (PIANP), the integral membrane proteins (ITM2B/C) and endoplasmatic reticulum proteins such as Reticulocalbin 2 and Calnexin (Schwenk et al., 2016). The functional consequences of these protein-protein interactions will also have to be elucidated, in order to gain a more complete understanding of $GABA_B$ receptor physiology and signaling.

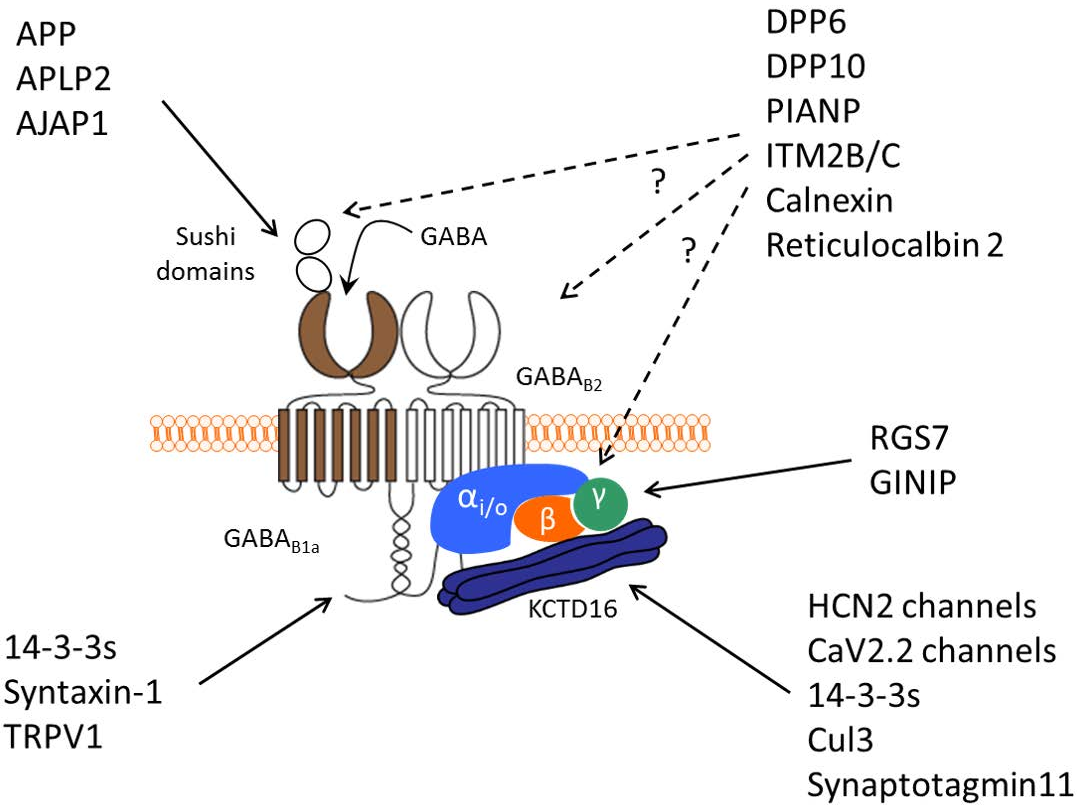


**Figure 17. Several constituents of the $GABA_B$ receptor complex mediate the biochemical connections to peripheral $GABA_B$ interactors.** KCTD16 serves as a scaffold for peripheral $GABA_B$ interactors such as HCN2 and CaV2.2 channels, Syt11, 14-3-3s and Cul3. Several proteins (APP, AJAP1, APLP2) specifically interact with the Sushi domains of $GABA_{B1a}$. Another group of proteins (14-3-3s, syntaxin-1, TRPV1) is binding to the intracellular C-terminus of the $GABA_{B1}$ subunit. Some interactors such as RGS7 and GINIP directly bind G proteins and modulate their signaling. Several interactions remain to be described in more detail (dashed lines).

So far, KCTD proteins have been implicated in several diverse biological processes. As might be anticipated given their possession of a potassium channel tetramerization domain, some KCTDs are known to play a role in the regulation of potassium ion channels, e.g. overexpression of the potassium channel regulatory protein (KCNRG) was shown to strongly inhibit potassium currents (Ivanov et al., 2003). KCNRG was also postulated as a cancer suppressor protein (Ivanov et al., 2003). However, not all KCTDs control potassium currents in this manner, as KCTD5 was shown not to affect potassium currents (Dementieva et al., 2009). KCTD1 was shown to be a regulator of transcription of AP-2α (Ding et al., 2009). KCTDs also control proliferation and apoptosis (Birerdinc et al., 2009), play roles in DNA replication (Zhou et al., 2005, Yang et al., 2009) and are essential for mitosis (Kittler et al., 2007). In agreement with KCTDs being substrate adaptors of CRL3 complexes, KCTD11 ubiquitinates and degrades HDAC1, thereby down-regulating hedgehog-signaling and suppressing tumors (Canettieri et al., 2010, Correale et al., 2011). Similarly, the KCTD subfamily of BACURDs regulate RhoA signaling by promoting ubiquitination and subsequent degradation of RhoA (Chen et al., 2009).

It will also be interesting to see whether GPCR-related functions solely exist for the subfamily of $GABA_B$ receptor-associated KCTDs or whether other members of the KCTDs family also associate with GPCRs. Interestingly, different KCTD proteins were identified in tandem affinity purifications of individual G proteins, KCTD5 was found to be associated with Gβ2 and likewise KCTD2 and KCTD5 interact with Gγ2 (Ahmed et al., 2010). Involvement in GPCR physiology was also found in proteins similar to the KCTDs. E.g. the Kelch-like protein 12 (KLHL12), which also belongs to the BTB protein superfamily, was found to be ubiquitinating and degrading dopamine D4 receptors, by functioning as a substrate adaptor for CRL3 complexes (Rondou et al., 2008).

In this work, the biological functions of the KCTD protein family are further extended, with the addition of important $GABA_B$ scaffolding functions to two downstream signaling complexes and the unexpected discovery of novel interactors of CRL3 complexes. This role for KCTDs opens a wide range of new regulation mechanisms for $GABA_B$ receptors as well as their linked signaling complexes. Furthermore, the results of this work have important implications for the modulation of presynaptic neurotransmission by $GABA_B$ receptors.

# References


Adelfinger L, Turecek R, Ivankova K, Jensen AA, Moss SJ, Gassmann M, Bettler B (2014) GABAB receptor phosphorylation regulates KCTD12-induced K+ current desensitization. Biochemical Pharmacology 91:369-379.

Ahmed SM, Daulat AM, Meunier A, Angers S (2010) G Protein βγ Subunits Regulate Cell Adhesion through Rap1a and Its Effector Radil. Journal of Biological Chemistry 285:6538-6551.

Altier C, Khosravani H, Evans RM, Hameed S, Peloquin JB, Vartian BA, Chen L, Beedle AM, Ferguson SSG, Mezghrani A, Dubel SJ, Bourinet E, McRory JE, Zamponi GW (2006) ORL1 receptor-mediated internalization of N-type calcium channels. Nat Neurosci 9:31-40.

Angelicheva D, Tournev I, Guergueltcheva V, Mihaylova V, Azmanov DN, Morar B, Radionova M, Smith SJ, Zlatareva D, Stevens JM, Kaneva R, Bojinova V, Carter K, Brown M, Jablensky A, Kalaydjieva L, Sander JW (2009) Partial epilepsy syndrome in a Gypsy family linked to 5q31.3-q32. Epilepsia 50:1679-1688.

Arikkath J, Campbell KP (2003) Auxiliary subunits: essential components of the voltage-gated calcium channel complex. Current Opinion in Neurobiology 13:298-307.

Azizieh R, Orduz D, Van Bogaert P, Bouschet T, Rodriguez W, Schiffmann S, Pirson I, Abramowicz M (2011) Progressive Myoclonic Epilepsy-Associated Gene KCTD7 is a Regulator of Potassium Conductance in Neurons. Mol Neurobiol 44:111-121.

Bayón Y, Trinidad AG, de la Puerta ML, del Carmen Rodríguez M, Bogetz J, Rojas A, De Pereda JM, Rahmouni S, Williams S, Matsuzawa S-i, Reed JC, Crespo MS, Mustelin T, Alonso A (2008) KCTD5, a putative substrate adaptor for cullin3 ubiquitin ligases. FEBS Journal 275:3900-3910.

Benes FM (2009) Amygdalocortical Circuitry in Schizophrenia: From Circuits to Molecules. Neuropsychopharmacology 35:239-257.

Bennett EJ, Rush J, Gygi SP, Harper JW (2010) Dynamics of Cullin-RING Ubiquitin Ligase Network Revealed by Systematic Quantitative Proteomics. Cell 143:951-965.

Berndsen CE, Wolberger C (2014) New insights into ubiquitin E3 ligase mechanism. Nat Struct Mol Biol 21:301-307.

Bernheim L, Beech DJ, Hille B (1991) A diffusible second messenger mediates one of the pathways coupling receptors to calcium channels in rat sympathetic neurons. Neuron 6:859-867.

Bettler B, Kaupmann K, Bowery N (1998) GABAB receptors: drugs meet clones. Current Opinion in Neurobiology 8:345-350.

Bettler B, Kaupmann K, Mosbacher J, Gassmann M (2004) Molecular Structure and Physiological Functions of GABAB Receptors. Physiological Reviews 84:835-867.

Biermann B, Ivankova-Susankova K, Bradaia A, Abdel Aziz S, Besseyrias V, Kapfhammer JP, Missler M, Gassmann M, Bettler B (2010) The Sushi Domains of GABAB Receptors Function as Axonal Targeting Signals. The Journal of Neuroscience 30:1385-1394.

Birerdinc A, Nohelty E, Marakhonov A, Manyam G, Panov I, Coon S, Nikitin E, Skoblov M, Chandhoke V, Baranova A (2009) Pro-apoptotic and antiproliferative activity of human KCNRG, a putative tumor suppressor in 13q14 region. Tumor Biology 31:33-45.

Booker SA, Althof D, Gross A, Loreth D, Müller J, Unger A, Fakler B, Varro A, Watanabe M, Gassmann M, Bettler B, Shigemoto R, Vida I, Kulik Á (2016) KCTD12 Auxiliary Proteins Modulate Kinetics of GABAB Receptor-Mediated Inhibition in Cholecystokinin-Containing Interneurons. Cerebral Cortex.

Bowery NG (1993) GABAB Receptor Pharmacology. Annual Review of Pharmacology and Toxicology 33:109-147.

Brock C, Boudier L, Maurel D, Blahos J, Pin J-P (2005) Assembly-dependent Surface Targeting of the Heterodimeric GABA(B) Receptor Is Controlled by COPI but Not 14-3-3. Molecular Biology of the Cell 16:5572-5578.

Brody DL, Yue DT (2000) Relief of G-Protein Inhibition of Calcium Channels and Short-Term Synaptic Facilitation in Cultured Hippocampal Neurons. The Journal of Neuroscience 20:889-898.

Canettieri G, Di Marcotullio L, Greco A, Coni S, Antonucci L, Infante P, Pietrosanti L, De Smaele E, Ferretti E, Miele E, Pelloni M, De Simone G, Pedone EM, Gallinari P, Giorgi A, Steinkuhler C, Vitagliano L, Pedone C, Schinin ME, Screpanti I, Gulino A (2010) Histone deacetylase and Cullin3-RENKCTD11 ubiquitin ligase interplay regulates Hedgehog signalling through Gli acetylation. Nat Cell Biol 12:132-142.

Canning P, Cooper CDO, Krojer T, Murray JW, Pike ACW, Chaikuad A, Keates T, Thangaratnarajah C, Hojzan V, Marsden BD, Gileadi O, Knapp S, von Delft F, Bullock AN (2013) Structural Basis for Cul3 Protein Assembly with the BTB-Kelch Family of E3 Ubiquitin Ligases. Journal of Biological Chemistry 288:7803-7814.

Cantí C, Page KM, Stephens GJ, Dolphin AC (1999) Identification of Residues in the N Terminus of α1B Critical for Inhibition of the Voltage-Dependent Calcium Channel by Gβγ. The Journal of Neuroscience 19:6855-6864.

Cardozo DL, Bean BP (1995) Voltage-dependent calcium channels in rat midbrain dopamine neurons: modulation by dopamine and GABAB receptors. Journal of Neurophysiology 74:1137-1148.

Catterall WA, Few AP (2008) Calcium Channel Regulation and Presynaptic Plasticity. Neuron 59:882-901.

Cauchi S, Proença C, Choquet H, Gaget S, Graeve F, Marre M, Balkau B, Tichet J, Meyre D, Vaxillaire M, Froguel P (2008) Analysis of novel risk loci for type 2 diabetes in a general French population: the D.E.S.I.R. study. Journal of Molecular Medicine 86:341-348.

Chalifoux JR, Carter AG (2010) GABAB Receptors Modulate NMDA Receptor Calcium Signals in Dendritic Spines. Neuron 66:101-113.

Chen Y, Yang Z, Meng M, Zhao Y, Dong N, Yan H, Liu L, Ding M, Peng HB, Shao F (2009) Cullin Mediates Degradation of RhoA through Evolutionarily Conserved BTB Adaptors to Control Actin Cytoskeleton Structure and Cell Movement. Molecular Cell 35:841-855.

Correale S, Pirone L, Di Marcotullio L, De Smaele E, Greco A, Mazzà D, Moretti M, Alterio V, Vitagliano L, Di Gaetano S, Gulino A, Pedone EM (2011) Molecular organization of the cullin E3 ligase adaptor KCTD11. Biochimie 93:715-724.

Couve A, Kittler JT, Uren JM, Calver AR, Pangalos MN, Walsh FS, Moss SJ (2001) Association of GABAB Receptors and Members of the 14-3-3 Family of Signaling Proteins. Molecular and Cellular Neuroscience 17:317-328.

Couve A, Thomas P, Calver AR, Hirst WD, Pangalos MN, Walsh FS, Smart TG, Moss SJ (2002) Cyclic AMP-dependent protein kinase phosphorylation facilitates GABAB receptor-effector coupling. Nat Neurosci 5:415-424.

Davies CH, Starkey SJ, Pozza MF, Collingridge GL (1991) GABAB autoreceptors regulate the induction of LTP. Nature 349:609-611.

De Jongh KS, Warner C, Catterall WA (1990) Subunits of purified calcium channels. α2 and δ are encoded by the same gene. Journal of Biological Chemistry 265:14738-14741.

De Smaele E, Di Marcotullio L, Moretti M, Pelloni M, Occhione MA, Infante P, Cucchi D, Greco A, Pietrosanti L, Todorovic J, Coni S, Canettieri G, Ferretti E, Bei R, Maroder M, Screpanti I, Gulino A (2011) Identification and Characterization of KCASH2 and KCASH3, 2 Novel Cullin3 Adaptors Suppressing Histone Deacetylase and Hedgehog Activity in Medulloblastoma. Neoplasia (New York, NY) 13:374-385.

Dementieva IS, Tereshko V, McCrossan ZA, Solomaha E, Araki D, Xu C, Grigorieff N, Goldstein SAN (2009) Pentameric Assembly of Potassium Channel Tetramerization Domain-Containing Protein 5. Journal of Molecular Biology 387:175-191.

Deng P-Y, Xiao Z, Yang C, Rojanathammanee L, Grisanti L, Watt J, Geiger JD, Liu R, Porter JE, Lei S (2009) GABAB Receptor Activation Inhibits Neuronal Excitability and Spatial Learning in the Entorhinal Cortex by Activating TREK-2 K+ Channels. Neuron 63:230-243.

Ding X, Luo C, Zhou J, Zhong Y, Hu X, Zhou F, Ren K, Gan L, He A, Zhu J, Gao X, Zhang J (2009) The interaction of KCTD1 with transcription factor AP-2α inhibits its transactivation. Journal of Cellular Biochemistry 106:285-295.

Dolphin AC (2003) β Subunits of Voltage-Gated Calcium Channels. Journal of Bioenergetics and Biomembranes 35:599-620.

Errington Wesley J, Khan MQ, Bueler Stephanie A, Rubinstein John L, Chakrabartty A, Privé Gilbert G (2012) Adaptor Protein Self-Assembly Drives the Control of a Cullin-RING Ubiquitin Ligase. Structure 20:1141-1153.

Ertel EA, Campbell KP, Harpold MM, Hofmann F, Mori Y, Perez-Reyes E, Schwartz A, Snutch TP, Tanabe T, Birnbaumer L, Tsien RW, Catterall WA (2000) Nomenclature of Voltage-Gated Calcium Channels. Neuron 25:533-535.

Evans RM, You H, Hameed S, Altier C, Mezghrani A, Bourinet E, Zamponi GW (2010) Heterodimerization of ORL1 and Opioid Receptors and Its Consequences for N-type Calcium Channel Regulation. Journal of Biological Chemistry 285:1032-1040.

Fajardo-Serrano A, Wydeven N, Young D, Watanabe M, Shigemoto R, Martemyanov KA, Wickman K, Luján R (2013) Association of Rgs7/Gβ5 complexes with Girk channels and GABA(B) receptors in hippocampal CA1 pyramidal neurons. Hippocampus 23:1231-1245.

Fedulova SA, Kostyuk PG, Veselovsky NS (1985) Two types of calcium channels in the somatic membrane of new-born rat dorsal root ganglion neurones. The Journal of Physiology 359:431-446.

Field MJ, Oles RJ, Lewis AS, McCleary S, Hughes J, Singh L (1997) Gabapentin (neurontin) and S-(+)-3-isobutylgaba represent a novel class of selective antihyperalgesic agents. British Journal of Pharmacology 121:1513-1522.

Filip M, Frankowska M, Sadakierska-Chudy A, Suder A, Szumiec Ł, Mierzejewski P, Bienkowski P, Przegaliński E, Cryan JF (2015) GABAB receptors as a therapeutic strategy in substance use disorders: Focus on positive allosteric modulators. Neuropharmacology 88:36-47.

Froestl W, Gallagher M, Jenkins H, Madrid A, Melcher T, Teichman S, Mondadori CG, Pearlman R (2004) SGS742: the first GABAB receptor antagonist in clinical trials. Biochemical Pharmacology 68:1479-1487.

Furukawa M, He YJ, Borchers C, Xiong Y (2003) Targeting of protein ubiquitination by BTB-Cullin 3-Roc1 ubiquitin ligases. Nat Cell Biol 5:1001-1007.

Furukawa M, Ohta T, Xiong Y (2002) Activation of UBC5 Ubiquitin-conjugating Enzyme by the RING Finger of ROC1 and Assembly of Active Ubiquitin Ligases by All Cullins. Journal of Biological Chemistry 277:15758-15765.

Gaillard S, Lo Re L, Mantilleri A, Hepp R, Urien L, Malapert P, Alonso S, Deage M, Kambrun C, Landry M, Low Sarah A, Alloui A, Lambolez B, Scherrer G, Le Feuvre Y, Bourinet E, Moqrich A (2014) GINIP, a Gαi-Interacting Protein, Functions as a Key Modulator of Peripheral GABAB Receptor-Mediated Analgesia. Neuron 84:123-136.

Galan JM, Haguenauer-Tsapis R (1997) Ubiquitin Lys63 is involved in ubiquitination of a yeast plasma membrane protein. The EMBO Journal 16:5847-5854.

Gassmann M, Bettler B (2012) Regulation of neuronal GABAB receptor functions by subunit composition. Nat Rev Neurosci 13:380-394.

Gee NS, Brown JP, Dissanayake VUK, Offord J, Thurlow R, Woodruff GN (1996) The Novel Anticonvulsant Drug, Gabapentin (Neurontin), Binds to the α2δ Subunit of a Calcium Channel. Journal of Biological Chemistry 271:5768-5776.

Genschik P, Sumara I, Lechner E (2013) The emerging family of CULLIN3-RING ubiquitin ligases (CRL3s): cellular functions and disease implications. The EMBO Journal 32:2307-2320.

Goldstein G, Scheid M, Hammerling U, Schlesinger DH, Niall HD, Boyse EA (1975) Isolation of a polypeptide that has lymphocyte-differentiating properties and is probably represented universally in living cells. Proceedings of the National Academy of Sciences of the United States of America 72:11-15.

Gowda CR, Lundt LP (2014) Mechanism of action of narcolepsy medications. CNS Spectrums 19:25-34.

Grampp T, Notz V, Broll I, Fischer N, Benke D (2008) Constitutive, agonist-accelerated, recycling and lysosomal degradation of GABAB receptors in cortical neurons. Molecular and Cellular Neuroscience 39:628-637.

Guetg N, Aziz SA, Holbro N, Turecek R, Rose T, Seddik R, Gassmann M, Moes S, Jenoe P, Oertner TG, Casanova E, Bettler B (2010) NMDA receptor-dependent GABAB receptor internalization via CaMKII phosphorylation of serine 867 in GABAB1. Proceedings of the National Academy of Sciences 107:13924-13929.

Gurnett CA, Felix R, Campbell KP (1997) Extracellular Interaction of the Voltage-dependent Ca2+ Channel α2δ and α1 Subunits. Journal of Biological Chemistry 272:18508-18512.

Hanack C, Moroni M, Lima Wanessa C, Wende H, Kirchner M, Adelfinger L, Schrenk-Siemens K, Tappe-Theodor A, Wetzel C, Kuich PH, Gassmann M, Roggenkamp D, Bettler B, Lewin Gary R, Selbach M, Siemens J (2015) GABA Blocks Pathological but Not Acute TRPV1 Pain Signals. Cell 160:759-770.

Harry JB, Kobrinsky E, Abernethy DR, Soldatov NM (2004) New Short Splice Variants of the Human Cardiac Cavβ2 Subunit: Redefining the major functional motifs implemented in modulation of the Cav1.2 channel. Journal of Biological Chemistry 279:46367-46372.

Hasegawa T, Asanuma H, Ogino J, Hirohashi Y, Shinomura Y, Iwaki H, Kikuchi H, Kondo T (2013) Use of potassium channel tetramerization domain-containing 12 as a biomarker for diagnosis and prognosis of gastrointestinal stromal tumor. Human Pathology 44:1271-1277.

Herlitze S, Hockerman GH, Scheuer T, Catterall WA (1997) Molecular determinants of inactivation and G protein modulation in the intracellular loop connecting domains I and II of the calcium channel α1A subunit. Proceedings of the National Academy of Sciences 94:1512-1516.

Hershko A, Ciechanover A (1998) The ubiquitin system. Annual Review of Biochemistry 67:425-479.

Ivankova K, Turecek R, Fritzius T, Seddik R, Prezeau L, Comps-Agrar L, Pin J-P, Fakler B, Besseyrias V, Gassmann M, Bettler B (2013) Up-regulation of GABAB Receptor Signaling by Constitutive Assembly with the K+ Channel Tetramerization Domain-containing Protein 12 (KCTD12). Journal of Biological Chemistry 288:24848-24856.

Ivanov DV, Tyazhelova TV, Lemonnier L, Kononenko N, Pestova AA, Nikitin EA, Prevarskaya N, Skryma R, Panchin YV, Yankovsky NK, Baranova AV (2003) A new human gene KCNRG encoding potassium channel regulating protein is a cancer suppressor gene candidate located in 13q14.3. FEBS Letters 539:156-160.

Jerng HH, Kunjilwar K, Pfaffinger PJ (2005) Multiprotein assembly of Kv4.2, KChIP3 and DPP10 produces ternary channel complexes with ISA-like properties. The Journal of Physiology 568:767-788.

Kaulin YA, De Santiago-Castillo JA, Rocha CA, Nadal MS, Rudy B, Covarrubias M (2009) The Dipeptidyl-Peptidase-Like Protein DPP6 Determines the Unitary Conductance of Neuronal Kv4.2 Channels. The Journal of Neuroscience 29:3242-3251.

Kaupmann K, Huggel K, Heid J, Flor PJ, Bischoff S, Mickel SJ, McMaster G, Angst C, Bittiger H, Froestl W, Bettler B (1997) Expression cloning of GABAB receptors uncovers similarity to metabotropic glutamate receptors. Nature 386:239-246.

Kaupmann K, Malitschek B, Schuler V, Heid J, Froestl W, Beck P, Mosbacher J, Bischoff S, Kulik A, Shigemoto R, Karschin A, Bettler B (1998a) GABAB-receptor subtypes assemble into functional heteromeric complexes. Nature 396:683-687.

Kaupmann K, Schuler V, Mosbacher J, Bischoff S, Bittiger H, Heid J, Froestl W, Leonhard S, Pfaff T, Karschin A, Bettler B (1998b) Human γ-aminobutyric acid type B receptors are differentially expressed and regulate inwardly rectifying K+ channels. Proceedings of the National Academy of Sciences 95:14991-14996.

Kerr LM, Yoshikami D (1984) A venom peptide with a novel presynaptic blocking action. Nature 308:282-284.

Kikuta K, Gotoh M, Kanda T, Tochigi N, Shimoda T, Hasegawa T, Katai H, Shimada Y, Suehara Y, Kawai A, Hirohashi S, Kondo T (2010) Pfetin as a Prognostic Biomarker in Gastrointestinal Stromal Tumor: Novel Monoclonal Antibody and External Validation Study in Multiple Clinical Facilities. Japanese Journal of Clinical Oncology 40:60-72.

Kim W, Bennett Eric J, Huttlin Edward L, Guo A, Li J, Possemato A, Sowa Mathew E, Rad R, Rush J, Comb Michael J, Harper JW, Gygi Steven P (2011) Systematic and Quantitative Assessment of the Ubiquitin-Modified Proteome. Molecular Cell 44:325-340.

Kipreos ET, Lander LE, Wing JP, He WW, Hedgecock EM (1996) cul-1 Is Required for Cell Cycle Exit in C. elegans and Identifies a Novel Gene Family. Cell 85:829-839.

Kitano J, Nishida M, Itsukaichi Y, Minami I, Ogawa M, Hirano T, Mori Y, Nakanishi S (2003) Direct Interaction and Functional Coupling between Metabotropic Glutamate Receptor Subtype 1 and Voltage-sensitive Cav2.1 Ca2+ Channel. Journal of Biological Chemistry 278:25101-25108.

Kittler R, Pelletier L, Heninger A-K, Slabicki M, Theis M, Miroslaw L, Poser I, Lawo S, Grabner H, Kozak K, Wagner J, Surendranath V, Richter C, Bowen W, Jackson AL, Habermann B, Hyman AA, Buchholz F (2007) Genome-scale RNAi profiling of cell division in human tissue culture cells. Nat Cell Biol 9:1401-1412.

Kiyonaka S, Wakamori M, Miki T, Uriu Y, Nonaka M, Bito H, Beedle AM, Mori E, Hara Y, De Waard M, Kanagawa M, Itakura M, Takahashi M, Campbell KP, Mori Y (2007) RIM1 confers sustained activity and neurotransmitter vesicle anchoring to presynaptic Ca2+ channels. Nat Neurosci 10:691-701.

Komander D, Rape M (2012) The Ubiquitin Code. Annual Review of Biochemistry 81:203-229.

Kondo T, Suehara Y, Kikuta K, Kubota D, Tajima T, Mukaihara K, Ichikawa H, Kawai A (2013) Proteomic approach toward personalized sarcoma treatment: Lessons from prognostic biomarker discovery in gastrointestinal stromal tumor. PROTEOMICS – Clinical Applications 7:70-78.

Kubota D, Mukaihara K, Yoshida A, Suehara Y, Saito T, Okubo T, Gotoh M, Orita H, Tsuda H, Kaneko K, Kawai A, Kondo T (2013) The Prognostic Value of Pfetin: A Validation Study in Gastrointestinal Stromal Tumors Using a Commercially Available Antibody. Japanese Journal of Clinical Oncology 43:669-675.

Kubota D, Okubo T, Saito T, Suehara Y, Yoshida A, Kikuta K, Tsuda H, Katai H, Shimada Y, Kaneko K, Kawai A, Kondo T (2012) Validation Study on Pfetin and ATP-dependent RNA Helicase DDX39 as Prognostic Biomarkers in Gastrointestinal Stromal Tumour. Japanese Journal of Clinical Oncology 42:730-741.

Lahaie N, Kralikova M, Pr, eacutezeau L, Blahos J, Bouvier M (2016) Post-endocytotic deubiquitination and degradation of the metabotropic γ-aminobutyric acid receptor by the ubiquitin specific protease 14. Journal of Biological Chemistry.

Lee MTM, Chen CH, Lee CS, Chen CC, Chong MY, Ouyang WC, Chiu NY, Chuo LJ, Chen CY, Tan HKL, Lane HY, Chang TJ, Lin CH, Jou SH, Hou YM, Feng J, Lai TJ, Tung CL, Chen TJ, Chang CJ, Lung FW, Chen CK, Shiah IS, Liu CY, Teng PR, Chen KH, Shen LJ, Cheng CS, Chang TP, Li CF, Chou CH, Chen CY, Wang KHT, Fann CSJ, Wu JY, Chen YT, Cheng ATA (2011) Genome-wide association study of bipolar I disorder in the Han Chinese population. Mol Psychiatry 16:548-556.

Leone MA, Vigna-Taglianti F, Avanzi G, Brambilla R, Faggiano F (2010) Gamma-hydroxybutyrate (GHB) for treatment of alcohol withdrawal and prevention of relapses. Cochrane Database of Systematic Reviews.

Li B, Zhong H, Scheuer T, Catterall WA (2004) Functional Role of a C-Terminal Gβγ-Binding Domain of Cav2.2 Channels. Molecular Pharmacology 66:761-769.

Li W, Bengtson MH, Ulbrich A, Matsuda A, Reddy VA, Orth A, Chanda SK, Batalov S, Joazeiro CAP (2008) Genome-Wide and Functional Annotation of Human E3 Ubiquitin Ligases Identifies MULAN, a Mitochondrial E3 that Regulates the Organelle's Dynamics and Signaling. PLoS ONE 3:e1487.

Liu J, Furukawa M, Matsumoto T, Xiong Y (2002) NEDD8 Modification of CUL1 Dissociates p120CAND1, an Inhibitor of CUL1-SKP1 Binding and SCF Ligases. Molecular Cell 10:1511-1518.

Liu Z, Xiang Y, Sun G (2013) The KCTD family of proteins: structure, function, disease relevance. Cell & Bioscience 3:1-5.

Maier PJ, Marin I, Grampp T, Sommer A, Benke D (2010) Sustained Glutamate Receptor Activation Down-regulates GABAB Receptors by Shifting the Balance from Recycling to Lysosomal Degradation. Journal of Biological Chemistry 285:35606-35614.

Maitre M, Klein C, Mensah-Nyagan AG (2016) Mechanisms for the Specific Properties of γ-Hydroxybutyrate in Brain. Medicinal Research Reviews 36:363-388.

Marín I (2009) Diversification of the cullin family. BMC Evolutionary Biology 9:1-11.

Mathias N, Johnson SL, Winey M, Adams AE, Goetsch L, Pringle JR, Byers B, Goebl MG (1996) Cdc53p acts in concert with Cdc4p and Cdc34p to control the G1-to-S-phase transition and identifies a conserved family of proteins. Molecular and Cellular Biology 16:6634-6643.

Metz M, Gassmann M, Fakler B, Schaeren-Wiemers N, Bettler B (2011) Distribution of the auxiliary GABAB receptor subunits KCTD8, 12, 12b, and 16 in the mouse brain. J Comp Neurol 519:1435-1454.

Metzger MB, Pruneda JN, Klevit RE, Weissman AM (2014) RING-type E3 ligases: Master manipulators of E2 ubiquitin-conjugating enzymes and ubiquitination. Biochimica et Biophysica Acta (BBA) - Molecular Cell Research 1843:47-60.

Mitra R, Morad M (1986) Two types of calcium channels in guinea pig ventricular myocytes. Proceedings of the National Academy of Sciences 83:5340-5344.

Müller CS, Haupt A, Bildl W, Schindler J, Knaus H-G, Meissner M, Rammner B, Striessnig J, Flockerzi V, Fakler B, Schulte U (2010) Quantitative proteomics of the Cav2 channel nano-environments in the mammalian brain. Proceedings of the National Academy of Sciences 107:14950-14957.

Na CH, Jones DR, Yang Y, Wang X, Xu Y, Peng J (2012) Synaptic Protein Ubiquitination in Rat Brain Revealed by Antibody-based Ubiquitome Analysis. Journal of Proteome Research 11:4722-4732.

Nadal MS, Ozaita A, Amarillo Y, de Miera EV-S, Ma Y, Mo W, Goldberg EM, Misumi Y, Ikehara Y, Neubert TA, Rudy B (2003) The CD26-Related Dipeptidyl Aminopeptidase-like Protein DPPX Is a Critical Component of Neuronal A-Type K+ Channels. Neuron 37:449-461.

Neher E (1998) Vesicle Pools and Ca2+ Microdomains: New Tools for Understanding Their Roles in Neurotransmitter Release. Neuron 20:389-399.

Obermair GJ, Tuluc P, Flucher BE (2008) Auxiliary Ca2+ channel subunits: lessons learned from muscle. Current Opinion in Pharmacology 8:311-318.

Ohh M, Kim WY, Moslehi JJ, Chen Y, Chau V, Read MA, Kaelin WG (2002) An intact NEDD8 pathway is required for Cullin-dependent ubiquitylation in mammalian cells. EMBO reports 3:177-182.

Ohta T, Michel JJ, Schottelius AJ, Xiong Y (1999) ROC1, a Homolog of APC11, Represents a Family of Cullin Partners with an Associated Ubiquitin Ligase Activity. Molecular Cell 3:535-541.

Olsen RW, Sieghart W (2008) International Union of Pharmacology. LXX. Subtypes of γ-Aminobutyric AcidA Receptors: Classification on the Basis of Subunit Composition, Pharmacology, and Function. Update. Pharmacological Reviews 60:243-260.

Orita H, Ito T, Kushida T, Sakurada M, Maekawa H, Wada R, Suehara Y, Kubota D, Sato K (2014) Pfetin as a Risk Factor of Recurrence in Gastrointestinal Stromal Tumors. BioMed Research International 2014:4.

Osaka F, Kawasaki H, Aida N, Saeki M, Chiba T, Kawashima S, Tanaka K, Kato S (1998) A new NEDD8-ligating system for cullin-4A. Genes & Development 12:2263-2268.

Pagano A, Rovelli G, Mosbacher J, Lohmann T, Duthey B, Stauffer D, Ristig D, Schuler V, Meigel I, Lampert C, Stein T, Prézeau L, Blahos J, Pin J-P, Froestl W, Kuhn R, Heid J, Kaupmann K, Bettler B (2001) C-Terminal Interaction Is Essential for Surface Trafficking But Not for Heteromeric Assembly of GABAB Receptors. The Journal of Neuroscience 21:1189-1202.

Pérez-Garci E, Gassmann M, Bettler B, Larkum ME (2006) The GABAB1b Isoform Mediates Long-Lasting Inhibition of Dendritic Ca2+ Spikes in Layer 5 Somatosensory Pyramidal Neurons. Neuron 50:603-616.

Perez-Reyes E (2003) Molecular Physiology of Low-Voltage-Activated T-type Calcium Channels. Physiological Reviews 83:117-161.

Pin J-P, Galvez T, Prézeau L (2003) Evolution, structure, and activation mechanism of family 3/C G-protein-coupled receptors. Pharmacology & Therapeutics 98:325-354.

Pontier SM, Lahaie N, Ginham R, St-Gelais F, Bonin H, Bell DJ, Flynn H, Trudeau LE, McIlhinney J, White JH, Bouvier M (2006) Coordinated action of NSF and PKC regulates GABAB receptor signaling efficacy. The EMBO Journal 25:2698-2709.

Pragnell M, De Waard M, Mori Y, Tanabe T, Snutch TP, Campbell KP (1994) Calcium channel beta-subunit binds to a conserved motif in the I-II cytoplasmic linker of the α1-subunit. Nature 368:67-70.

Rajalu M, Fritzius T, Adelfinger L, Jacquier V, Besseyrias V, Gassmann M, Bettler B (2015) Pharmacological characterization of GABAB receptor subtypes assembled with auxiliary KCTD subunits. Neuropharmacology 88:145-154.

Raveh A, Turecek R, Bettler B (2015) Chapter Six - Mechanisms of Fast Desensitization of GABAB Receptor-Gated Currents. In: Advances in Pharmacology, vol. Volume 73 (Uwe, R., ed), pp 145-165: Academic Press.

Rettig J, Sheng ZH, Kim DK, Hodson CD, Snutch TP, Catterall WA (1996) Isoform-specific interaction of the α1A subunits of brain Ca2+ channels with the presynaptic proteins syntaxin and SNAP-25. Proceedings of the National Academy of Sciences 93:7363-7368.

Robbins MJ, Calver AR, Filippov AK, Hirst WD, Russell RB, Wood MD, Nasir S, Couve A, Brown DA, Moss SJ, Pangalos MN (2001) GABAB2 Is Essential for G-Protein Coupling of the GABAB Receptor Heterodimer. The Journal of Neuroscience 21:8043-8052.

Rondou P, Haegeman G, Vanhoenacker P, Van Craenenbroeck K (2008) BTB Protein KLHL12 Targets the Dopamine D4 Receptor for Ubiquitination by a Cul3-based E3 Ligase. Journal of Biological Chemistry 283:11083-11096.

Sand PG, Langguth B, Itzhacki J, Bauer A, Geis S, Cárdenas Conejo Zugey E, Pimentel V, Kleinjung T (2012) Resequencing of the auxiliary GABAB receptor subunit gene KCTD12 in chronic tinnitus. Frontiers in Systems Neuroscience 6.

Sarikas A, Hartmann T, Pan Z-Q (2011) The cullin protein family. Genome Biology 12:220-220.

Schwenk J, Metz M, Zolles G, Turecek R, Fritzius T, Bildl W, Tarusawa E, Kulik A, Unger A, Ivankova K, Seddik R, Tiao JY, Rajalu M, Trojanova J, Rohde V, Gassmann M, Schulte U, Fakler B, Bettler B

(2010) Native GABAB receptors are heteromultimers with a family of auxiliary subunits. Nature 465:231-235.

Schwenk J, Perez-Garci E, Schneider A, Kollewe A, Gauthier-Kemper A, Fritzius T, Raveh A, Dinamarca MC, Hanuschkin A, Bildl W, Klingauf J, Gassmann M, Schulte U, Bettler B, Fakler B (2016) Modular composition and dynamics of native GABAB receptors identified by high-resolution proteomics. Nat Neurosci 19:233-242.

Seddik R, Jungblut SP, Silander OK, Rajalu M, Fritzius T, Besseyrias V, Jacquier V, Fakler B, Gassmann M, Bettler B (2012) Opposite Effects of KCTD Subunit Domains on GABAB Receptor-mediated Desensitization. Journal of Biological Chemistry 287:39869-39877.

Sheng Z-H, Yokoyama CT, Catterall WA (1997) Interaction of the synprint site of N-type Ca2+ channels with the C2B domain of synaptotagmin I. Proceedings of the National Academy of Sciences 94:5405-5410.

Sibille E, Wang Y, Joeyen-Waldorf J, Gaiteri C, Surget A, Oh S, Belzung C, Tseng GC, Lewis DA (2009) A Molecular Signature of Depression in the Amygdala. American Journal of Psychiatry 166:1011-1024.

Simms Brett A, Zamponi Gerald W (2014) Neuronal Voltage-Gated Calcium Channels: Structure, Function, and Dysfunction. Neuron 82:24-45.

Singer D, Biel M, Lotan I, Flockerzi V, Hofmann F, Dascal N (1991) The roles of the subunits in the function of the calcium channel. Science 253:1553-1557.

Skaar JR, Pagan JK, Pagano M (2013) Mechanisms and function of substrate recruitment by F-box proteins. Nature reviews Molecular cell biology 14:10.1038/nrm3582.

Skoblov M, Marakhonov A, Marakasova E, Guskova A, Chandhoke V, Birerdinc A, Baranova A (2013) Protein partners of KCTD proteins provide insights about their functional roles in cell differentiation and vertebrate development. BioEssays 35:586-596.

Smaldone G, Pirone L, Balasco N, Di Gaetano S, Pedone EM, Vitagliano L (2015) Cullin 3 Recognition Is Not a Universal Property among KCTD Proteins. PLoS ONE 10:e0126808.

Sodickson DL, Bean BP (1996) GABAB Receptor-Activated Inwardly Rectifying Potassium Current in Dissociated Hippocampal CA3 Neurons. The Journal of Neuroscience 16:6374-6385.

Stephens G, Mochida S (2013) Modulation of Presynaptic Calcium Channels: Springer.

Stogios PJ, Downs GS, Jauhal JJ, Nandra SK, Privé GG (2005) Sequence and structural analysis of BTB domain proteins. Genome Biology 6:1-18.

Südhof TC (2014) The Molecular Machinery of Neurotransmitter Release (Nobel Lecture). Angewandte Chemie International Edition 53:12696-12717.

Suehara Y, Kondo T, Seki K, Shibata T, Fujii K, Gotoh M, Hasegawa T, Shimada Y, Sasako M, Shimoda T, Kurosawa H, Beppu Y, Kawai A, Hirohashi S (2008) Pfetin as a Prognostic Biomarker of Gastrointestinal Stromal Tumors Revealed by Proteomics. Clinical Cancer Research 14:1707-1717.

Surget A, Wang Y, Leman S, Ibarguen-Vargas Y, Edgar N, Griebel G, Belzung C, Sibille E (2008) Corticolimbic Transcriptome Changes are State-Dependent and Region-Specific in a Rodent Model of Depression and of Antidepressant Reversal. Neuropsychopharmacology 34:1363-1380.

Sweatt JD (2016) Neural Plasticity & Behavior – Sixty Years of Conceptual Advances. Journal of Neurochemistry.

Takahashi T, Forsythe ID, Tsujimoto T, Barnes-Davies M, Onodera K (1996) Presynaptic Calcium Current Modulation by a Metabotropic Glutamate Receptor. Science 274:594-597.

Takahashi T, Momiyama A (1993) Different types of calcium channels mediate central synaptic transmission. Nature 366:156-158.

Thrower JS, Hoffman L, Rechsteiner M, Pickart CM (2000) Recognition of the polyubiquitin proteolytic signal. The EMBO Journal 19:94-102.

Turecek R, Schwenk J, Fritzius T, Ivankova K, Zolles G, Adelfinger L, Jacquier V, Besseyrias V, Gassmann M, Schulte U, Fakler B, Bettler B (2014) Auxiliary GABAB Receptor Subunits Uncouple G Protein βγ Subunits from Effector Channels to Induce Desensitization. Neuron 82:1032-1044.

Urwyler S (2011) Allosteric Modulation of Family C G-Protein-Coupled Receptors: from Molecular Insights to Therapeutic Perspectives. Pharmacological Reviews 63:59-126.

Vertkin I, Styr B, Slomowitz E, Ofir N, Shapira I, Berner D, Fedorova T, Laviv T, Barak-Broner N, Greitzer-Antes D, Gassmann M, Bettler B, Lotan I, Slutsky I (2015) GABAB receptor deficiency causes failure of neuronal homeostasis in hippocampal networks. Proceedings of the National Academy of Sciences 112:E3291-E3299.

Vigot R, Barbieri S, Bräuner-Osborne H, Turecek R, Shigemoto R, Zhang Y-P, Luján R, Jacobson LH, Biermann B, Fritschy J-M, Vacher C-M, Müller M, Sansig G, Guetg N, Cryan JF, Kaupmann K, Gassmann M, Oertner TG, Bettler B (2006) Differential Compartmentalization and Distinct Functions of GABAB Receptor Variants. Neuron 50:589-601.

von Poser C, Ichtchenko K, Shao X, Rizo J, Südhof TC (1997) The Evolutionary Pressure to Inactivate: a subclass of synaptotagmins with an amino acid substitution that abolishes Ca2+ binding. Journal of Biological Chemistry 272:14314-14319.

Wagner SA, Beli P, Weinert BT, Nielsen ML, Cox J, Mann M, Choudhary C (2011) A Proteome-wide, Quantitative Survey of In Vivo Ubiquitylation Sites Reveals Widespread Regulatory Roles. Molecular & Cellular Proteomics : MCP 10:M111.013284.

Wang C, Wang Y, Hu M, Chai Z, Wu Q, Huang R, Han W, Zhang CX, Zhou Z (2016) Synaptotagmin-11 inhibits clathrin-mediated and bulk endocytosis. EMBO reports 17:47-63.

Wilkinson KD (2005) The discovery of ubiquitin-dependent proteolysis. Proceedings of the National Academy of Sciences 102:15280-15282.

Yang L, Liu N, Hu X, Zhang W, Wang T, Li H, Zhang B, Xiang S, Zhou J, Zhang J (2009) CK2 phosphorylates TNFAIP1 to affect its subcellular localization and interaction with PCNA. Molecular Biology Reports 37:2967-2973.

Zamponi GW, Bourinet E, Nelson D, Nargeot J, Snutch TP (1997) Crosstalk between G proteins and protein kinase C mediated by the calcium channel α1 subunit. Nature 385:442-446.

Zamponi GW, Currie KPM (2013) Regulation of CaV2 calcium channels by G protein coupled receptors. Biochimica et Biophysica Acta (BBA) - Biomembranes 1828:1629-1643.

Zemoura K, Schenkel M, Acuña MA, Yévenes GE, Ulrich Zeilhofer H, Benke D (2013) Endoplasmic Reticulum-associated Degradation Controls Cell Surface Expression of γ-Aminobutyric Acid, Type B Receptors. Journal of Biological Chemistry 288:34897-34905.

Zhang Y, Yamada Y, Fan M, Bangaru SD, Lin B, Yang J (2010) The β Subunit of Voltage-gated Ca2+ Channels Interacts with and Regulates the Activity of a Novel Isoform of Pax6. Journal of Biological Chemistry 285:2527-2536.

Zheng J, Yang X, Harrell JM, Ryzhikov S, Shim E-H, Lykke-Andersen K, Wei N, Sun H, Kobayashi R, Zhang H (2002) CAND1 Binds to Unneddylated CUL1 and Regulates the Formation of SCF Ubiquitin E3 Ligase Complex. Molecular Cell 10:1519-1526.

Zhou J, Hu X, Xiong X, Liu X, Liu Y, Ren K, Jiang T, Hu X, Zhang J (2005) Cloning of two rat PDIP1 related genes and their interactions with proliferating cell nuclear antigen. Journal of Experimental Zoology Part A: Comparative Experimental Biology 303A:227-240.

# Appendix: Publication

**$GABA_B$ receptor deficiency causes failure of neuronal homeostasis in hippocampal networks.**

Vertkin, I., B. Styr, E. Slomowitz, N. Ofir, I. Shapira, D. Berner, T. Fedorova, T. Laviv, N. Barak-Broner, D. Greitzer-Antes, M. Gassmann, B. Bettler, I. Lotan and I. Slutsky

*Proceedings of the National Academy of Sciences* 112(25): E3291-E3299.

**Personal contribution**

Co-immunoprecipitation experiments with mouse membrane preparations

Data analysis

# $GABA_B$ receptor deficiency causes failure of neuronal homeostasis in hippocampal networks

Irena Vertkin[a], Boaz Styr[a], Edden Slomowitz[a], Nir Ofir[a,b], Ilana Shapira[a], David Berner[c], Tatiana Fedorova[a,b], Tal Laviv[a,b,1], Noa Barak-Broner[a], Dafna Greitzer-Antes[a,2], Martin Gassmann[c], Bernhard Bettler[c], Ilana Lotan[a,b], and Inna Slutsky[a,b,3]

[a]Department of Physiology and Pharmacology, Sackler Faculty of Medicine, Tel Aviv University, 69978 Tel Aviv, Israel; [b]Sagol School of Neuroscience, Tel Aviv University, 69978 Tel Aviv, Israel; and [c]Department of Biomedicine, Institute of Physiology, Pharmazentrum, University of Basel, CH-4056 Basel, Switzerland

Edited by Gina G. Turrigiano, Brandeis University, Waltham, MA, and approved May 14, 2015 (received for review January 8, 2015)

**Stabilization of neuronal activity by homeostatic control systems is fundamental for proper functioning of neural circuits. Failure in neuronal homeostasis has been hypothesized to underlie common pathophysiological mechanisms in a variety of brain disorders. However, the key molecules regulating homeostasis in central mammalian neural circuits remain obscure. Here, we show that selective inactivation of $GABA_B$, but not $GABA_A$, receptors impairs firing rate homeostasis by disrupting synaptic homeostatic plasticity in hippocampal networks. Pharmacological $GABA_B$ receptor ($GABA_BR$) blockade or genetic deletion of the $GB_{1a}$ receptor subunit disrupts homeostatic regulation of synaptic vesicle release. $GABA_BRs$ mediate adaptive presynaptic enhancement to neuronal inactivity by two principle mechanisms: First, neuronal silencing promotes syntaxin-1 switch from a closed to an open conformation to accelerate soluble N-ethylmaleimide-sensitive factor attachment protein receptor (SNARE) complex assembly, and second, it boosts spike-evoked presynaptic calcium flux. In both cases, neuronal inactivity removes tonic block imposed by the presynaptic, $GB_{1a}$-containing receptors on syntaxin-1 opening and calcium entry to enhance probability of vesicle fusion. We identified the $GB_{1a}$ intracellular domain essential for the presynaptic homeostatic response by tuning intermolecular interactions among the receptor, syntaxin-1, and the $Ca_V2.2$ channel. The presynaptic adaptations were accompanied by scaling of excitatory quantal amplitude via the postsynaptic, $GB_{1b}$-containing receptors. Thus, $GABA_BRs$ sense chronic perturbations in GABA levels and transduce it to homeostatic changes in synaptic strength. Our results reveal a novel role for $GABA_BR$ as a key regulator of population firing stability and propose that disruption of homeostatic synaptic plasticity may underlie seizure's persistence in the absence of functional $GABA_BRs$.**

homeostatic plasticity | $GABA_B$ receptor | synaptic vesicle release | syntaxin-1 | FRET

Neural circuits achieve an ongoing balance between plasticity and stability to enable adaptations to constantly changing environments while maintaining neuronal activity within a stable regime. Hebbian-like plasticity, reflected by persistent changes in synaptic and intrinsic properties, is crucial for refinement of neural circuits and information storage; however, alone it is unlikely to account for the stable functioning of neural networks (1). In the last 2 decades, major progress has been made toward understanding the homeostatic negative feedback systems underlying restoration of a baseline neuronal function after prolonged activity perturbations (2–4). Homeostatic processes may counteract the instability by adjusting intrinsic neuronal excitability, inhibition-to-excitation balance, and synaptic strength via postsynaptic or presynaptic modifications (5, 6) through a profound molecular reorganization of synaptic proteins (7, 8). These stabilizing mechanisms have been collectively termed homeostatic plasticity. Homeostatic mechanisms enable invariant firing rates and patterns of neural networks composed from intrinsically unstable activity patterns of individual neurons (9).

However, nervous systems are not always capable of maintaining constant output. Although some mutations, genetic knockouts, or pharmacologic perturbations induce a compensatory response that restores network firing properties around a predefined "set point" (10), the others remain uncompensated, or their compensation leads to pathological function (11). The inability of neural networks to compensate for a perturbation may result in epilepsy and various types of psychiatric disorders (12). Therefore, determining under which conditions activity-dependent regulation fails to compensate for a perturbation and identifying the key regulatory molecules of neuronal homeostasis is critical for understanding the function and malfunction of central neural circuits.

In this work, we explored the mechanisms underlying the failure in stabilizing hippocampal network activity by combining long-term extracellular spike recordings by multielectrode arrays (MEAs), intracellular patch-clamp recordings of synaptic responses, imaging of synaptic vesicle exocytosis, and calcium dynamics, together with FRET-based analysis of intermolecular interactions at individual synapses. Our results demonstrate that metabotropic, G protein-coupled receptors for GABA, $GABA_BRs$, are essential for firing rate homeostasis in hippocampal networks. We explored the mechanisms by which $GABA_BRs$ gate homeostatic synaptic

## Significance

How neuronal circuits maintain stable activity despite continuous environmental changes is one of the most intriguing questions in neuroscience. Previous studies proposed that deficits in homeostatic control systems may underlie common neurological symptoms in a variety of brain disorders. However, the key regulatory molecules that control homeostasis of central neural circuits remain obscure. We show here that basal activity of $GABA_B$ receptors is required for firing rate homeostasis in hippocampal networks. We identified the principal mechanisms by which $GABA_B$ receptors control homeostatic augmentation of synaptic strength to chronic neuronal silencing. We propose that deficits in $GABA_B$ receptor signaling, associated with epilepsy and psychiatric disorders, may lead to aberrant brain activity by erasing homeostatic plasticity.

Author contributions: I.V. and I. Slutsky designed research; I.V., B.S., E.S., N.O., I. Shapira, D.B., T.F., and T.L. performed research; N.B.-B., D.G.-A., M.G., B.B., and I.L. contributed new reagents/analytic tools; I.V., B.S., E.S., N.O., I. Shapira, D.B., T.F., T.L., M.G., B.B., and I. Slutsky analyzed data; and I.V. and I. Slutsky wrote the paper.

The authors declare no conflict of interest.

This article is a PNAS Direct Submission.

Freely available online through the PNAS open access option.

[1]Present address: Max Planck Florida Institute for Neuroscience, Jupiter, FL 33468-0998.

[2]Present address: Department of Medicine, University of Toronto, Toronto, ON, Canada M5S 1A8.

[3]To whom correspondence should be addressed. Email: islutsky@post.tau.ac.il.

This article contains supporting information online at www.pnas.org/lookup/suppl/doi:10.1073/pnas.1424810112/-/DCSupplemental.

plasticity. Our study raises the possibility that persistence of epileptic seizures in $GABA_BR$-deficient mice (13–15) is directly linked to impairments in a homeostatic control system.

## Results

**$GABA_BR$ Blockade Disrupts Firing Rate Homeostasis.** Mice lacking functional $GABA_BRs$ because of $GB_1$ or $GB_2$ subunit deletion display continuous spontaneous seizure activity (13–16). These findings are quite counterintuitive in light of a wide range of G protein-coupled receptors that mediate synaptic inhibition and might compensate for $GABA_BR$ loss of function. Therefore, we hypothesized that functional $GABA_BRs$ may play an essential role in neuronal homeostasis. To test this hypothesis, we examined homeostasis of mean firing rate of a neuronal population after chronic blockade of $GABA_BRs$. To chronically monitor neuronal activity in stable neural populations, we grew hippocampal cultures on MEAs for ~3 wk. Each MEA contains 59 recording electrodes, with each electrode capable of recording the activity of several adjacent neurons (Fig. 1*A*). Spikes were detected and analyzed using principal component analysis to obtain well-separated single units that were consistent throughout at least 2 d of recording (*SI Appendix*, *Methods*). To assess how chronic inhibition of the basal $GABA_BR$ activity affects mean firing rate of neural network, we measured spiking activity during a baseline recording period and for 2 d after application of CGP54626 (CGP), a selective $GABA_BR$ antagonist. Fig. 1*B* illustrates raster plots during periods of baseline, 1 h, and 48 h after 1 μM CGP application in a single experiment. Indeed, CGP causes an acute increase of 67 ± 13% in the mean firing rate (Fig. 1*C*), confirming proconvulsive properties of $GABA_BR$ antagonists in vivo (17). However, to our surprise, mean firing rate was not normalized during 2 d in the constant presence of CGP. After 2 d, firing rate remained 67 ± 18% higher in the presence of $GABA_BR$ antagonist ($P < 0.01$; Fig. 1*C*). Notably, under control conditions, network spike rates were stable during the 2 d of recording (no treatment, $P > 0.2$ between 1 h and 48 h; Fig. 1*D*).

To confirm that the lack of firing rate homeostasis is specific to the $GABA_BR$ blockade, we examined how chronic blockade of $GABA_ARs$ affects the population firing rate in hippocampal networks. Application of $GABA_AR$ antagonist gabazine (30 μM) caused a fast and pronounced increase in the population firing rate to 330 ± 32%, which gradually declined over the course of 2 d in the presence of gabazine (Fig. 1*E*), despite the constant presence of the antagonist. Washout of gabazine after 2 d caused a significant decrease in firing rate, indicating sustained activity of both gabazine and the $GABA_ARs$ (*SI Appendix*, Fig. S1).

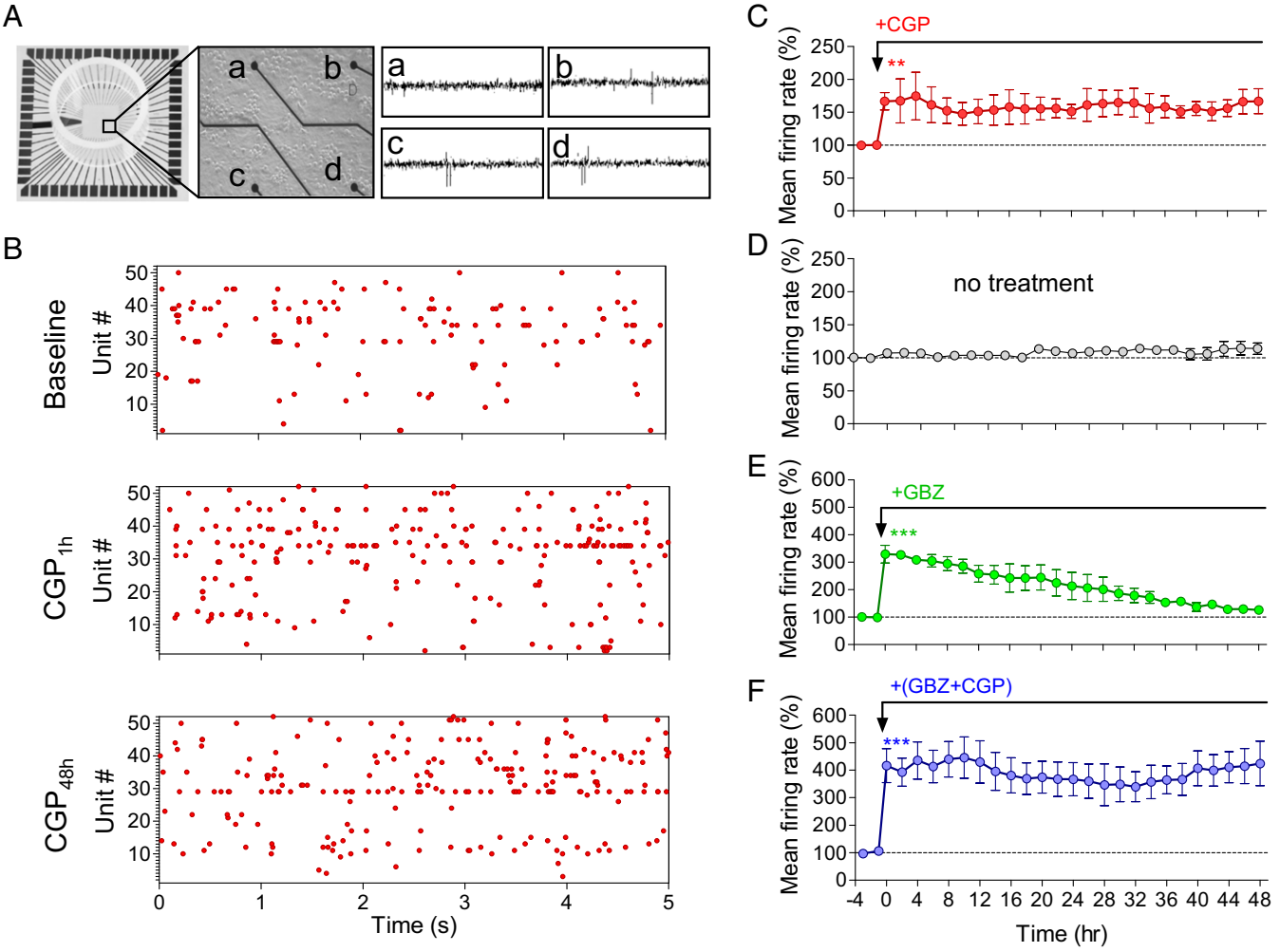


**Fig. 1.** $GABA_BR$ blockade disrupts firing rate homeostasis in hippocampal networks. (*A*, *Left*) Image of MEA dish. (*Middle*) Image of dissociated hippocampal culture plated on MEA. Black circles at the end of the black lines are the recording electrodes. (*Right*) Representative traces of recording from four MEA channels (*a*, *b*, *c*, and *d*). (*B*) Representative raster plot of MEA recording before and 1 and 48 h after application of the $GABA_BR$ antagonist CGP (1 μM). (*C–F*) Mean firing rate of hippocampal neuronal cultures incubated with CGP ($n = 4$; *C*), no treatment (Cnt, $n = 6$; *D*), gabazine (GBZ, 30 μM, $n = 4$; *E*), and CGP+GBZ ($n = 4$; *F*) during 2 d of MEA recordings.

Moreover, a $GABA_BR$ agonist, baclofen, triggered a pronounced block of firing rate that was precisely restored to the baseline level after a period of 2 d (9). The observed compensatory responses to increase in spiking activity by $GABA_AR$ antagonist or decrease in spiking activity by $GABA_BR$ agonist confirm the idea that homeostatic mechanisms maintain stable circuit function by keeping neuronal firing rate around a "set point" (10, 18).

Given a 3.4-fold difference in the magnitude of the initial firing rate increase produced by $GABA_AR$ versus $GABA_BR$ blockade, it is plausible that the lack of firing rate renormalization in the presence of CGP was a result of its relatively weak effect on firing rate. If this is the case, concurrent blockade of $GABA_ARs$ and $GABA_BRs$ would result in a reversal of firing rate, as in the presence of the $GABA_AR$ blocker alone. However, coapplication of gabazine and CGP triggered an initial increase in firing rate by 416 ± 61% that remained at 415 ± 63% for 2 d in the presence of the GABAR blockers ($P < 0.001$; Fig. 1*F*), suggesting selective $GABA_BR$ blockade truly disrupts firing rate renormalization. Altogether, these results demonstrate that ongoing $GABA_BR$ activity is required for firing rate homeostasis in hippocampal networks.

**$GB_{1a}$-Containing $GABA_BRs$ Mediate Homeostatic Increase in Evoked Vesicle Release.** What are the mechanisms underlying disruption of firing rate homeostasis by $GABA_BR$ blockade? To address this question, we assessed the dependency of synaptic homeostatic responses that normally contribute to firing rate homeostasis on the $GABA_BR$ function during activity changes. As a perturbation, we applied tetrodotoxin for 48 h ($TTX_{48h}$) to silence spiking activity, a classical paradigm in homeostasis research. First, we asked whether active $GABA_BRs$ are required for inactivity-induced increase in spike-evoked vesicle exocytosis estimated by the FM1-43 method (19). To this end, the total pool of recycling vesicles was stained by maximal stimulation (600 stimuli at 10 Hz) and subsequently destained by 1 Hz stimulation (Fig. 2*A* and *SI Appendix*, Fig. S2*A*). $TTX_{48h}$ induced a 1.4-fold increase in the destaining rate constant (measured as $1/\tau_{decay}$, whereas $\tau_{decay}$ is an exponential time course) and, thus, vesicle exocytosis ($P < 0.001$; Fig. 2 *B* and *G*). However, the adaptive enhancement of release probability (*Pr*) to inactivity was abolished when neurons were treated with TTX in the presence of CGP over the course of 48 h [$(TTX + CGP)_{48h}$; $P > 0.4$; Fig. 2 *C* and *G*]. Importantly, CGP application acutely increased FM destaining rate ($P < 0.01$; *SI Appendix*, Fig. S2*B*), which remained elevated for 48 h in the presence of CGP ($CGP_{48h}$; $P < 0.01$; Fig. 2 *C* and *G*), indicating that the expected compensatory reduction in *Pr* was impaired under the $GABA_BR$ blockade. Acute application of CGP after $TTX_{48h}$ treatment during FM destaining did not alter adaptive increase in vesicle exocytosis (*SI Appendix*, Fig. S2*C*). It is noteworthy that *Pr* was not saturated under $GABA_BR$ blockade, as presynaptic homeostatic compensation by $TTX_{48h}$ was normally expressed in high-*Pr* boutons under elevated extracellular $Ca^{2+}$ levels (Fig. 2 *D* and *G* and *SI Appendix*, Fig. S2*D*). Moreover, $GABA_AR$ blockade by gabazine for 48 h induced an adaptive reduction in *Pr* that was prevented by CGP coapplication (*SI Appendix*, Fig. S3). Thus, the failure in the homeostatic mechanisms is not associated with modulation of basal *Pr*. Taken together, these results indicate that basal $GABA_BR$ activity is necessary to achieve a compensatory increase in spike-evoked synaptic vesicle exocytosis in hippocampal synapses.

Which isoform of the $GABA_BRs$ mediates homeostatic increase in evoked vesicle release? $GABA_BRs$ are obligatory heterodimers, requiring two homologous subunits, $GB_1$ and $GB_2$, for functional expression (20). In hippocampal synapses, the $GB_{1a}$ isoform is predominantly expressed at glutamatergic presynaptic

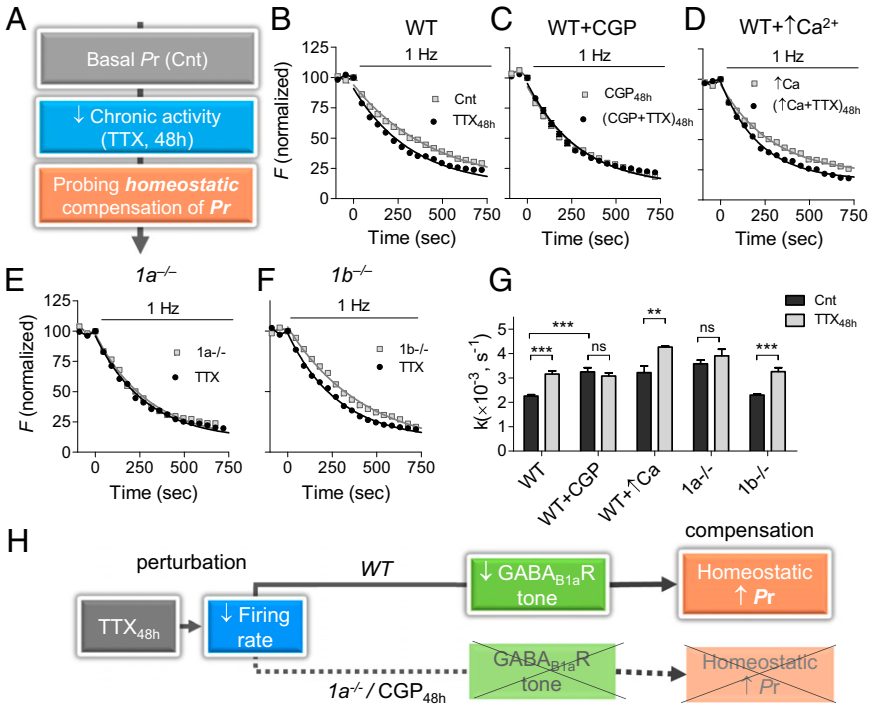


**Fig. 2.** Presynaptic homeostatic response is impaired by $GABA_BR$ blockade or $GB_{1a}$ deletion. (*A*) Experimental protocol for determining changes in synaptic vesicle exocytosis after prolonged inactivity by $TTX_{48h}$ (0.5 μM, 48 h). (*B–F*) Representative FM destaining rate curves of 50 synapses incubated with/without $TTX_{48h}$ in WT neurons (*B*), WT neurons treated by $CGP_{48h}$ (1 μM CGP for 48 h; *C*), WT neurons grown in increased (2 mM) $Ca^{2+}$ concentration (*D*), $1a^{-/-}$ neurons (*E*), and $1b^{-/-}$ neurons (*F*). (*G*) Effect of $TTX_{48h}$ on average destaining rate constants in WT neurons ($n = 687–701$), WT neurons incubated with $CGP_{48h}$ ($n = 593–748$), WT neurons in presence of high $Ca^{2+}$ ($n = 278–331$), $1a^{-/-}$ neurons ($n = 313–327$), and $1b^{-/-}$ neurons ($n = 303–313$). (*H*) Schematic illustration of $TTX_{48h}$-induced *Pr* homeostatic regulation by neuronal inactivity via $GABA_{B1a}Rs$.

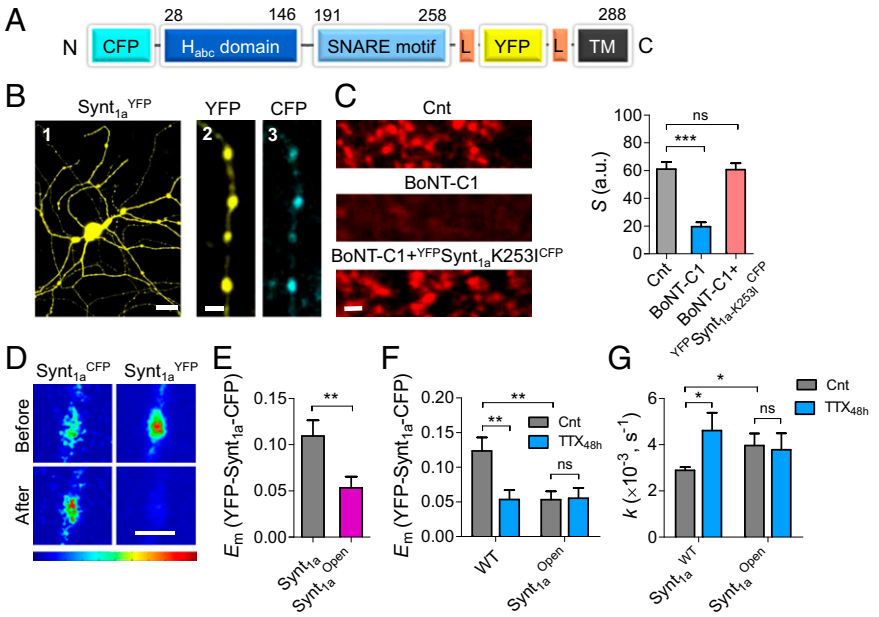


**Fig. 3.** Homeostatic mechanisms promote closed-to-open $Synt_{1a}$ conformational switch by neuronal inactivity. (*A*) Schematic illustration of $Synt_{1a}$ FRET construct (27). (*B*) Representative confocal image of a hippocampal neuron transfected with CFP-$Synt_{1a}$-YFP and zoom-in image of an axon. (*C*, *Left*) Synaptic vesicle recycling is blocked in neurons expressing BoNT-C1 light chain but is rescued by CFP-$Synt_{1a}$-K253I-YFP FRET probe. FM4-64 staining during 20-Hz stimulation (600 APs). (*Right*) Quantification of total presynaptic strength (*S*) in neurons expressing (*1*) CFP only (Cnt, $n = 8$) (*2*), BoNT-C1 ($n = 12$), and (*3*) BoNT-C1 + CFP-$Synt_{1a}$-K253I-YFP FRET probe ($n = 9$). (*D*) Pseudocolor-coded fluorescent images of CFP-$Synt_{1a}$-YFP protein expressing bouton before and after YFP photobleaching. (*E*) $Synt_{1a}^{Open}$ reduces $E_m$ ($n = 30$–$38$). (*F*) Summary of the $TTX_{48h}$ effect in neurons expressing wild-type $Synt_{1a}$ probe ($n = 23$–$34$) and $Synt_{1a}^{Open}$ ($n = 38$–$25$). (*G*) Average destaining rate constants in $Synt_{1a}^{WT}$ ($n = 284$), $Synt_{1a}^{WT}$ treated by $TTX_{48h}$ ($n = 181$), $Synt_{1a}^{Open}$ ($n = 270$), and $Synt_{1a}^{Open}$ treated by $TTX_{48h}$ ($n = 192$). [Scale bars, 20 μm (*B*, *1*) and 2 μm (*B*, *2* and *3*, and *D*)].

boutons, whereas $GB_{1b}$ is predominantly expressed at spines (21). Thus, we examined whether the presynaptic homeostatic response is disrupted in $1a^{-/-}$ boutons lacking the $GB_{1a}$ receptor subunit (21). The $1a^{-/-}$ boutons did not display a presynaptic response to activity blockade (Fig. 2 *E* and *G*). The deficits in presynaptic homeostatic plasticity were specific for the $GB_{1a}$ isoform, as $1b^{-/-}$ boutons displayed a typical adaption to prolonged synaptic inactivity (Fig. 2 *F* and *G*). Notably, acute application of CGP increased evoked synaptic vesicle release in the wild-type and $1b^{-/-}$, but not $1a^{-/-}$, boutons (*SI Appendix*, Fig. S4), confirming that the $GB_{1a}$-containing receptors mediate inhibition of *Pr* by local GABA levels. Although our previous data demonstrated a correlation between inactivity-induced reduction in the $GB_{1a}$ receptor activity and increase in *Pr* (22), our current results suggest that the basal $GB_{1a}$ receptor activity is required for homeostatic *Pr* regulation (Fig. 2*H*).

In contrast to inactivity-induced regulation of spike-evoked vesicle exocytosis, neither acute (*SI Appendix*, Fig. S5) nor chronic (*SI Appendix*, Fig. S6) application of CGP affected miniature excitatory postsynaptic current (mEPSC) frequency. Moreover, $TTX_{48h}$ alone or in the presence of $CGP_{48h}$ did not significantly change mEPSC frequency (*SI Appendix*, Fig. S6). It is worth mentioning that $TTX_{48h}$ reduced short-term synaptic facilitation during spike bursts measured by double-patch recordings (*SI Appendix*, Fig. S7), indicating an increase in *Pr* (23). Thus, the difference between spike-evoked and spontaneous vesicle release regulation observed under our experimental conditions reflects differential regulation of exocytosis during spontaneous and evoked synaptic activity (24). Although $GABA_BR$ blockade did not affect regulation of mEPSC frequency, it impaired inactivity-induced increase in mEPSC amplitude, suggesting the postsynaptic $GABA_BRs$ are involved in this regulation. Indeed, the effect of $TTX_{48h}$ was absent in $1b^{-/-}$ neurons (*SI Appendix*, Fig. S8), suggesting the $GB_{1b}$-containg postsynaptic $GABA_BRs$ play an important role in synaptic scaling.

**Inactivity Promotes Syntaxin-1 Conformational Switch.** What are the molecular mechanisms underlying the homeostatic increase in *Pr* by presynaptic $GABA_BRs$? SNARE-complex assembly is initiated by a syntaxin-1 ($Synt_1$) switch from its closed conformation (in which the N-terminal $H_{abc}$ domain of $Synt_1$ folds back onto its SNARE domain) into an open conformation (in which the SNARE domain becomes unmasked for SNARE-complex formation) (25). Rendering $Synt_1$ constitutively open induces an increase in *Pr* by enhancing SNARE-complex assembly per vesicle (26). However, activity-dependent mechanisms regulating $Synt_1$ conformational switch are not fully understood.

To assess whether chronic inactivity promotes $Synt_1$ opening, we used a recently developed intramolecular $Synt_{1a}$ FRET probe (CFP-$Synt_{1a}$-YFP) that reports the closed-to-open transition as a decrease in FRET efficiency (27). The $Synt_{1a}$ sensor contains CFP fluorophore inserted at the N terminus and YFP inserted after the SNARE motif (Fig. 3*A*) and is well expressed in processes of hippocampal neurons (Fig. 3*B*). The engineered $Synt_{1a}$ FRET reporter has been shown to assemble into endogenous SNARE complexes and was able to reconstitute dense-core vesicle exocytosis in PC12 cells (27). Furthermore, we show that neurons transfected with the light chain of BoNT-C1 are not capable of synaptic vesicle recycling, even during strong stimulation (600 pulses at 20 Hz; Fig. 3*C*). However, coexpression of BoNT-C1, together with BoNT-C1-insensitive CFP-$Synt_{1a}$K253I-YFP mutant reporter, restores synaptic vesicle recycling to the level observed in wild-type neurons (Fig. 3*C*). These results strongly suggest the CFP-$Synt_{1a}$-YFP FRET reporter is functional, supporting synaptic vesicle exocytosis in hippocampal neurons.

To monitor $Synt_{1a}$ conformational changes, we measured the steady-state FRET efficiency ($E_m$), using the acceptor photobleaching method at presynaptic boutons expressing CFP-$Synt_{1a}$-YFP

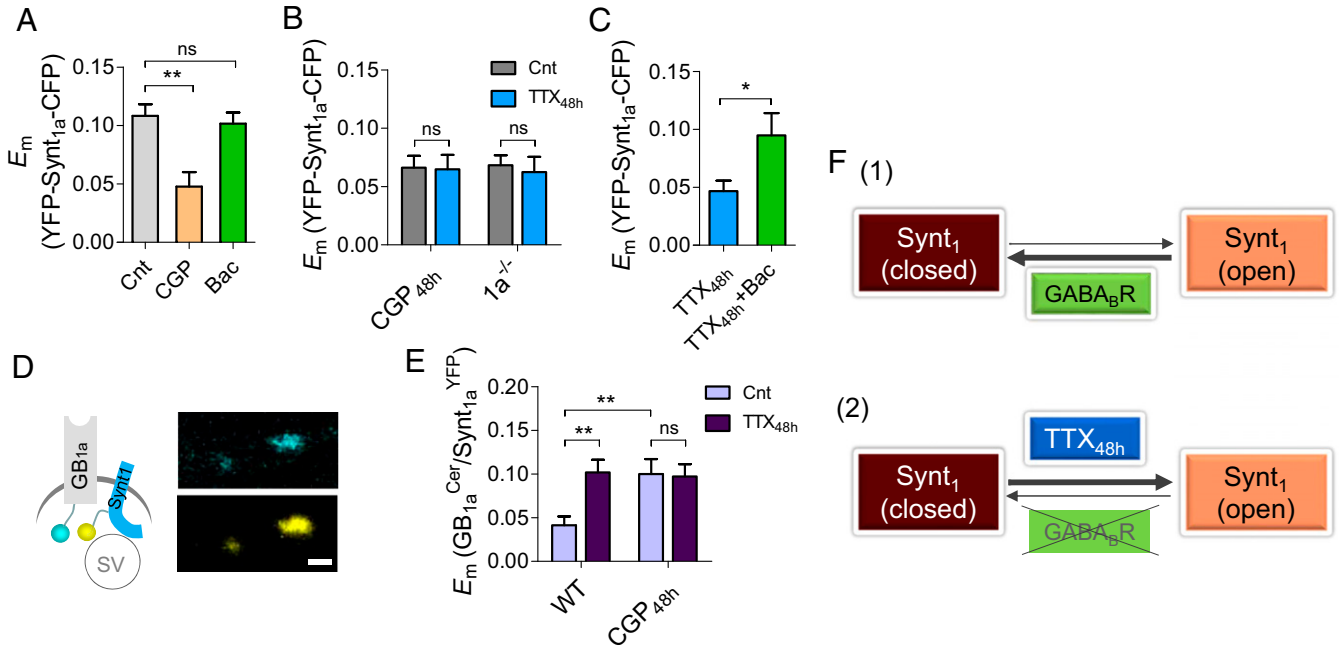


**Fig. 4.** Neuronal inactivity promotes $Synt_1$ opening by removal of $GABA_BR$-mediated block. (*A*) Acute application of CGP reduced CFP-$Synt_{1a}$-YFP $E_m$ ($n = 38$), whereas 10 μM baclofen did not affect it ($n = 88$) in WT neurons. (*B*) Summary of the $TTX_{48h}$ effect on CFP-$Synt_{1a}$-YFP $E_m$ in the presence of $CGP_{48h}$ in WT ($n = 42$–45) and in $1a^{-/-}$ ($n = 40$–80) neurons. (*C*) Baclofen (10 μM) rescued $TTX_{48h}$-induced FRET reduction ($n = 25$–40). (*D*) Representative confocal images of boutons cotransfected with $GB_{1a}^{Cer}$ and $Synt_{1a}^{YFP}$. (Scale bar, 1 μm.) (*E*) Effect of $TTX_{48h}$ on $GB_{1a}^{Cer}/Synt_{1a}^{YFP}$ $E_m$ ($n = 48$–57). $CGP_{48h}$ increases $GB_{1a}^{Cer}/Synt_{1a}^{YFP}$ $E_m$ and abolishes $TTX_{48h}$-induced $E_m$ changes ($n = 41$–69). (*F*) Schematic illustration of $Synt_1$ conformational switch regulation by neuronal inactivity via $GABA_BRs$.

(Fig. 3*B*, *2* and *3*). High-magnification confocal images show an increase in CFP fluorescence after YFP photobleaching (Fig. 3*D*), indicating dequenching of the donor and the presence of FRET. On average, CFP-$Synt_{1a}$-YFP FRET efficiency across hippocampal boutons was 0.12 ± 0.02 (Fig. 3*E*). To validate that the probe reports closed-to-open transition as a decrease in FRET efficiency, we used the $Synt_{1a}^{Open}$ FRET probe with L165E/L166E mutations, rendering $Synt_1$ in a constitutively open conformation (25). Indeed, $Synt_{1a}^{Open}$ displayed 56% lower FRET efficiency in comparison with the wild-type $Synt_{1a}$ probe (0.053 ± 0.01; $P <$ 0.01; Fig. 3*E*).

Next, we asked whether $Synt_{1a}$ conformation is homeostatically regulated by chronic neuronal inactivity to promote *Pr* augmentation. Indeed, $TTX_{48h}$ induced a reduction in $Synt_{1a}$ FRET to 0.05 ± 0.01 ($P < 0.01$; Fig. 3*F*). Notably, the reduction magnitude by $TTX_{48h}$ was similar to that exhibited by $Synt_{1a}^{Open}$ and was occluded by $Synt_{1a}^{Open}$. At the functional level, $Synt_{1a}^{Open}$ increased the rate of vesicle exocytosis ($P < 0.05$; Fig. 3*G*), supporting results of earlier studies (26, 28). Most important, $Synt_{1a}^{Open}$ occluded the effect of $TTX_{48h}$ on *Pr* ($P > 0.7$; Fig. 3*G*), suggesting a functional importance of $Synt_{1a}$ opening in compensatory *Pr* augmentation.

**Removal of $GABA_BR$ Block Mediates Inactivity-Induced Syntaxin-1 Opening.** To examine whether $GABA_BR$ tone is required for inactivity-induced $Synt_{1a}$ opening, we first asked whether $Synt_{1a}$ conformation is regulated by basal $GABA_BR$ activity. Acute application of $GABA_BR$ antagonist CGP reduced mean FRET level to 0.048 ± 0.01 ($P < 0.01$; Fig. 4*A*). Application of $GABA_BR$ agonist baclofen (10 μM) did not affect FRET ($P >$ 0.05; Fig. 4*A*), indicating that basal GABA levels are sufficient to stabilize a closed $Synt_{1a}$ conformation. Next, we asked whether $GABA_BR$ blockade interferes with $TTX_{48h}$-induced $Synt_{1a}$ opening. $CGP_{48h}$ caused a reduction in $Synt_{1a}$ FRET ($P < 0.01$; Fig. 4*B*) and occluded the effect of $TTX_{48h}$ on $Syn_{1a}$ conformational change (Fig. 4*B*). The effect of $CGP_{48h}$ was mimicked by deletion of the $GB_{1a}$ receptor subunit: $Synt_{1a}$ FRET was twofold lower in $1a^{-/-}$ boutons and insensitive to chronic reduction in spiking activity by $TTX_{48h}$ (Fig. 4*B*). Importantly, acute application of baclofen restored $Synt_{1a}$ FRET in $TTX_{48h}$-treated neurons (Fig. 4*C*), suggesting prolonged silencing may promote $Synt_{1a}$ opening by reducing the extracellular GABA levels (22).

Having established the necessity for $GB_{1a}$-containing $GABA_BRs$ in the homeostatic conformational change of $Synt_{1a}$, we explored a possibility of $Synt_{1a}$ and $GB_{1a}$ interactions. To quantify activity-dependent changes in $GB_{1a}$–$Synt_{1a}$ interactions at individual presynaptic sites, we used the FRET approach. To preserve the functionality of the $Synt_{1a}$ FRET reporter, we replaced CFP by its nonfluorescent mutant CFP-W66A, and a Cerulean (Cer)-tagged $GB_{1a}$ subunit at the C terminus ($GB_{1a}^{Cer}$) was used as a donor (Fig. 4*D*). Basal $GB_{1a}^{Cer}/Synt_{1a}^{YFP}$ FRET efficiency was 0.04 ± 0.01 and underwent a 2.4-fold increase by $TTX_{48h}$ ($P < 0.01$; Fig. 4*E*). Notably, blockade of $GABA_BRs$ produced a similar effect ($P < 0.01$; Fig. 4*E*), indicating that $GB_{1a}/Synt_{1a}$ interactions are regulated by basal GABA. Moreover, $CGP_{48h}$ occluded $TTX_{48h}$-induced $GB_{1a}^{Cer}/Synt_{1a}^{YFP}$ FRET changes ($P = 0.9$; Fig. 4*E*). To determine the existence of endogenous protein complexes containing $Synt_1$ and $GABA_BRs$, we performed coimmunoprecipitation experiments with solubilized mouse brain membranes. Anti-$Synt_1$ antibodies coprecipitated a significant amount of $GB_1$ proteins together with $Synt_1$ from WT, but not from full $GB_1$-KO mice (*SI Appendix*, Fig. S9). Taken together, these results indicate that $Synt_{1a}$ conformational change constitutes a critical step in presynaptic homeostatic response, that basal $GABA_BR$ activity maintains $Synt_{1a}$ in a closed conformation (Fig. 4*F*, *1*), and that prolonged inactivity removes a $GABA_BR$-imposed clamping of a closed $Synt_{1a}$ conformation, allowing $Synt_{1a}$ shift toward its open conformation (Fig. 4*F*, *2*).

**$GB_{1a}$ Is Required for Homeostatic Increase in Presynaptic Calcium Flux.** Next, we examined whether the $GB_{1a}$ receptor subunit controls homeostatic regulation of presynaptic $Ca^{2+}$ transients (29),

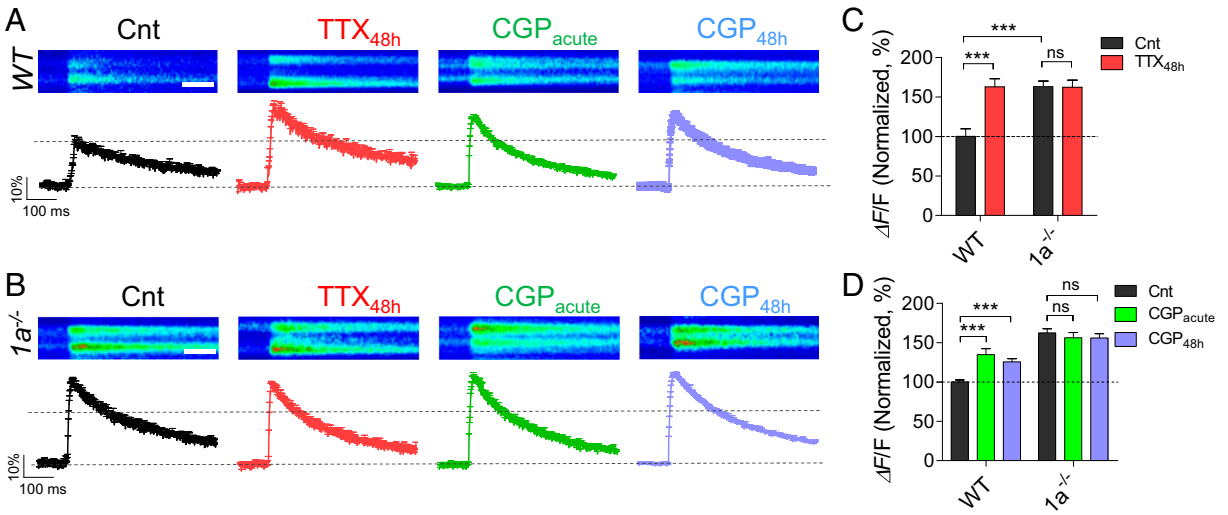


**Fig. 5.** Homeostatic increase in presynaptic calcium flux is impaired by $GB_{1a}$ deletion. (*A* and *B*) $TTX_{48h}$ increased spike-dependent presynaptic $Ca^{2+}$ entry in boutons of WT, but not in $1a^{-/-}$ neurons. (*Top*) Representative images of $Ca^{2+}$ transients (average of seven traces) evoked by 0.2-Hz stimulation during a 500-Hz line scan in boutons under control, or $TTX_{48h}$, $CGP_{acute}$, and $CGP_{48h}$ conditions in WT (*A*) and $1a^{-/-}$ (*B*) neurons. (Scale bar, 100 ms.) (*Bottom*) Averaged $Ca^{2+}$ transients, quantified as $\Delta F/F$, in control ($n = 20$), $TTX_{48h}$ ($n = 15$), $CGP_{acute}$ ($n = 29$), and $CGP_{48h}$ ($n = 37$) conditions in WT (*A*) and $1a^{-/-}$ (*B*, $n = 20$, 21, 23, and 66 for Cnt, $TTX_{48h}$, $CGP_{acute}$, and $CGP_{48h}$, respectively) neurons. (*C*) Summary of $TTX_{48h}$ effect (percentage of control) on $Ca^{2+}$ transients in boutons of WT versus $1a^{-/-}$ neurons (the same data as in *A* and *B*). Note that $Ca^{2+}$ transients were higher in $1a^{-/-}$ boutons than in WT ones. (*D*) Summary of $CGP_{acute}$ and $CGP_{48h}$ effects (percentage of control) on $Ca^{2+}$ transients in WT versus $1a^{-/-}$ boutons (the same data as in *A* and *B*).

in addition to regulating $Synt_1$ conformational switch, to adapt *Pr* to chronic activity perturbations. Thus, we measured presynaptic $Ca^{2+}$ transients evoked by 0.1-Hz stimulation, using high-affinity fluorescent calcium indicator Oregon Green 488 BAPTA-1 AM (Fig. 5*A*) at functional boutons identified by the FM4-64 marker. Although the size of action-potential dependent fluorescence transients ($\Delta F/F$) varied between different boutons, presynaptic $Ca^{2+}$ flux was significantly larger in $TTX_{48h}$-treated WT neurons ($P < 0.0001$; Fig. 5 *A* and *C*). Importantly, presynaptic $Ca^{2+}$ flux was higher in boutons of $1a^{-/-}$ neurons ($P < 0.0001$; Fig. 5 *B* and *C*), occluding the effect of $TTX_{48h}$ on further potentiation of calcium transients. It is noteworthy that $Ca^{2+}$ transients were not saturated by single action potential in $1a^{-/-}$ boutons (*SI Appendix*, Fig. S10). Furthermore, acute application of CGP increased presynaptic $Ca^{2+}$ flux that remained stable over the course of 2 d in the presence of CGP in WT ($P < 0.001$; Fig. 5 *A* and *D*), but not in $1a^{-/-}$ ($P > 0.4$; Fig. 5 *B* and *D*), neurons. This lack of compensation at the level of $Ca^{2+}$ flux was specific for the $GABA_BR$ deficit, as $GABA_AR$ blockade by gabazine has been previously shown to trigger an adaptive reduction in presynaptic $Ca^{2+}$ transients (29). These results indicate that $GB_{1a}$-containing $GABA_BRs$ normally inhibit presynaptic $Ca^{2+}$ flux evoked by single action potential and that removal of the $GABA_BR$-mediated block is essential for homeostatic potentiation of $Ca^{2+}$ flux by chronic inactivity.

**$GB_{1a}$PCT Mediates Presynaptic Homeostatic Response.** Next, we searched for the molecular domain in the $GB_{1a}$ protein that mediates the presynaptic homeostatic response. In our previous work, we identified the proximal C-terminal domain of the $GB_{1a}$ protein (R857-S877; $GB_{1a}$PCT; Fig. 6*A*) as essential for the compartmentalization of the presynaptic signaling complex of $GABA_BRs$, Gβγ G protein subunits, and $Ca_V2.2$ channels in hippocampal boutons (30). Interestingly, deletion of $GB_{1a}$PCT domain specifically impaired $Ca_V2.2$/Gβγ interaction and function, leaving $G\alpha_{i/o}$-dependent signaling unaltered.

First, we assessed the functional role of the $GB_{1a}$PCT domain in the homeostatic increase of *Pr* by comparing the effect of $TTX_{48h}$ on FM4-64 destaining rates in $1a^{-/-}$ neurons transfected with $GB_{1a}$WT-CFP versus $GB_{1a}\Delta$PCT-CFP proteins. Expression of the $GB_{1a}$WT-CFP protein rescued inactivity-induced potentiation of vesicle exocytosis in $1a^{-/-}$ neurons ($P < 0.01$; Fig. 6 *B* and *D* in comparison with Fig. 2*G*). In contrast, $TTX_{48h}$-induced presynaptic enhancement remained impaired in boutons expressing $GB_{1a}\Delta$PCT-CFP ($P > 0.8$; Fig. 6 *C* and *D*). Moreover, deletion of the $GB_{1a}$PCT domain abolished inactivity-induced increase in presynaptic calcium transients ($P > 0.8$; Fig. 6 *E*–*G*). Thus, the $GB_{1a}$PCT domain is necessary for presynaptic adaptations to prolonged inactivity in hippocampal networks.

Finally, we examined whether inactivity induces conformational $GABA_BR/Ca_V2.2$ changes, and if so, whether the $GB_{1a}$PCT domain is involved in this homeostatic regulation. We monitored FRET efficiency between the YFP-tagged $GB_{1a}$ receptor subunit at the C terminus and the CFP-tagged α1 subunit of the $Ca_V2.2$ channel at the N terminus ($GB_{1a}^{YFP}/Ca_V2.2^{CFP}$). $TTX_{48h}$ induced an increase in $GB_{1a}^{YFP}/Ca_V2.2^{CFP}$ FRET ($P < 0.05$; Fig. 6*H*), indicating that chronic neuronal silencing alters $GB_{1a}/Ca_V2.2$ interactions. Importantly, deletion of the $GB_{1a}$PCT domain disrupted $TTX_{48h}$-induced homeostatic $GB_{1a}^{YFP}/Ca_V2.2^{CFP}$ changes ($P = 0.49$; Fig. 6*H*). Moreover, $GB_{1a}$PCT deletion occluded $TTX_{48h}$-induced homeostatic $GB_{1a}^{Cer}/GB_2^{Cit}$ and $GB_{1a}^{YFP}/Synt_{1a}^{CFP}$ changes (*SI Appendix*, Fig. S11). A physical interaction between endogenous $GABA_BRs$ and $Ca_V2.2$ was revealed by coimmunoprecipitation experiments (*SI Appendix*, Fig. S9), confirming previous proteomic data (31). These results suggest that homeostatic mechanisms modulate $GB_{1a}/Ca_V2.2$ and $GB_{1a}/Synt_{1a}$ interactions in the $GABA_BR$ presynaptic signaling complex via the $GB_{1a}$PCT domain.

## Discussion

The ability of neuronal circuits to stabilize their firing properties in the face of environmental or genetic changes is critical for normal neuronal functioning. Despite extensive research on a wide repertoire of possible homeostatic mechanisms, the key regulators of firing rate homeostasis in mammalian central neural circuits remain obscure. In this work, we identified the $GABA_BR$ as a key homeostatic signaling molecule stabilizing mean firing rate in hippocampal networks. $GABA_BRs$ enable inactivity-induced homeostatic increase in synaptic strength by three principle mechanisms:

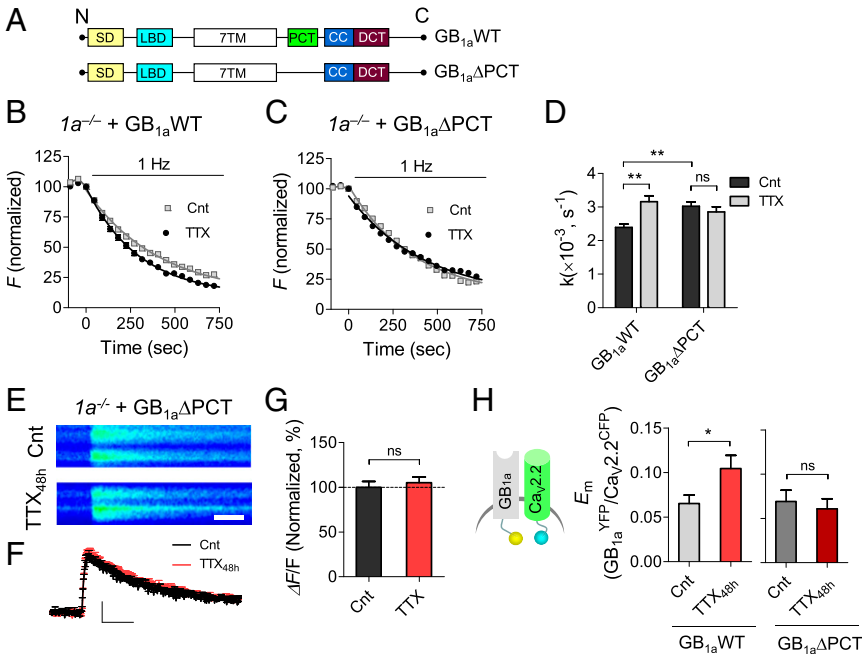


**Fig. 6.** The $GB_{1a}$PCT domain is required for presynaptic homeostatic response. (*A*) Schematics show $GB_{1a}$WT and $GB_{1a}$ΔPCT constructs. 7TM, seven-transmembrane domain; CC, coiled-coiled domain; DCT, distal C-terminal domain; LBD, ligand-binding domain; PCT, proximal C-terminal domain; SD, two sushi domains. (*B* and *C*) Representative FM destaining rate curves of 50 synapses pretreated with/without $TTX_{48h}$ in $1a^{-/-}$ neurons transfected with $GB_{1a}$WT (*B*) or $GB_{1a}$ΔPCT (*C*). (*D*) Expression of $GB_{1a}$WT ($n$ = 609–642), but not of $GB_{1a}$ΔPCT ($n$ = 598–721), restores presynaptic homeostatic adaptation in $1a^{-/-}$ neurons. (*E* and *F*) $TTX_{48h}$ did not alter spike-dependent presynaptic $Ca^{2+}$ entry in boutons expressing $GB_{1a}$ΔPCT in $1a^{-/-}$ neurons. Representative images of $Ca^{2+}$ transients (average of seven traces) evoked by 0.2-Hz stimulation in boutons of control and $TTX_{48h}$-treated $GB_{1a}$ΔPCT-expressing boutons (*E*). Averaged $Ca^{2+}$ transients in control ($n$ = 44) and $TTX_{48h}$ ($n$ = 37) conditions (*F*). (*G*) Summary of $TTX_{48h}$ effect on $Ca^{2+}$ transients in boutons expressing $GB_{1a}$ΔPCT protein (the same data as in *F*). (*H*) Effect of $TTX_{48h}$ on $GB_{1a}{}^{YFP}/Ca_V2.2^{CFP}$ $E_m$ ($n$ = 40–88). Deletion of PCT domain abolishes $TTX_{48h}$-induced change in $GB_{1a}{}^{YFP}/Ca_V2.2^{CFP}$ $E_m$ ($n$ = 44–55).

promoting synatxin-1 conformational switch to enhance SNARE-complex assembly, augmenting presynaptic $Ca^{2+}$ flux to promote spike-evoked vesicle exocytosis, and increasing the quantal excitatory amplitude. Thus, $GABA_BRs$, in addition to modulation of short-term (32, 33) and long-term, Hebbian (21) synaptic plasticity, are essential for maintaining firing stability of neural circuits.

**$GABA_BRs$ and Synaptic Homeostatic Plasticity.** Homeostatic regulation of synaptic strength represents a basic mechanism of neuronal adaptation to constant changes in ongoing activity levels. Strong evidence exists on homeostatic augmentation of *P*r and readily releasable pool size in response to prolong inactivity in hippocampal neurons (19, 22, 34–42). These homeostatic adaptations are associated with modulation of presynaptic $Ca^{2+}$ flux (29) and remodeling of a large number of proteins in presynaptic cytomatrix (7). Recent studies have identified the mechanisms underlying presynaptic homeostatic signaling in *Drosophila* neuromuscular junction, implicating epithelial sodium leak channels (43) and endostatin (44) as homeostatic regulators of the presynaptic $Ca_V2$ channels (for review, see ref. 5). However, the critical molecules controlling presynaptic homeostasis in mammalian central synapses are not fully understood.

In this work, we show that chronic neuronal silencing induces an adaptive increase in evoked basal vesicle release through $GABA_BRs$ by removing tonic inhibition of $Synt_1$ conformational switch and of presynaptic $Ca^{2+}$ flux. These results are important for several reasons. First, they reveal a crucial role for $GABA_BRs$ in presynaptic homeostasis. Taking into account a wide variety of G protein-coupled receptors that mediate presynaptic inhibition, the requirement for the $GABA_BR$ tone in presynaptic homeostatic response is particularly striking. Second, they demonstrate, for the first time, the role of the extracellular GABA in determining $Synt_1$ conformation via the presynaptic $GB_{1a}$-containing $GABA_BRs$. Either genetic $GB_{1a}$ deletion or pharmacological $GABA_BR$ blockade stabilizes an open $Synt_1$ conformation in analogy to mutations rendering $Synt_1$ constitutively open, occluding adaptive response to neuronal silencing. Notably, addition of $GABA_BR$ agonist after prolonged inactivity stabilizes a closed $Synt_1$ conformation, suggesting reduction in local GABA levels induces an adaptive $Synt_{1a}$ response. Third, in addition to the well-known role of $GABA_BRs$ in the presynaptic $Ca^{2+}$ flux inhibition, at a rapid timescale of minutes (22, 45), our work revealed the necessity for basal $GABA_BR$ activity in presynaptic adaptations of $Ca^{2+}$ transients to chronic activity perturbations at extended timescales of days. Deletion of the $GB_{1a}$PCT domain blocks presynaptic homeostatic plasticity by disrupting GABA-mediated conformational changes within the presynaptic $GB_{1a}$/$Ca_V2.2$/$Synt_1$ signaling complex. Thus, endogenous molecular "brakes" imposed by $GABA_BRs$ on $Ca_V2.2$ channels and SNARE complex assembly are essential for presynaptic homeostasis in hippocampal neurons.

It is important to note that in the present study, chronic inactivity by TTX induced a compensatory increase in mEPSC amplitude via the postsynaptic $GB_{1b}$-containing receptors without affecting mEPSC frequency. Given a pronounced effect of $TTX_{48h}$ on spike-evoked synaptic vesicle exocytosis, these results suggest complete blockade of spikes does not trigger compensatory changes in spontaneous vesicle release. In previous studies, mEPSC frequency was found to be immune to chronic TTX treatment in some cases (18, 41), while being up-regulated by AMPA receptor blockade (36, 41), either by suppression of neuronal excitability (38) or by increase in the $GABA_BR$-mediated inhibition (9). Thus, the induction of presynaptic homeostatic changes may require minimal spiking activity (41).

**$GABA_BR$-Mediated Neuronal Homeostasis and Brain Disorders.** It is tempting to speculate that many distinct neurologic and psychiatric disorders with different etiologies share common dysfunctions in pathways related to homeostatic plasticity. However, the molecular mechanisms by which defective homeostatic signaling may lead to common disease pathophysiology remain to be determined. Only a few molecular links, such as the schizophrenia-associated gene dysbindin, have been established between homeostatic system impairments and brain dysfunctions (46). Our study demonstrates that ongoing $GABA_BR$ activity is essential for population firing rate homeostasis in hippocampal networks. This may explain why aberrant neuronal activity remains uncompensated in mice lacking functional $GABA_BRs$ as a result of deletion of either the $GB_1$ (13) or $GB_2$ (15) receptor subunit. Interestingly, $1a^{-/-}$, but not $1b^{-/-}$, mice exhibit spontaneous epileptiform activity (16), suggesting the presynaptic $GB_{1a}$-containing receptors may play a more prominent role in firing rate homeostasis. Strikingly, our results show that homeostatic plasticity is impaired in synaptic networks displaying enhanced ongoing synaptic $Ca^{2+}$ flux because of removal of the $GABA_BR$-mediated block. Thus, $Ca_V2$ channel gain of function may be as detrimental for neuronal homeostasis as $Ca_V2$ loss of function (47, 48), indicating that an optimal level of ongoing synaptic $Ca^{2+}$ flux may be essential for homeostatic regulation. It remains to be seen whether the loss of functional $GABA_BRs$, associated with epilepsy and a wide range of psychiatric disorders (49), contributes to pathophysiology shared by these disorders through erasing critical pathways in homeostatic control systems.

## Materials and Methods

**Hippocampal Cell Culture.** Primary cultures of CA3-CA1 hippocampal neurons were prepared from WT, $1a^{-/-}$, and $1b^{-/-}$ (BALB/c background) mice (21) on postnatal days 0–2, as described (50). The experiments were performed in mature (14–28 d in vitro) cultures. All animal experiments were approved by the Tel Aviv University Committee on Animal Care.

**MEA Preparation and Recordings.** Cultures were plated on MEA plates containing 59 TiN recording and one internal reference electrodes [Multi Channel Systems (MCS)]. Electrodes are 30 μm in diameter and spaced 500 μm apart. Data were acquired using a MEA1060-Inv-BC-Standard amplifier (MCS) with frequency limits of 5,000 Hz and a sampling rate of 10 kHz per electrode mounted on an Olympus IX71 inverted microscope. Recordings were carried out under constant 37 °C and 5% $CO_2$ conditions, identical to incubator conditions. Spike sorting and analysis are described in ref. 9 and in *SI Appendix, Spike Sorting and Data Analysis*.

**Molecular Biology.** $GB_{1a}$WT-, $GB_{1a}$ΔPCT-, $GB_2$-, and $Ca_V2.2$-tagged proteins used throughout the study were constructed as described before (30). $Synt_{1a}$ (CSYS-5RK), $Synt_{1a}^{Open}$, and $Synt_{1a}$K253I are as described in ref. 27. W66A point mutation was introduced to silence YFP in the YFP-$Synt_{1a}$-CFP construct (Fig. 4 *D* and *E* and *SI Appendix*, Fig. S11). BoNT/C1α-51-IRES-EGFP was designed and then generated by ProGen Israel, Protein and Gene Engineering Company. Transient cDNA transfections have been performed using Lipofectamine-2000 reagents, and neurons were typically imaged 18–48 h after transfection.

**Estimation of Synaptic Vesicle Release Using FM Dyes.** Activity-dependent FM1-43 or FM4-64 styryl dyes have been used to estimate synaptic vesicle exocytosis and presynaptic plasticity, as described (22). The experiments were conducted at room temperature in extracellular Tyrode solution containing (in mM): NaCl, 145; KCl, 3; glucose, 15; Hepes, 10; $MgCl_2$, 1.2; $CaCl_2$, 1.2, with pH adjusted to 7.4 with NaOH. The extracellular medium contained nonselective antagonist of ionotropic glutamate receptors (kynurenic acid, 0.5 mM) to block recurrent neuronal activity. Synaptic vesicles were loaded with 15 μM FM4-64 in all of the experiments with GFP/CFP/YFP transfection, whereas 10 μM FM1-43 was used in all of the nontransfected neurons.

**Detecting Presynaptic Calcium Transients.** Fluorescent calcium indicator Oregon Green 488 BAPTA-1 AM was dissolved in DMSO to yield a concentration of 1 mM. For cell loading, cultures were incubated at 37 °C for 30 min with 3 μM of this solution diluted in a standard extracellular solution. Imaging was performed using FV1000 Olympus confocal microscopes, under 488 nm (excitation) and 510–570 nm (emission), using 500-Hz line scanning.

**FRET Imaging and Analysis.** Intensity-based FRET imaging was carried as described before (22, 30). Donor dequenching resulting from the desensitized acceptor was measured from Cer/CFP emission (460–500 nm) before and after the acceptor (YFP) photobleaching. Mean FRET efficiency, $E_m$, was then calculated using the equation $E_m = 1 - I_{DA}/I_D$, where $I_{DA}$ is the peak of donor emission in the presence of the acceptor and $I_D$ is the peak after acceptor photobleaching.

**Statistical Analysis.** Error bars shown in the figures represent SEM. Where applicable, the number of experiments (cultures) or the number of boutons is defined by *n*. All the experiments were repeated at least in three different batches of cultures. One-way ANOVA analysis with post hoc Bonferroni's was used to compare several conditions. Student's unpaired, two-tailed *t* test has been used in the experiments in which two different populations of synapses were compared. Student's paired, two-tailed *t* test has been used in the experiments where before and after treatments were compared at the same population of synapses. $*P < 0.05$; $**P < 0.01$; $***P < 0.001$; ns, nonsignificant.

**ACKNOWLEDGMENTS.** This work was supported by European Research Council Starting Grant 281403 (to I. Slutsky), the Israel Science Foundation (398/13 to I.S.; 234/14 to I.L.), the Binational Science Foundation (2013244 to I. Slutsky; 2009049 to I.L.), Swiss National Science Foundation (31003A_152970 to B.B.), and the Legacy Heritage Biomedical Program of the Israel Science Foundation (1195/14 to I. Slutsky). I. Slutsky is grateful to the Sheila and Denis Cohen Charitable Trust and Rosetrees Trust of the United Kingdom for their support. I.V. is grateful to the TEVA National Network of Excellence in Neuroscience for the award of a postdoctoral fellowship.

1. Turrigiano GG, Nelson SB (2000) Hebb and homeostasis in neuronal plasticity. *Curr Opin Neurobiol* 10(3):358–364.
2. Turrigiano GG, Nelson SB (2004) Homeostatic plasticity in the developing nervous system. *Nat Rev Neurosci* 5(2):97–107.
3. Davis GW (2006) Homeostatic control of neural activity: from phenomenology to molecular design. *Annu Rev Neurosci* 29:307–323.
4. Marder E, Goaillard JM (2006) Variability, compensation and homeostasis in neuron and network function. *Nat Rev Neurosci* 7(7):563–574.
5. Davis GW, Müller M (2015) Homeostatic control of presynaptic neurotransmitter release. *Annu Rev Physiol* 77:251–270.
6. Turrigiano G (2011) Too many cooks? Intrinsic and synaptic homeostatic mechanisms in cortical circuit refinement. *Annu Rev Neurosci* 34:89–103.
7. Lazarevic V, Schöne C, Heine M, Gundelfinger ED, Fejtova A (2011) Extensive remodeling of the presynaptic cytomatrix upon homeostatic adaptation to network activity silencing. *J Neurosci* 31(28):10189–10200.
8. Ehlers MD (2003) Activity level controls postsynaptic composition and signaling via the ubiquitin-proteasome system. *Nat Neurosci* 6(3):231–242.
9. Slomowitz E, et al. (2015) Interplay between population firing stability and single neuron dynamics in hippocampal networks. *eLife* 4:e04378.
10. Hengen KB, Lambo ME, Van Hooser SD, Katz DB, Turrigiano GG (2013) Firing rate homeostasis in visual cortex of freely behaving rodents. *Neuron* 80(2):335–342.
11. O'Leary T, Williams AH, Franci A, Marder E (2014) Cell types, network homeostasis, and pathological compensation from a biologically plausible ion channel expression model. *Neuron* 82(4):809–821.
12. Ramocki MB, Zoghbi HY (2008) Failure of neuronal homeostasis results in common neuropsychiatric phenotypes. *Nature* 455(7215):912–918.
13. Schuler V, et al. (2001) Epilepsy, hyperalgesia, impaired memory, and loss of pre- and postsynaptic GABA(B) responses in mice lacking GABA(B(1)). *Neuron* 31(1):47–58.
14. Prosser HM, et al. (2001) Epileptogenesis and enhanced prepulse inhibition in GABA (B1)-deficient mice. *Mol Cell Neurosci* 17(6):1059–1070.
15. Gassmann M, et al. (2004) Redistribution of GABAB(1) protein and atypical GABAB responses in GABAB(2)-deficient mice. *J Neurosci* 24(27):6086–6097.
16. Vienne J, Bettler B, Franken P, Tafti M (2010) Differential effects of GABAB receptor subtypes, gamma-hydroxybutyric Acid, and Baclofen on EEG activity and sleep regulation. *J Neurosci* 30(42):14194–14204.
17. Badran S, Schmutz M, Olpe HR (1997) Comparative in vivo and in vitro studies with the potent GABAB receptor antagonist, CGP 56999A. *Eur J Pharmacol* 333(2-3): 135–142.
18. Turrigiano GG, Leslie KR, Desai NS, Rutherford LC, Nelson SB (1998) Activity-dependent scaling of quantal amplitude in neocortical neurons. *Nature* 391(6670): 892–896.
19. Murthy VN, Schikorski T, Stevens CF, Zhu Y (2001) Inactivity produces increases in neurotransmitter release and synapse size. *Neuron* 32(4):673–682.
20. Bettler B, Kaupmann K, Mosbacher J, Gassmann M (2004) Molecular structure and physiological functions of GABA(B) receptors. *Physiol Rev* 84(3):835–867.
21. Vigot R, et al. (2006) Differential compartmentalization and distinct functions of GABAB receptor variants. *Neuron* 50(4):589–601.

22. Laviv T, et al. (2010) Basal GABA regulates GABA(B)R conformation and release probability at single hippocampal synapses. *Neuron* 67(2):253–267.
23. Dobrunz LE, Stevens CF (1997) Heterogeneity of release probability, facilitation, and depletion at central synapses. *Neuron* 18(6):995–1008.
24. Raingo J, et al. (2012) VAMP4 directs synaptic vesicles to a pool that selectively maintains asynchronous neurotransmission. *Nat Neurosci* 15(5):738–745.
25. Dulubova I, et al. (1999) A conformational switch in syntaxin during exocytosis: role of munc18. *EMBO J* 18(16):4372–4382.
26. Acuna C, et al. (2014) Microsecond dissection of neurotransmitter release: SNARE-complex assembly dictates speed and $Ca^{2+}$ sensitivity. *Neuron* 82(5):1088–1100.
27. Greitzer-Antes D, et al. (2013) Tracking Ca2+-dependent and Ca2+-independent conformational transitions in syntaxin 1A during exocytosis in neuroendocrine cells. *J Cell Sci* 126(Pt 13):2914–2923.
28. Gerber SH, et al. (2008) Conformational switch of syntaxin-1 controls synaptic vesicle fusion. *Science* 321(5895):1507–1510.
29. Zhao C, Dreosti E, Lagnado L (2011) Homeostatic synaptic plasticity through changes in presynaptic calcium influx. *J Neurosci* 31(20):7492–7496.
30. Laviv T, et al. (2011) Compartmentalization of the GABAB receptor signaling complex is required for presynaptic inhibition at hippocampal synapses. *J Neurosci* 31(35):12523–12532.
31. Müller CS, et al. (2010) Quantitative proteomics of the Cav2 channel nano-environments in the mammalian brain. *Proc Natl Acad Sci USA* 107(34):14950–14957.
32. Varela JA, et al. (1997) A quantitative description of short-term plasticity at excitatory synapses in layer 2/3 of rat primary visual cortex. *J Neurosci* 17(20): 7926–7940.
33. Kreitzer AC, Regehr WG (2000) Modulation of transmission during trains at a cerebellar synapse. *J Neurosci* 20(4):1348–1357.
34. Lee KJ, et al. (2013) Mossy fiber-CA3 synapses mediate homeostatic plasticity in mature hippocampal neurons. *Neuron* 77(1):99–114.
35. Kim J, Tsien RW (2008) Synapse-specific adaptations to inactivity in hippocampal circuits achieve homeostatic gain control while dampening network reverberation. *Neuron* 58(6):925–937.
36. Thiagarajan TC, Lindskog M, Tsien RW (2005) Adaptation to synaptic inactivity in hippocampal neurons. *Neuron* 47(5):725–737.
37. Branco T, Staras K, Darcy KJ, Goda Y (2008) Local dendritic activity sets release probability at hippocampal synapses. *Neuron* 59(3):475–485.
38. Burrone J, O'Byrne M, Murthy VN (2002) Multiple forms of synaptic plasticity triggered by selective suppression of activity in individual neurons. *Nature* 420(6914):414–418.
39. Wierenga CJ, Walsh MF, Turrigiano GG (2006) Temporal regulation of the expression locus of homeostatic plasticity. *J Neurophysiol* 96(4):2127–2133.
40. Bacci A, et al. (2001) Chronic blockade of glutamate receptors enhances presynaptic release and downregulates the interaction between synaptophysin-synaptobrevin-vesicle-associated membrane protein 2. *J Neurosci* 21(17):6588–6596.
41. Jakawich SK, et al. (2010) Local presynaptic activity gates homeostatic changes in presynaptic function driven by dendritic BDNF synthesis. *Neuron* 68(6):1143–1158.
42. Mitra A, Mitra SS, Tsien RW (2012) Heterogeneous reallocation of presynaptic efficacy in recurrent excitatory circuits adapting to inactivity. *Nat Neurosci* 15(2):250–257.
43. Younger MA, Müller M, Tong A, Pym EC, Davis GW (2013) A presynaptic ENaC channel drives homeostatic plasticity. *Neuron* 79(6):1183–1196.
44. Wang T, Hauswirth AG, Tong A, Dickman DK, Davis GW (2014) Endostatin is a trans-synaptic signal for homeostatic synaptic plasticity. *Neuron* 83(3):616–629.
45. Wu LG, Saggau P (1995) GABAB receptor-mediated presynaptic inhibition in guinea-pig hippocampus is caused by reduction of presynaptic Ca2+ influx. *J Physiol* 485(Pt 3): 649–657.
46. Dickman DK, Davis GW (2009) The schizophrenia susceptibility gene dysbindin controls synaptic homeostasis. *Science* 326(5956):1127–1130.
47. Frank CA, Kennedy MJ, Goold CP, Marek KW, Davis GW (2006) Mechanisms underlying the rapid induction and sustained expression of synaptic homeostasis. *Neuron* 52(4): 663–677.
48. Müller M, Davis GW (2012) Transsynaptic control of presynaptic $Ca^{2+}$ influx achieves homeostatic potentiation of neurotransmitter release. *Curr Biol* 22(12): 1102–1108.
49. Gassmann M, Bettler B (2012) Regulation of neuronal GABA(B) receptor functions by subunit composition. *Nat Rev Neurosci* 13(6):380–394.
50. Slutsky I, Sadeghpour S, Li B, Liu G (2004) Enhancement of synaptic plasticity through chronically reduced Ca2+ flux during uncorrelated activity. *Neuron* 44(5): 835–849.

# $GABA_B$ receptor deficiency causes failure of neuronal homeostasis in hippocampal networks

Irena Vertkin, Boaz Styr, Edden Slomowitz, Nir Ofir, Ilana Shapira, David Berner, Tatiana Fedorova, Tal Laviv, Noa Barak-Broner, Dafna Greitzer-Antes, Martin Gassmann, Bernhard Bettler, Ilana Lotan and Inna Slutsky

***SI Appendix***

## Materials and Methods

**Hippocampal cell culture**. Primary cultures of CA3-CA1 hippocampal neurons were prepared from WT, *1a*$^{-/-}$, and *1b*$^{-/-}$ (BALB/c background) mice on postnatal days 0–2, as described (1). The generation of the *1a*$^{-/-}$ and *1b*$^{-/-}$ mice has been described previously (2). The experiments were performed in mature (13 - 28 days *in vitro*) cultures. All animal experiments were approved by the Tel Aviv University Committee on Animal Care.

**MEA preparation and recordings**. Cultures were plated on MEA plates containing 59 TiN recording and one internal reference electrodes (Multi Channel Systems (MCS)). Electrodes are 30 μm in diameter and spaced 500 μm apart. Data was acquired using a MEA1060-Inv-BC-Standard amplifier (MCS) with frequency limits of 5000 Hz and a sampling rate of 10 kHz per electrode mounted on an Olympus IX71 inverted microscope. Recordings were carried out under constant 37℃ and 5% $CO_2$ conditions, identical to incubator conditions.

**Spike sorting and data analysis**. Raw data was filtered, offline, at 200 Hz using a Butterworth high-pass filter. Spikes cutouts were then detected, offline, using MC Rack software (MCS) based on a fixed threshold set to between 4-5 standard deviations from noise levels as described (3). To reduce processing time, only the first twenty minutes of each hour were used for analysis. Spike cutouts were then transferred to Offline Sorter (Plexon Inc.) for spike sorting. Spikes were plotted in 2-D or 3-D principal component (PC) space and unit clusters were semi-automatically detected using K-means

clustering algorithm followed by template sorting. Clusters were then manually inspected to insure stability throughout experiment. All analysis was performed using custom-written scripts in MATLAB (Mathworks). Network mean firing rates were calculated by averaging the mean firing rates of all units for a given time-point.

**Whole-cell recordings in hippocampal culture**. Experiments were performed at room temperature in a recording chamber on the stage of FV300 inverted confocal microscope. Extracellular Tyrode solution contained (in mM): NaCl, 145; KCl, 3; glucose, 15; HEPES, 10; $MgCl_2$, 1.2; $CaCl_2$, 1.2; pH adjusted to 7.4 with NaOH. mEPSCs were recorded using the following intracellular solution (in mM): Cs-$MeSO_3$, 120; HEPES, 10; NaCl, 10; $CaCl_2$, 0.5; $Mg^{2+}$-ATP, 2; $Na_3GTP$, 0.3; EGTA, 10; pH adjusted to 7.25 with NaOH. Serial resistance was not compensated. For mEPSCs recordings, Tetrodotoxin (TTX; 1 μM), amino-phosphonopentanoate (AP-5; 50 μM), and gabazine (30 μM) were added to the Tyrode solution. Access resistance was between 5 - 10 MΩ. Neurons were excluded from the analysis if RMP was > - 55 mV, serial resistance was > 10 MΩ or if any of these parameters changed by >20% during the recording.

Dual whole-cell perforated patchclamp recordings were made on two inter-connected cultured hippocampal pyramidal neurons. Perforated patch pipettes were front filled with a solution containing CsOH, 127 mM; D-gluconic acid, 127 mM; CsCl, 4 mM; HEPES, 10 mM; NaCl, 8 mM; and EGTA, 0.4 mM; pH was adjusted to 7.25 with CsOH and then back filled with the same solution containing 150–200 ng/ml amphotericin B. The presynaptic cell was stimulated by 1 ms step depolarization from -70 to +30 mV in voltage-clamp mode. The postsynaptic cells were held in voltage-clamp at -70 mV. Only neurons with monosynaptic connections were used. The access resistances of both pre- and postsynaptic neurons were monitored online and were typically 7–20 MΩ. Recordings with access resistance > 20 MΩ or that varied substantially were rejected from analysis.

Signals were recorded using a MultiClamp 700B amplifier, digitized by DigiData1440A (Molecular Devices) at 10 kHz, and filtered at 2 kHz. mEPSCs were analyzed using MiniAnalysis (Synaptosoft), evoked EPSC using pClamp10 (Molecular Devices). For comparison of mEPSC amplitude or frequency under different conditions, 200 mEPSCs were randomly selected for each cell and pooled for each condition.

**Molecular biology**. $GB_{1a}$WT, $GB_{1a}$ΔPCT, $GB_2$ and Cav2.2 tagged proteins used throughout the study were constructed as described before (4). $Syt_{1a}$ (CSYS-5RK), $Syt_{1a}^{Open}$ and $Syt_{1a}$-K253I as described in (5). W66A point mutation was introduced to silence YFP in the YFP-$Synt_{1a}$-CFP construct (Fig. 4*D-E* and *SI Appendix*, Fig. S11). BoNT/C1α-51-IRES-EGFP was designed and then generated by ProGen Israel, Protein and Gene Engineering Company. BoNT/C1α-51, triple mutant BoNT/C1 light chain (shown to cleave Syntaxin and spare SNAP-25; a kind gift from Meyer Jackson (6)), flanked by HindIII and EcoRI sites was cloned into the N-terminus of Internal Ribosome Entry Site (IRES) cDNA sequence followed by an EGFP, in PCDNA3. Transient cDNA transfections have been performed using Lipofectamine-2000 reagents and neurons were typically imaged 18-48h after transfection.

**Estimation of synaptic vesicle release using FM dyes.** Activity-dependent FM1-43 or FM4-64 styryl dyes have been used to estimate synaptic vesicle exocytosis and presynaptic plasticity. Action potentials have been elicited by passing 50 mA constant current for 1 ms (~50% above the threshold for eliciting action potential) through two platinum wires, separated by ~7 mm and close to the surface of the coverslip. The experiments were conducted at room temperature in extracellular Tyrode solution contained (in mM): NaCl, 145; KCl, 3; glucose, 15; HEPES, 10; $MgCl_2$, 1.2; $CaCl_2$, 1.2; pH adjusted to 7.4 with NaOH. The extracellular medium contained non-selective antagonist of ionotropic glutamate receptors (kynurenic acid, 0.5 mM) to block recurrent neuronal activity. Synaptic vesicles were loaded with 15 μM FM4-64 in all the experiments with GFP/CFP/YFP transfection, while 10 μM FM1-43 was used in all the non-transfected neurons. FM was loaded by

bathing the cultures in a medium containing dye. FM was present 5 sec before and 30 sec after the electrical stimulation. After dye loading, external dye was washed away in $Ca^{2+}$-free solution containing ADVASEP-7 (0.1 mM) to scavenge membrane-bound FM. The fluorescence of individual synapses was determined from the difference between images obtained after staining and after destining ($\Delta F$). To estimate vesicle release during low frequency stimulation, we quantified FM destaining rate during 1 Hz stimulation following staining of boutons by maximal stimulation of 600 action potentials at 20 Hz (7, 8).

Images were obtained with an Olympus (FV300 or FV1000) confocal laser inverted microscopes. The 488-nm line of an argon laser was used for excitation, and the emitted light was filtered using a 510-nm long-pass filter and detected by a photomultiplier. A 60 × 1.2 NA water-immersion objective was used for imaging. The confocal aperture was partially open and image resolution was 57 - 92 nm / pixel. The gain of the photomultiplier was adjusted to maximize the signal-to-noise ratio without causing saturation by the strongest signals. The image after FM dye unloading was subtracted from the initial image; thus, only those terminals containing activity-dependent releasable FM dye (~90% of total staining) were analyzed. For detection of $FM^+$ puncta, $\Delta F$ images have been analyzed (only the puncta exhibiting ≥ 90% destaining were subjected to analysis) as described before (7).

**Detecting presynaptic calcium transients.** Fluorescent calcium indicator Oregon Green 488 BAPTA-1 AM was dissolved in DMSO to yield a concentration of 1 mM. For cell loading, cultures were incubated at 37 °C for 30 min with 3 μM of this solution diluted in a standard extracellular solution. Imaging was performed using FV1000 Olympus confocal microscopes, under 488 nm (excitation) and 510 - 570 nm (emission), using 500 Hz line scanning.

**FRET imaging and analysis.** Intensity-based FRET imaging was carried as described before (4, 8). Donor dequenching due to the desensitized acceptor was measured from Cer/CFP emission (460-500 nm) before and after the acceptor (YFP) photobleaching. Photobleaching of YFP was carried out with

515 nm laser line, by a single point activation module for rapid and efficient multi-region bleaching. Images were acquired without averaging. Image acquisition parameters were optimized for maximal signal-to-noise ratio and minimal phototoxicity. Images were 512 × 512 pixels, with a pixel width of 92 – 110 nm. Z-stacks were collected from 3-4 µm optical slice, at 0.6 - 0.8µm steps. Mean FRET efficiency, $E_m$, was then calculated using the equation $E_m = 1 - I_{DA}/I_D$, where $I_{DA}$ is the peak of donor emission in the presence of the acceptor and $I_D$ is the peak after acceptor photobleaching. Detection of signals was done as described earlier (8). Briefly, regions of interest (ROIs) were marked at boutons that underwent YFP photobleaching. Average intensity of ROI was subtracted from background ROI intensity in close proximity to the bouton. All the boutons that exhibited acceptor photobleaching by >90% of initial fluorescence intensity were included in the analysis. Non-bleached boutons at the same image area were analyzed to ensure lack of non-specific photobleaching due to image acquisition.

**Co-immunoprecipitation**. Adult mouse brain membranes were prepared as described previously (2) and solubilized in NP-40 lysis buffer (100mM NaCl, 20mM Tris, 0.5% Nonidet P-40, 1mM EDTA) supplemented with protease inhibitors (complete EDTA-free, Roche). After pre-clearing with protein A-agarose beads (Roche), solubilized brain membranes were incubated overnight at 4° with anti-CaV2.2 (ACC-002, Alomone Labs) or anti-Syntaxin 1 (ANR-002, Alomone Labs) antibodies. Subsequently antibody/protein complexes were captured by incubation with Protein A-agarose beads for 40 min at 4°, washed six times in lysis buffer and eluted with 1x reducing SDS-PAGE sample buffer. For Western Blotting, protein samples were resolved using standard SDS–PAGE and probed with the primary antibodies anti-CaV2.2 (1:500, AB5154, Millipore), anti-Syntaxin 1 (1:1000, S1172, Sigma) anti-$GABA_{B1}$ (1:500, ab55051, Abcam) and peroxidase-coupled secondary antibodies (1:10000, GE Healthcare Life Sciences) or the Clean Blot IP reagent (1:200, Thermo Fisher Scientific). The chemiluminescence detection kit SuperSignal West (Thermo Scientific) was used for visualization.

**Chemical reagents.** FM4-64 (SynaptoRed C2), FM1-43 (SynaptoGreen C4) and Advasep-7 were purchased from Biotium; CGP54626 and baclofen from Tocris; TTX from Alomon labs, kynurenic acid from Sigma-Aldrich, Calcium Green 488 BAPTA-1 AM from Invitrogen.

**Statistical analysis.** Error bars shown in the figures represent standard error of the mean (s.e.m.). Where applicable, the number of experiments (cultures) or the number of boutons is defined by *n*. All the experiments were repeated at least in 3 different batches of cultures. One-way ANOVA analysis with *post hoc* Bonferroni's was used to compare several conditions. Student's un-paired, two-tailed *t*-test has been used in the experiments where two different populations of synapses were compared. Student's paired, two-tailed *t*-test has been used in the experiments where before and after treatments were compared at the same population of synapses. * $P < 0.05$; ** $P < 0.01$; *** $P < 0.001$, ns – non significant.

**References:**


1. Slutsky I, Sadeghpour S, Li B, & Liu G (2004) Enhancement of synaptic plasticity through chronically reduced Ca2+ flux during uncorrelated activity. *Neuron* 44(5):835-849.
2. Vigot R, *et al.* (2006) Differential compartmentalization and distinct functions of GABAB receptor variants. *Neuron* 50(4):589-601.
3. Slomowitz E, *et al.* (2015) Interplay between population firing stability and single neuron dynamics in hippocampal networks. *eLife* 10.7554/eLife.04378.
4. Laviv T, *et al.* (2011) Compartmentalization of the GABAB Receptor Signaling Complex Is Required for Presynaptic Inhibition at Hippocampal Synapses. *The Journal of Neuroscience* 31(35):12523-12532.
5. Greitzer-Antes D, *et al.* (2013) Tracking Ca2+-dependent and Ca2+-independent conformational transitions in syntaxin 1A during exocytosis in neuroendocrine cells. *Journal of Cell Science* 126(13):2914-2923.
6. Wang D, *et al.* (2011) Syntaxin Requirement for Ca2+-Triggered Exocytosis in Neurons and Endocrine Cells Demonstrated with an Engineered Neurotoxin. *Biochemistry* 50(14):2711-2713.
7. Abramov E, *et al.* (2009) Amyloid-[beta] as a positive endogenous regulator of release probability at hippocampal synapses. *Nat Neurosci* 12(12):1567-1576.
8. Laviv T, *et al.* (2010) Basal GABA Regulates GABA(B)R Conformation and Release Probability at Single Hippocampal Synapses. *Neuron* 67(2):253-267.

## Supplementary Figures

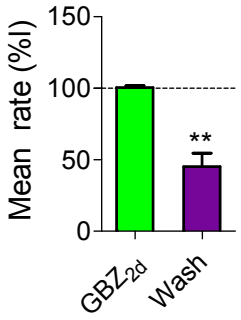


**Figure S1.** Washout of gabazine causes a decrease in mean firing rate after 2 days gabazine incubation. The average firing rate was reduced by 60% ($P$ = 0.0011, paired, two-tailed $t$-test).

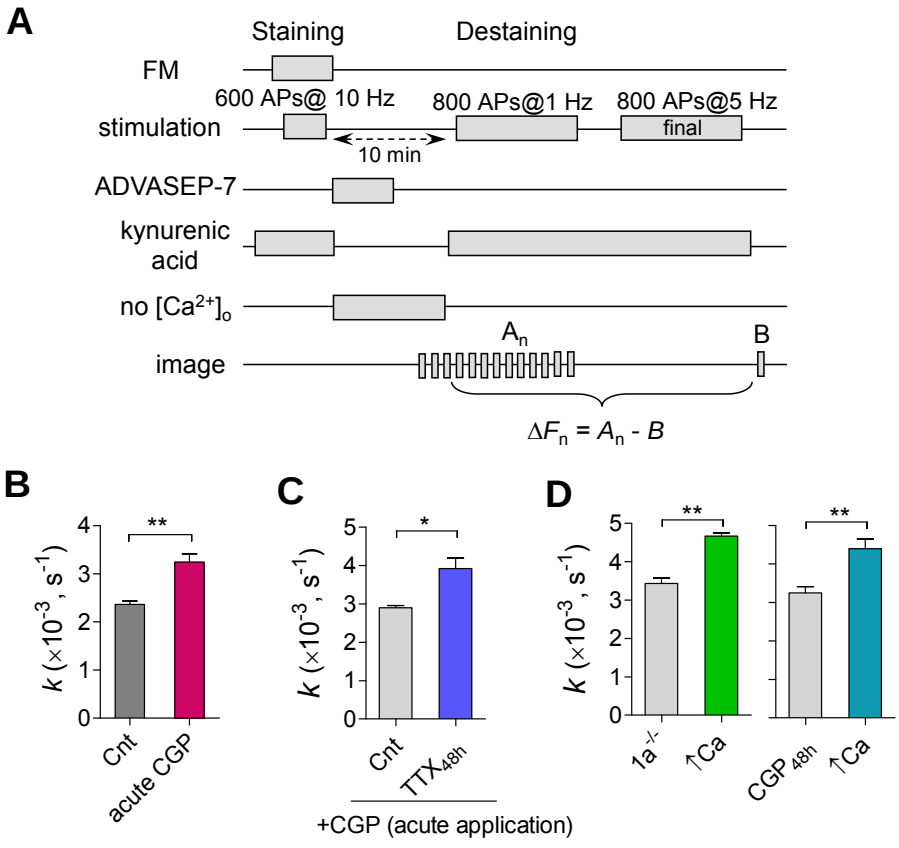


**Figure S2.** Measuring synaptic vesicle exocytosis by FM dyes. (*A*) Experimental protocol to estimate the rate of synaptic vesicle exocytosis by FM dyes. (*B*) Acute application of CGP54626 increases the FM destaining rate ($n$ = 688 – 762). (*C*) Application of CGP54626 during FM destaining does not prevent $TTX_{48h}$-induced increase in the FM destaining rate ($n$ = 305 - 321). Unpaired, two-tailed $t$-

test. (*D*) Increase in the extracellular $Ca^{2+}$ from 1.2 to 2.5 mM induced an increase in the FM destaining rate in *1a*$^{-/-}$ (*n* = 250 - 295) and $CGP_{48h}$-treated (*n* = 270 - 310) cultures.

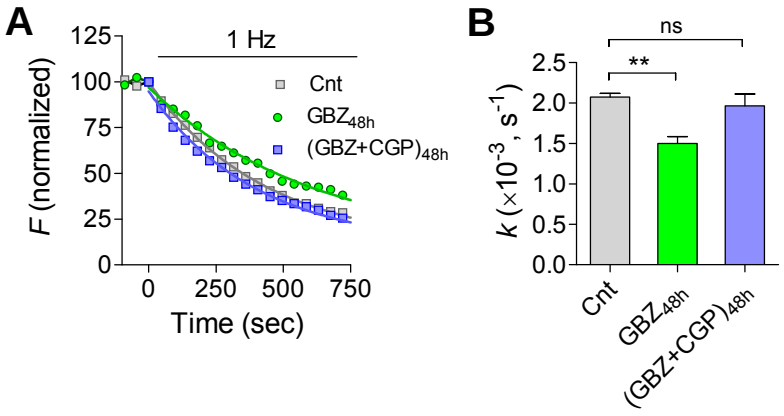


**Figure S3**. Blockade of $GABA_BRs$ prevents homeostatic decrease in *P*r by gabazine. (*A*) Representative FM destaining rate curves of 80 synapses under control conditions (Cnt), 2 days after gabazine incubation ($GBZ_{48h}$) and 2 days after concurrent gabazine and CGP54626 incubation ($(GBZ+CGP)_{48h}$) . (*B*) Effect of $GBZ_{48h}$ and $(GBZ+CGP)_{48h}$ on average destaining rate constants (*n* = 385 – 450, unpaired, two-tailed *t*-test).

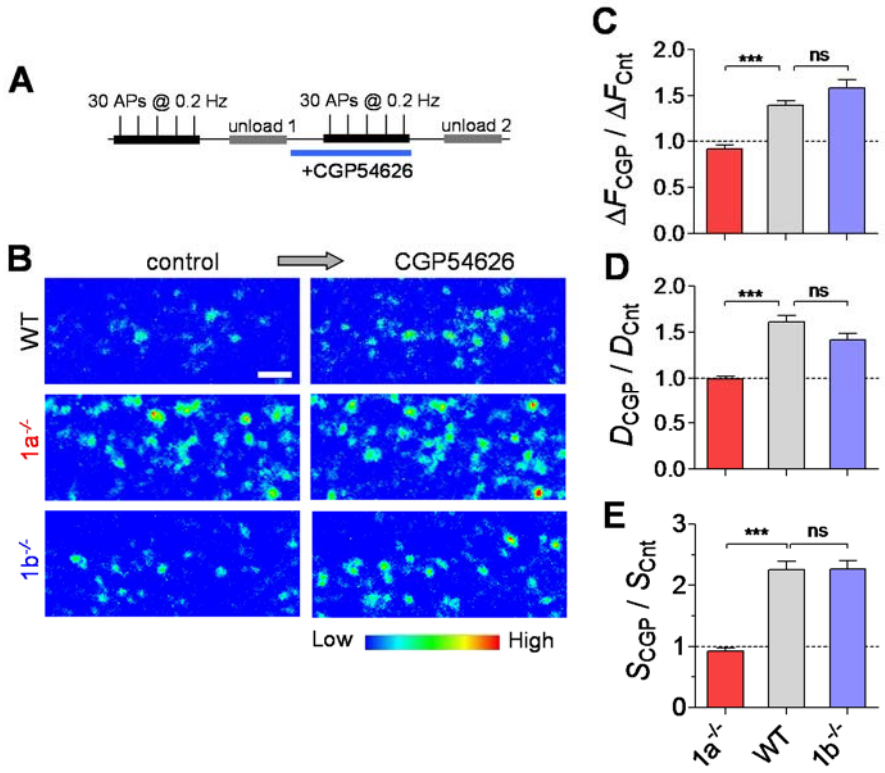


**Figure S4**. Impaired basal $GABA_BR$-mediated inhibition in *1a*$^{-/-}$ boutons. (*A*) Experimental protocol used to determine tonic inhibition. Synaptic vesicle recycling evoked by 30 AP @ 0.2 Hz was assessed before and 10 min after application of CGP54626 (1 μM). (*B*) Representative $\Delta F$ images before and after CGP54626 application in WT, *1a*$^{-/-}$ and *1b*$^{-/-}$ cultures. Scale bar: 2 μm. (*C-E*) Tonic inhibition expressed as fold changes in $\Delta F$, *D* (FM-(+) puncta density) and *S* (total presynaptic strength, $S = \Delta F \times D$) across synaptic populations in *WT* ($n$ = 18), *1a*$^{-/-}$ ($n$ = 17) and *1b*$^{-/-}$ ($n$ = 17) cultures. One way ANOVA with *post hoc* Bonferroni's multiple comparison tests.

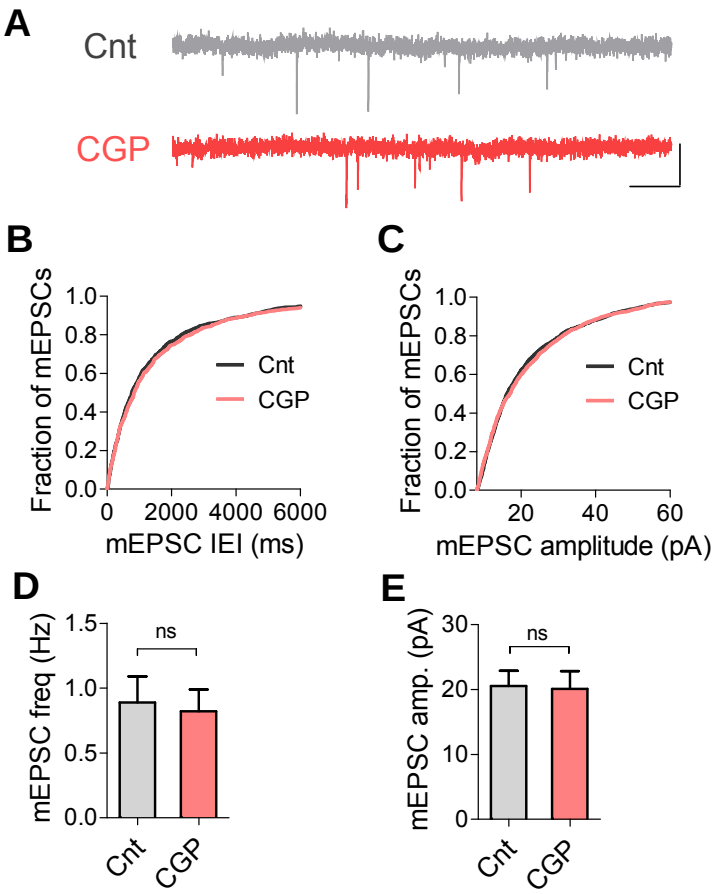


**Figure S5**. Acute effect of CGP54626 on mEPSCs. (*A*) Representative traces of mEPSCs in control and after acute (10 min) application of CGP54626. Scale bar: 20 pA, 0.5 sec. (*B-C*) Cumulative distributions of the mEPSC peak amplitude (*B*) and inter-event intervals (*D*) before and after CGP application ($n$ = 9). (*D-E*) Average mean peak amplitude (*D*, $P > 0.7$) and frequency (*E*, $P > 0.2$) of mEPSCs (the same experiments as in *B-C*). Paired, two-tailed *t*-tests.

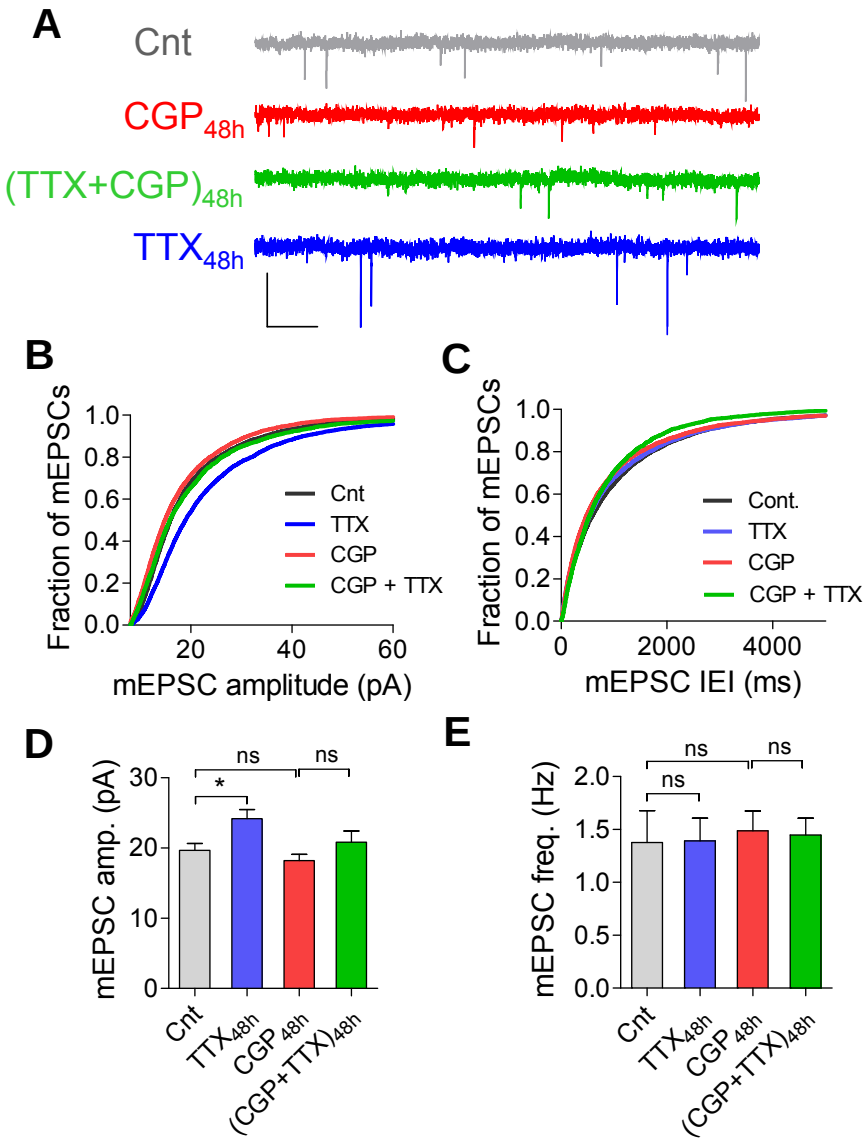


**Figure S6.** Postsynaptic scaling of mEPSC amplitude requires active $GABA_BRs$. (*A*) Representative traces of mEPSCs in control, after $TTX_{48h}$, $CGP_{48h}$ and $(TTX+CGP)_{48h}$ pre-incubation. Scale bar: 40 pA, 0.5 sec. (*B-C*) Cumulative distributions of the mEPSC peak amplitude (*B*) and inter-event intervals (*D*) under control ($n$ = 21), after $TTX_{48h}$ ($n$ = 29), $CGP_{48h}$ ($n$ = 27) and $(TTX+CGP)_{48h}$ ($n$ = 17) conditions. Differences between the control and $TTX_{48h}$ conditions for the displayed mEPSC amplitude cumulative distributions are statistically significant ($P$ < 0.05, K-S test). Differences between mEPSC inter-event interval distributions ($P$ = 0.95, K-S test) are not significant. (*D-E*) Average mean peak amplitude (*D*) and frequency (*E*) of mEPSCs (the same experiments as in B-C). ANOVA analysis with *post hoc* Bonferroni's multiple comparison tests.

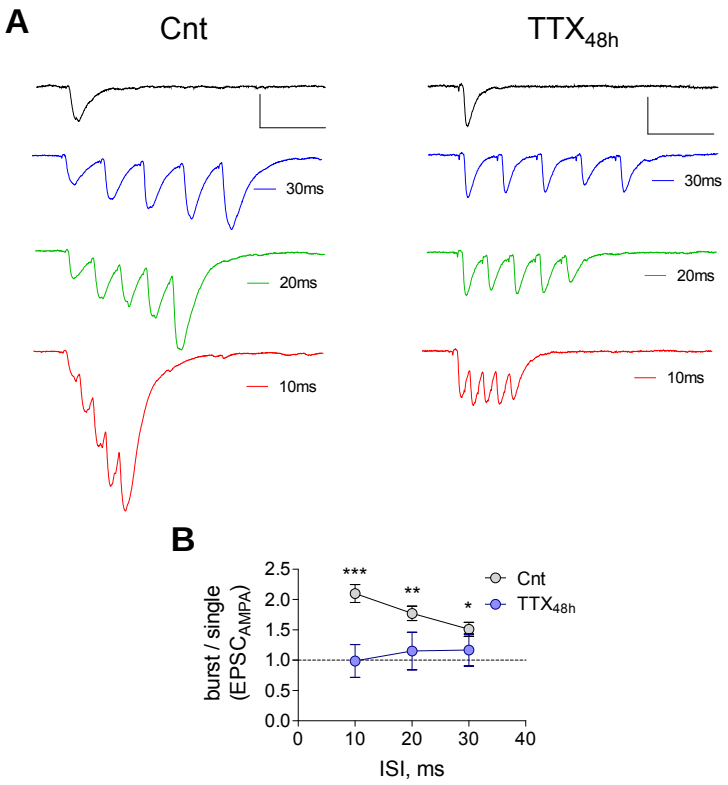


**Figure S7.** Chronic inactivity by TTX triggers a reduction in short-term synaptic facilitation measured between paired of neurons. (*A*) Double-patch recordings of evoked AMPAR-mediated EPSCs at -70 mV (in the presence of 50 μM AP-5). Neurons were stimulated by single (0.1 Hz) and bursting (bursts of 5 APs, inter-spike-interval 30, 20 and 10 ms, inter-burst-interval 10 sec) inputs in control and $TTX_{48h}$-treated cultures. (*B*) Short-term facilitation of EPSC charge transfer (burst/single ratio, calculated as $Q_{burst}/Q_{single}*5$) is lower in $TTX_{48h}$-treated cultures ($n$ = 8).

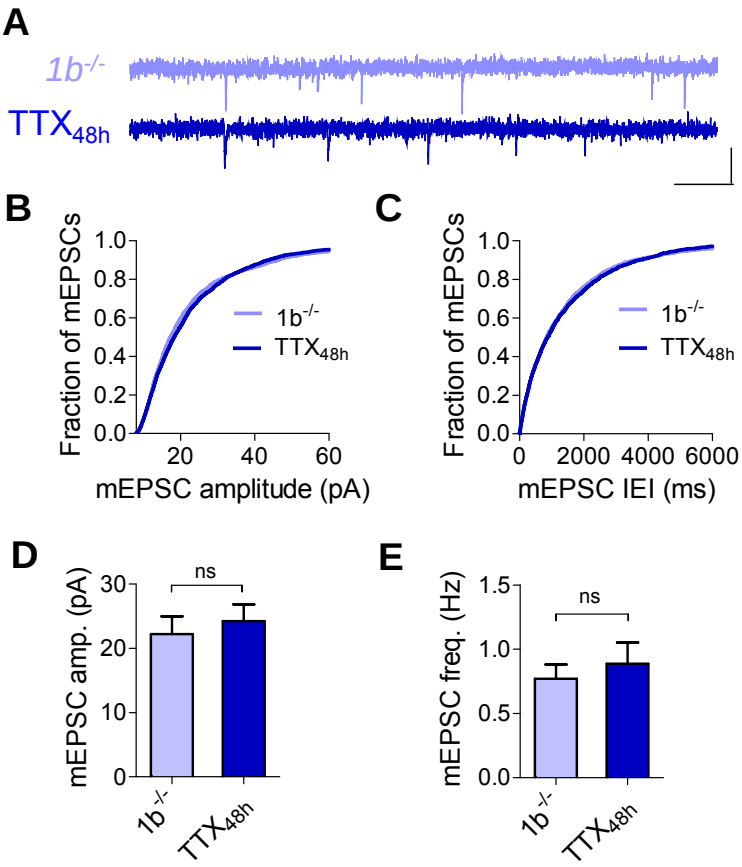


**Figure S8.** $GB_{1b}$-containing $GABA_BRs$ mediate postsynaptic scaling of mEPSC amplitude. (*A*) Representative traces of mEPSCs in control and $TTX_{48h}$ *1b*$^{-/-}$ cultures. Scale bar: 20 pA, 0.5 sec. (*B-C*) Cumulative distributions of the mEPSC peak amplitude (*B*) and inter-event intervals (*D*) in control ($n$ = 13) and $TTX_{48h}$-treated ($n$ = 13) cultures. (*D-E*) Average mean peak amplitude (*D*, $P > 0.6$) and frequency (*E*, $P > 0.5$) of mEPSCs (the same experiments as in *B-C*). Unpaired, two-tailed *t*-tests.

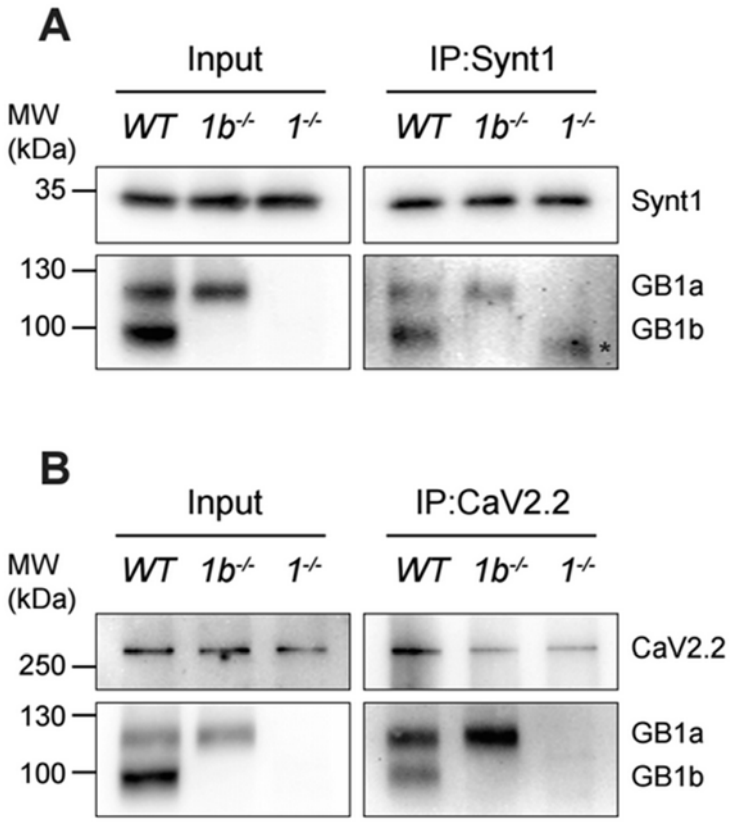


**Figure S9.** Endogenous $GABA_BRs$ co-immunoprecipitate with syntaxin-1 and $Ca_V2.2$. (*A-B*) Solubilized brain membranes from WT, *1b*$^{-/-}$ and *1*$^{-/-}$ mice were immunoprecipitated (IP) with anti-syntaxin-1 (*A*) and anti-$Ca_V2.2$ (*B*) antibodies and analyzed by western blotting with the indicated antibodies. Of note, the anti-GB1 antibody recognizes the common C-terminus of $GB_{1a}$ and $GB_{1b}$. Asterisk indicates a cross-reacting band visible after the long exposure required for detection of $GABA_BRs$ in anti-syntaxin-1 IPs. Left panels show input brain membranes used for immunoprecipitation. MW, molecular weight.

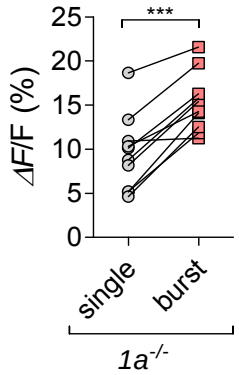


**Figure S10.** Calcium transients evoked by single spikes are not saturated in *1a*$^{-/-}$ presynaptic boutons. Calcium transients evoked by spike bursts (5 spikes at 100 Hz, 5 sec inter-burst-interval) were significantly higher than those evoked by single spikes ($n$ = 10, paired, two-tailed $t$-test).

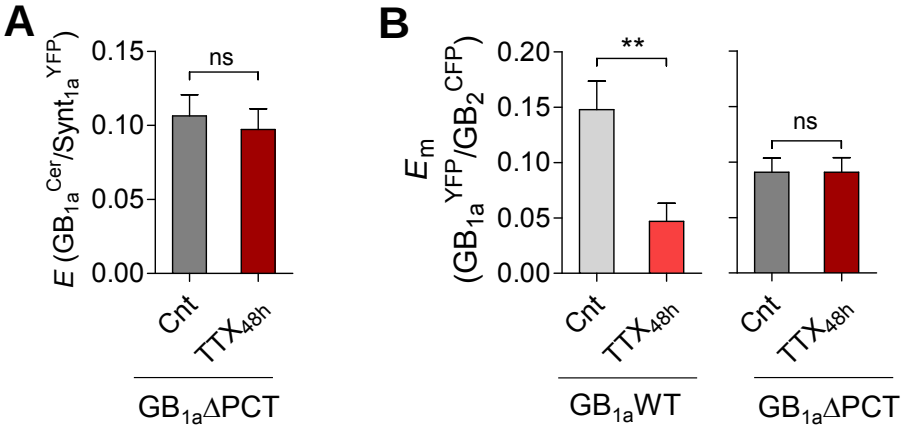


**Figure S11.** $GB_{1a}$-PCT domain determines $GB_{1a}/GB_2$ and $GB_{1a}/Synt_{1a}$ inter-molecular changes by chronic inactivity. (*A*) Deletion of PCT domain increases $GB_{1a}^{Cer}/Synt_{1a}^{YFP}$ FRET efficiency and abolishes $TTX_{48h}$-induced FRET changes ($n$ = 58 - 69). (*B*) Effect of $TTX_{48h}$ on $E_m$ between $GB_{1a}^{YFP}/GB_2^{Cer}$ in $GB_{1a}$WT ($n$ = 17 - 29) and $GB_{1a}\Delta$PCT ($n$ = 24 - 28) expressing neurons. Unpaired, two-tail, student $t$-tests.

# Acknowledgements

First, I want to thank Prof. Bernhard “Benny” Bettler for giving me the great opportunity to do my PhD thesis in his lab and for his supervision of it.

I also want to thank Prof. Markus Rüegg and Prof. Martin Spiess for their help and serving as members of my PhD committee.

My thanks also go to Martin Gassmann for his supervision and the discussions of my work.

Thanks also go to Adi and Margarita for proofreading the thesis, the nice discussions and coffee breaks.

I also want to thank Lisa for her help and discussions related to the Cullin 3-project and Rosta for the easy and fruitful collaboration on the N-type calcium channel-project. Thanks also go to Ruth for teaching me many techniques and to Thorsten, Valérie, Adi and Margarita for their technical help over the years.

Many thanks also go to all the unmentioned present and past lab members for their help and discussions. Furthermore, thanks for all the fun we had together, during and after work.

Last but not least, I want to express my gratitude to several people for the good times and the support over the years: my girlfriend Julia, all of my friends (especially the “Clan”: Dave, Erik, Manuel, Sämi, Ade, Ingie, Huebi and their partners; as well as Anna, Fäbi, Hannes and Melissa) and all of my family (especially my parents Ruth and Jörg as well as my brother Christian).